

STEADY FLOW AND CIRCULATIONS
IN SOUND FIELDS

by

JOHN MILTON ANDRES

B.S., California Institute of Technology
(1949)

M.S., California Institute of Technology
(1950)

SUBMITTED IN PARTIAL FULFILLMENT OF THE
REQUIREMENTS FOR THE DEGREE OF
DOCTOR OF PHILOSOPHY

at the

MASSACHUSETTS INSTITUTE OF TECHNOLOGY

June, 1953

Signature of Author Signature redacted
Department of Physics, May 18, 1953

Certified by Signature redacted
Thesis Supervisor

Accepted by Signature redacted
Chairman, Departmental Committee on Graduate Students

MR ✓

Physics
Thesis
1953



STEADY FLOW AND CIRCULATIONS

IN SOUND FIELDS

by

John Milton Andres

Submitted to the Department of Physics on May 18, 1953, in partial fulfillment of the requirements for the degree of Doctor of Philosophy.

ABSTRACT

The phenomenon of acoustic streaming has been observed and discussed for many years. One of the more interesting aspects of the streaming near obstacles is its dependence upon the geometry of the obstacle and the intensity and frequency of the acoustic wave striking the obstacle. The direction of the streaming motion has been observed to change under certain conditions.

It is pointed out in this thesis that the type of streaming which occurs is determined by two dimensionless parameters, $R = U_0 a / \nu$, and s/a , where U_0 is the particle velocity amplitude in the incident wave, s is the particle displacement amplitude, a is the radius for the case of a cylindrical obstacle and ν is the kinematic viscosity of the medium. Theoretical treatments are given for the limiting cases of very large and very small R , and the calculated flow patterns are in agreement with those observed experimentally.

The treatment for large R is based upon the mathematical theory of the boundary layer introduced by Prandtl. A perturbation calculation is carried through to terms of fourth order, and represents an extension of work done by Schlichting*. The calculations are rather laborious and involve several simple extensions of the perturbation technique. The resulting expression for the stationary streaming flow is applied to several examples, including the flow near a circular cylinder.

The treatment for small R is based upon the Oseen approximation to the Navier-Stokes equations. A perturbation technique is again used to calculate the streaming near a circular cylinder.

Experiments have been conducted in the range of intermediate values of R and indicate that two types of flow exist,

*H. Schlichting, Phys. Z. 33, 327 (1932).

Hayden (Ray) Aug. 13, 1953

one corresponding to that calculated for large R and the other to that for small R . The transition point between the two types of flow has been determined experimentally for a circular cylinder as a function of the parameters R and s/a .

A calculation of the rate at which energy is dissipated viscously near a circular cylinder in an oscillating flow for both the large and the small R cases is also included in this thesis.

Thesis Supervisor: Uno Ingard

Title: Assistant Professor of Physics

Acknowledgment

The author wishes to thank Professor Uno Ingard for the suggestions and encouragement given during the course of this research. The author also thanks the many other members of the Acoustics Laboratory who helped in the research work and in the preparation of this thesis.

Table of Contents

Abstract	
Acknowledgment	
List of Figures	
Chapter I.	Introduction and History of Problem 1
Chapter II.	The Reynolds Number as an Important Parameter in Streaming Problems 8
	The Case for Small R 14
	The Case for Large R 15
Chapter III.	The Calculation for the Case of Large Reynolds Numbers 21
	Schlichting's Treatment 23
	The Higher Order Terms 25
	Discussion 39
Chapter IV.	The Calculation for the Case of Small Reynolds Numbers 45
	The Velocities u_1 and v_1 49
	The Velocities u_2 and v_2 50
	Discussion 54
Chapter V.	Calculation of the Viscous Dissipation due to an Obstacle 63
	The Case for Large R 64
	The Case for Small R 70
	Discussion 74
Chapter VI.	A Discussion of Certain Experimental Observations 77
	Experimental Setup 77
	Observations 84
	Tables 88
	Appendix 1 101
	Appendix 2 108

Appendix 3	110
Appendix 4	113
Bibliography	115
Biographical Sketch	117

List of Figures

Figure 1.	Plot of ψ_{2b}, ψ'_{2b} as functions of η	26
Figure 2.	Plot of ψ_{4a}, ψ'_{4a} as functions of η	32
Figure 3.	Plot of ψ_{4b}, ψ'_{4b} as functions of η	33
Figure 4.	Plot of ψ_{4c}, ψ'_{4c} as functions of η	34
Figure 5.	Plot of $\psi_{2b} \times 100, \psi_{4a}, \psi_{4b}, \psi_{4c}$ as functions of η	35
Figure 6.	Streamline pattern near cylinder for case of large R, higher order terms neglected	40
Figure 7.	Streamline pattern near cylinder for case of large R, higher order terms considered	41
Figure 8.	Plot of $f(r/a, a/\delta)$ as function of r/a for several values of a/δ	56
Figure 9.	Streamline pattern near cylinder for case of small R, $a/\delta = 1$	57
Figure 10.	Streamline pattern near cylinder for case of small R, $a/\delta = 2$	58
Figure 11.	Streamline pattern near cylinder for case of small R, $a/\delta = 3$	59
Figure 12.	Plot of radial velocity function $\frac{f(r/a, a/\delta)}{r/a}$ as a function of r/a	60
Figure 13.	Plot of tangential velocity function $f'(r/a, a/\delta)$ as a function of r/a	61
Figure 14.	Plot of the viscous dissipation $W/4\pi v \frac{\rho}{2} U_0^2$ as a function of a/δ for both large R and small R cases	73
Figure 15.	"Phase diagram" plot in $s/a, R$ space, summing up results	89
Figure 16	(a, b) Photograph and schematic sketch of streaming flow $R = 75$ $s/a = .036$	90
Figure 17	(a, b) Photograph and schematic sketch of streaming flow $R = 20$ $s/a = .65$	91

Figure 18 (a, b) Photograph and schematic sketch of streaming flow $R = 8$ $s/a = .8$	92
Figure 19 (a, b) Photograph and schematic sketch of streaming flow $R = 2$ $s/a = .5$	93
Figure 20 (a, b) Photograph of "squeeze-out" phenomenon (before-after) $R = 270$ $s/a = .55$	94
Figure 21. Photograph of equipment setup to take streaming photographs	95
Figure 22. Photograph of equipment setup for visual observations of streaming	96
Figure 23. Photograph of equipment setup for travelling wave observations	97
Figure 24. Photograph of test section	98
Figure 25. Photograph of speaker and driver section	99
Figure 26. Photograph of test section and cylindrical obstacles	100

Chapter I

Introduction and History of Problem

When an acoustic wave is propagated in a viscous fluid, under certain conditions time-independent currents appear superimposed upon the periodic motion of the fluid. For many years this phenomenon has been known and a number of papers concerned with the subject have been published. The phenomenon is often referred to as acoustic streaming, and can occur both in the presence of solid obstacles and when no boundary surfaces are present. The former type of streaming has been observed to occur in tubes and in the neighborhood of spheres, cylinders, orifices, and other obstacles in a sound field. One of the first mathematical treatments of this type of flow was given by Rayleigh² in which he treated the circulating flow in standing wave tubes. A general analysis of streaming in the presence of boundaries appears in a paper by Schuster and Matz,¹⁰ and is applied to the problem treated by Rayleigh. The treatment of Schuster and Matz neglects the terms in the equations of motion which can give rise to streaming in the absence of boundaries. Eckart¹¹ seems to have been the first to discuss this latter type of streaming, one example of which is the streaming occurring in a medium in the vicinity of a narrow beam of sound (quartz wind).

A list of references to the papers on acoustic streaming is included in the bibliography of this thesis. Among the

1--22

more recent papers on the subject, those of Westervelt,¹⁹ Nyborg,²⁰ and Medwin and Rudnick²¹ are of considerable interest. Each of these papers contains a brief review of the general mathematical theory of acoustic streaming, beginning with the Navier-Stokes equations for a viscous compressible fluid, and points out how the streaming is generated by the combination of viscous and nonlinear terms appearing in these equations. Reference is made in these papers to earlier mathematical treatments in the light of their approximations and assumptions. In their paper Medwin and Rudnick²¹ distinguish explicitly between the volume source terms and the surface source terms giving rise to the two types of streaming discussed above. Westervelt gives a proof of the physically apparent fact that the streaming motion is solenoidal.

One of the more interesting aspects of the type of streaming occurring near boundaries is that the nature of the streaming seems to change with the intensity and frequency of the incident sound wave producing the flow. In addition the shape and direction of the steady circulating flows depend upon the geometry of the obstacle interacting with the incident sound field. For example, Carrière^{4,5,9} while studying the streaming near a circular cylinder observed flow patterns which are symmetric with respect to axes drawn through the cylinder in directions parallel to and perpendicular to the direction of propagation of the incident wave. He found the flow to be

directed toward the cylinder along the line of propagation. Schlichting⁷ and Andrade⁶ studying the streaming near a cylinder under somewhat different conditions observed a steady flow qualitatively similar to that described by Carrière, but which was moving in the opposite direction. Bouasse⁸ has noted these two types of flow near obstacles of a variety of shapes, and he has qualitatively correlated them with the amplitude of the oscillating motion of the fluid near the obstacle. Westervelt¹⁹ more recently has again pointed to the discrepancies between Carrière and Andrade and Schlichting, and also has assigned them to differences in the intensity of the wave incident upon the cylinder. Ingard and Labate,¹³ in their experiments with various shapes and sizes of orifices in a sound field, have noted these distinct types of flow occurring as the amplitude of oscillation is varied with respect to the dimensions of the orifice, and they present "phase diagrams" indicating the onset of flow reversal and turbulence as a function of frequency and amplitude.

It has been recognized that the change in the nature of the circulating flow manifested as a reversal of flow must be a consequence of the nonlinearity of the equations governing the motion of the fluid, but the theoretical treatment of these equations is difficult, and cannot be carried out without approximations. It is difficult to know just what type of approximations are appropriate for a given experiment and

the experiments cited do not seem to indicate any direction of attack. If the parameters important in describing the experiments were known, the type of approximation to be used in the theoretical treatment could be more easily selected.

As seen in the experiments referred to above, the intensity and frequency of the incident wave as well as the geometry of the obstacle seem to play a vital role. In this thesis it is pointed out that the situation in any given case can be completely specified in terms of two dimensionless parameters. This can be seen from an application of the elements of dimensional analysis to the problem. Thus in treating a streaming problem it makes sense to speak of the conditions of the problem or experiment in terms of these two dimensionless parameters. The variables, intensity, frequency, etc., are absorbed into the dimensionless parameters. The parameters which prove most useful in the analysis which follows are the Reynolds number, $R = \frac{U_0 a}{\nu}$ and the ratio s/a . The letter U_0 stands for the velocity amplitude of the incident wave, a represents the radius of the cylinder in the problem treated, ν is the kinematic viscosity coefficient, and s represents the amplitude of the periodic particle motion in the incident wave.

If one looks at the experiments above in terms of the parameters R and s/a a theoretical approach to the problem immediately suggests itself. It will be seen that the experiment of Carriere corresponds to a small value of R ,

and the experiments of Andrade and Schlichting correspond to large values of R . The streaming patterns which they observed will be shown to agree qualitatively with patterns obtained theoretically using the approximations valid in each of the two cases. Thus, the case in which R is large can be attacked by using the mathematical theory of the boundary layer. Indeed Schlichting⁷ used this theory to calculate the steady flow corresponding to his experiment. The small Reynolds number case can be treated by using an approximation procedure introduced by Oseen.²⁷ In this thesis the Oseen approximation is carried through to give the steady flow near a circular cylinder, and the boundary layer treatment of Schlichting is extended to include higher order terms. This latter treatment shows the dependence of the streaming at high Reynolds numbers upon the parameter s/a . It is possible to calculate the rate at which energy is dissipated by viscosity in both of these cases, and these calculations are also included in the thesis. There is no known method by which the cases involving Reynolds numbers which are neither large nor small can be treated theoretically. A chapter is included in which experimental data covering this middle range is presented and discussed.

The accumulation of the material in this thesis did not strictly follow the outline of the exposition just presented, and it is of interest to trace the actual path that the research followed.

It was believed initially that the observed changes in the circulatory motions with changes in incident wave intensity could be explained by extending the treatment of Schlichting⁷ so as to include higher order terms. In particular a statement by Westervelt¹⁹ to the effect that the reversed circulations observed by Carrière occurred for large incident wave intensities led to the hope that the higher order calculation would predict such a reversal. When the Schlichting treatment was carried to fourth order giving terms in the steady velocity depending on intensity, it was indeed seen that the resulting expressions indicated a change in the sign of the velocity for sufficiently high intensity, and the extension was regarded as successful. This sign change is discussed in more detail later, and is now believed to indicate the failure of the perturbation procedure when s/a is increased beyond a certain point.

Attempts to observe a flow of the type described by Carrière at high intensities proved futile. When the circulation of smoke particles in the sound field near small obstacles was observed, it was realized that this flow observed by Carrière occurs for small incident wave intensities instead of large and for cylinders of small radii. It was then that the importance of the use of the parameters R and s/a to describe the conditions of the experiment was recognized, and the calculation for small R using the Oseen approximation followed. The experiments describing the flows

for intermediate values of R were carried out to complete the picture.

It is hoped that this work has indicated the value of the parameters R and s/a in describing the interaction of an acoustic wave with an obstacle. The problem of the flow near a cylinder which is treated in this thesis is one of the simpler problems illustrating the principles involved. Perhaps the solutions for this example will be of use in a treatment of the interaction of an acoustic wave with an orifice, a sharp edged obstacle, or with the very fine fibers in absorbent materials.

In the following chapters the material outlined here will be examined in greater detail.

Chapter II

The Reynolds Number as an Important Parameter in Streaming Problems

It is ordinarily assumed that acoustic motion can be accurately described by the following equations of force and continuity.²⁷

$$\rho \left[\frac{\partial \bar{v}}{\partial t} + (\bar{v} \cdot \nabla) \bar{v} \right] = -\nabla p + \left[\mu' + \frac{4}{3}\mu \right] \nabla \nabla \cdot \bar{v} - \mu \nabla_x \nabla_x \bar{v} \quad (2.1)$$

and

$$\frac{\partial \rho}{\partial t} + \nabla \cdot \rho \bar{v} = 0 \quad (2.2)$$

where μ is the dynamic shear viscosity, μ' is the dynamic bulk viscosity, p is the pressure, ρ is the density and \bar{v} the particle velocity, which vanishes at all rigid boundaries. It has been assumed here that μ' and μ are constants of the fluid. Several authors have recently considered μ' and μ to have a density and/or time dependence in connection with determining how acoustic streaming would behave (hypothetically) under such circumstances,^{19, 21} but it is not the concern of this thesis to investigate these questions. We shall primarily be concerned with streaming produced by the interaction of sound waves with obstacles where the nonlinear and shear viscosity terms play the major role in determining the fluid motion.

Since these terms are present even for the case of an incompressible fluid, we may still expect that the equations obtained by setting ρ constant in (2.1) and (2.2) will give rise to streaming in the presence of a boundary. In fact time-independent streaming is observed for the case of periodic flow around obstacles in liquids as well as in gases.

If the wave length of the incident sound wave is very large compared with the size of the obstacle, compressibility can be neglected in the acoustic case. Putting ρ constant in (2.1) and (2.2) gives

$$\frac{\partial \bar{v}}{\partial t} + (\bar{v} \cdot \nabla) \bar{v} = - \frac{1}{\rho} \nabla p - v \nabla_x \nabla_x \bar{v} \quad (2.3)$$

$$\nabla \cdot \bar{v} = 0 \quad (2.4)$$

where $v = \frac{\mu}{\rho}$, and $\bar{v} = 0$ on any boundary surface.

These equations, while appearing somewhat simpler than (2.1) and (2.2) are still virtually impossible to solve exactly except in special cases. Of course the main mathematical difficulty lies in the fact that the equations are not linear. In several of the exact solutions to these equations the quadratic terms appearing on the left side of (2.3) are identically zero, viz., the case of Poiseuille flow (laminar) through a pipe or the flow between rotating cylinders. If the viscous term is neglected, the equations simplify greatly and describe the general theory of inviscid liquids. In the case of streaming near an obstacle it is

the combination of both the viscous and nonlinear terms which are important. Indeed Eckart¹¹ and Fox and Herzfeld¹⁵ have pointed out that both types of terms are essential to the production of steady flow.

In the remainder of this thesis let us think in particular of the streaming produced by the periodic oscillation of a liquid to and fro around a circular cylinder. Such a case has been the subject of a number of experiments, and is perhaps the most simple example to be treated theoretically.

Before examining equations (2.3) and (2.4) further, certain considerations of a more general nature should be made. These considerations will enable us to attack the equations with a greater sense of purpose and direction. Considered briefly the problem facing us is this. We have a cylinder of radius \underline{a} in a plane oscillatory field of angular frequency ω and velocity amplitude U_0 , and in a liquid whose kinematic viscosity coefficient is ν . It has been observed that a time-independent streaming exists under such circumstances, and in addition as pointed out in the introduction, the streaming flow pattern may have a different shape or direction of flow depending upon the value of U_0 , ω and \underline{a} .^{4,6,7} We want to determine theoretically how this can occur, and obtain analytical expressions describing the behavior of the streaming in terms of U_0 , ω and \underline{a} , and compare our results with experiment.

Dimensional analysis²⁴ furnishes us with information on how the parameters U_0 , ω and \underline{a} and ν must fit together in any

analytical description of the streaming, and also furnishes us with a method of attacking the problem systematically. Let us review this subject a bit.

Suppose that the streaming velocity at a point r/a and ϕ is denoted by q . Here r and ϕ are the usual cylindrical position coordinates, and r/a expresses the distance from the cylinder in dimensionless form. Thus we have quantities $q(r/a, \phi)$, U_0 , a , ω , and ν . The dimensions of these quantities are given in the following table.

$q(r/a, \phi)$	LT^{-1}
U_0	LT^{-1}
a	L
ω	T^{-1}
ν	L^2T^{-1}

We can thus construct three independent dimensionless parameters

$$\pi_1 = \frac{q}{U_0} \quad \pi_2 = \frac{U_0}{\omega a} \quad \pi_3 = \frac{U_0 a}{\nu}$$

The Buckingham Pi Theorem²⁴ tells us that a functional relationship exists between these parameters. Thus

$$F(\pi_1, \pi_2, \pi_3) = 0$$

or equivalently

$$\pi_1 = f(\pi_2, \pi_3)$$

Thus

$$q(r/a, \phi) = U_0 f(U_0/\omega a, U_0 a/v)$$

The streaming velocity, in dimensionless form, q/U_0 , can be written as a function of the two dimensionless parameters $\frac{U_0}{\omega a}$ and $\frac{U_0 a}{v}$. If we denote the particle oscillation amplitude by the letter s , and recognize $\frac{U_0 a}{v}$ as the usual Reynolds number R we can write

$$q(r/a, \phi) = U_0 f(s/a, R) \quad (2.5)$$

The construction of dimensionless parameters is not unique, and an infinite number of choices can be made. The present choice of R and s/a is especially convenient since these quantities are a measure of the relative importance of the terms in equation (2.3). Thus the nonlinear term $(\bar{v} \cdot \nabla) \bar{v}$ is of order $\frac{U_0^2}{a}$, the viscous term, $\frac{v U_0}{a^2}$, and the time derivative term of order ωU_0 . The ratio of the nonlinear term to the viscous term is thus of order $\frac{U_0^2 a^2}{a v U_0} = \frac{U_0 a}{v} = R$ while the ratio of the nonlinear term to the time derivative term is $\frac{U_0^2}{a \omega U_0} = \frac{s}{a}$.

What we can do with equations (2.3) and (2.4) now clearly depends upon the relative size of the terms in (2.3), that is upon the values of the parameters R and s/a . Since we have seen that the values of R and s/a determine the streaming velocity at any point, the conditions of any particular

experiment will specify the value of R and s/a , and assist us in deciding upon a theoretical approach to the problem.

As an example let us consider the experiments reported by Carrière, Schlichting, and Andrade.^{4,6,7} For the case reported by Carrière, $\omega = 2\pi 50$, $s = .4 \times 10^{-1}$ cm, $\underline{a} = 1.25 \times 10^{-1}$ cm and ν for air is $0.15 \text{ cm}^2/\text{sec}$. Thus $R = \frac{\omega s a}{\nu} \approx 10$. In the experiment of Schlichting, $\omega = 3.1$, $s = 0.19$ cm, $\underline{a} = 4$ cm, and $\nu = .0117 \text{ cm}^2/\text{sec}$ for water. Thus $R = \frac{\omega s a}{\nu} \approx 1000$. Andrade⁶ does not seem to specify the value of \underline{s} for the photographs shown in his article. For a numerical estimate let us take $s/a = .1$. He gives: $a = .24$ cm, $\omega = 4900$, $\nu = .15 \text{ cm}^2/\text{sec}$ and thus $R = \frac{a^2 \omega}{\nu} \frac{s}{a} \approx 200$ for this experiment.

Comparing the value of R in the experiment of Carrière with those reported for Andrade and Schlichting, it is not surprising that the observed streaming patterns are different. Fortunately equations (2.3) and (2.4) can be attacked and solved for the two limiting cases of very small and very large R , assuming that s/a is small. The flow observed by Carrière resembles the flow obtained from the solution for small R , while the flow observed by Schlichting can be obtained from the solution for large R . The appropriate mathematical theory for the two cases is contained in the so-called Oseen approximation for small R and in the Prandtl boundary layer theory for large R .

The Case for Small R

In two dimensions, and for rectangular coordinates (2.3) and (2.4) can be written

$$\frac{\partial u}{\partial t} + u \frac{\partial u}{\partial x} + v \frac{\partial u}{\partial y} = - \frac{1}{\rho} \frac{\partial p}{\partial x} + \nu \nabla^2 u \quad (2.6)$$

$$\frac{\partial v}{\partial t} + u \frac{\partial v}{\partial x} + v \frac{\partial v}{\partial y} = - \frac{1}{\rho} \frac{\partial p}{\partial y} + \nu \nabla^2 v$$

$$\frac{\partial u}{\partial x} + \frac{\partial v}{\partial y} = 0$$

where u and v are the components of velocity in the x and y directions respectively. The components u and v both vanish on the rigid boundary surfaces. Since for small R the nonlinear terms are small compared with the viscous terms it may be expected that the nonlinear terms can be partially neglected in this case. In the absence of any obstacles we would have a uniform flow field. This uniform field is perturbed by the obstacle, and the perturbation effects decrease as the distance from the obstacle is increased. The expression for velocity can be split into two parts by writing

$$\begin{aligned} u &= U(t) + u' \\ v &= v' \end{aligned} \quad (2.7)$$

where the primed quantities represent the perturbing field, and the $U(t)$ is the original uniform velocity field. If the expressions (2.7) are substituted into (2.6) one obtains

$$\frac{\partial U}{\partial t} + \frac{\partial u'}{\partial t} + U \frac{\partial u'}{\partial x} + u' \frac{\partial u'}{\partial x} + v' \frac{\partial u'}{\partial y} = - \frac{1}{\rho} \frac{\partial p}{\partial x} + \nu \nabla^2 u' \quad (2.8)$$

$$\frac{\partial v'}{\partial t} + U \frac{\partial v'}{\partial x} + u' \frac{\partial v'}{\partial x} + v' \frac{\partial v'}{\partial y} = - \frac{1}{\rho} \frac{\partial p}{\partial y} + \nu \nabla^2 v'$$

$$\text{and } \frac{\partial u'}{\partial x} + \frac{\partial v'}{\partial y} = 0$$

The Oseen approximation consists in neglecting the nonlinear product terms in the primed quantities compared with the viscous primed terms. This is valid if R , which represents the relative magnitude of the terms, is small.

The linearized equations are

$$\frac{\partial U}{\partial t} + \frac{\partial u'}{\partial t} + U \frac{\partial u'}{\partial x} = - \frac{1}{\rho} \frac{\partial p}{\partial x} + \nu \nabla^2 u' \quad (2.9)$$

$$\frac{\partial v'}{\partial t} + U \frac{\partial v'}{\partial x} = - \frac{1}{\rho} \frac{\partial p}{\partial y} + \nu \nabla^2 v'$$

$$\text{and } \frac{\partial u'}{\partial x} + \frac{\partial v'}{\partial y} = 0$$

where $u' + U = 0$ and $v' = 0$ at the boundary surfaces. These equations will be solved for the case of the circular cylinder in an oscillating field, where $U(t) = U_0 \cos \omega t$.

The Case for Large R

When R is large the inertial terms and the viscous terms are of the same order of magnitude. The few exact solutions for such a case seem to agree with what is usually observed, in that the velocity of the fluid motion at high Reynolds

numbers changes rapidly from its zero value at a solid wall to its value in the main body of fluid. Even when the viscosity of the fluid is low, the very rapid change in the space derivatives of the velocity in the transition region will give rise to viscous terms of magnitude comparable to that of the inertial terms. Thus for a description of the flow past obstacles at large Reynolds numbers, it is appropriate to look to the equations governing the fluid in a layer in the immediate neighborhood of the body.

Prandtl²⁶ in 1904 first suggested examining this "boundary layer" and developed the equations of motion of the fluid in this layer. These equations are ordinarily developed by considering equations (2.6) and realizing that within the boundary layer the terms involving derivatives with respect to the direction normal to the boundary will be much larger than derivatives in the direction along the boundary.

Starting with equations (2.6) we take x along the boundary and y normal to it. The velocities u and v vanish at $y = 0$. The symbol δ is taken to represent the thickness of the boundary layer, i.e., the extent of the region in which the inertial and viscous terms are of the same order. In this distance δ the velocity changes from its midstream value $U(t)$ to zero. Thus considering U of the order of unity and δ small, $\frac{\partial u}{\partial y} \sim \delta^{-1}$, $\frac{\partial^2 u}{\partial y^2} \sim \delta^{-2}$ in the boundary layer. u , $\frac{\partial u}{\partial x}$, $\frac{\partial u}{\partial t}$, $\frac{\partial^2 u}{\partial x^2}$ are all considered to be of order unity. The continuity

equation says that $\frac{\partial v}{\partial y} \sim 1$ and hence $v \sim \delta$. Hence, $\frac{\partial v}{\partial t}$, $\frac{\partial v}{\partial x}$, $\frac{\partial^2 v}{\partial x^2}$ are of order δ and $\frac{\partial^2 v}{\partial y^2} \sim \delta^{-1}$. Now if equations (2.6) are examined and all terms of order δ and δ^2 are discarded, the first equation becomes:

$$\frac{\partial u}{\partial t} + u \frac{\partial u}{\partial x} + v \frac{\partial u}{\partial y} = - \frac{1}{\rho} \frac{\partial p}{\partial x} + \nu \frac{\partial^2 u}{\partial y^2} \quad (2.10a)$$

The second gives

$$- \frac{1}{\rho} \frac{\partial p}{\partial y} \approx 0 \quad (2.10b)$$

and finally

$$\frac{\partial u}{\partial x} + \frac{\partial v}{\partial y} = 0 \quad (2.10c)$$

Thus in order that the inertial terms and viscous terms are of the same order we must have $\nu \delta^{-2} \sim 1$ or $\delta \sim \nu^{1/2}$. The equation (2.10b) says that the total pressure change through the boundary layer is of order δ^2 . Thus the pressure gradient $-\frac{1}{\rho} \frac{\partial p}{\partial x}$ can be regarded as having the same value within the boundary layer as outside. The limiting form of (2.10a) in midstream gives

$$- \frac{1}{\rho} \frac{\partial p}{\partial x} = \frac{\partial U}{\partial t} + U \frac{\partial U}{\partial x} \quad (2.11)$$

A non-dimensional derivation of these equations points more clearly to their connection with large values of R . We shall follow a development given by Goldstein.²⁵

Taking U_0 as a typical velocity, d a typical length and $R = \frac{U_0 d}{\nu}$, the expression arrived at earlier stating that $\delta \sim \nu^{1/2}$ can be expressed non-dimensionally as $\frac{\delta}{d} \sim R^{-1/2}$. Thus as R increases the thickness of the boundary layer decreases. In order to get a true representation of what happens in the boundary layer as $R \rightarrow \infty$, it is necessary to multiply the scale of distances normal to the wall by $R^{1/2}$ so that the region we are examining does not vanish in this limit. Similarly, we multiply the normal velocity by $R^{1/2}$. This leads us to write:

$$x' = \frac{x}{d}; \quad y' = R^{1/2} \frac{y}{d}; \quad u' = \frac{u}{U_0}; \quad v' = R^{1/2} \frac{v}{U_0}$$

$$t' = t \frac{U_0}{d}; \quad p' = \frac{p}{\rho U_0^2}$$

If these are substituted into (2.6) the equations become

$$\frac{\partial u'}{\partial t'} + u' \frac{\partial u'}{\partial x'} + v' \frac{\partial u'}{\partial y'} = -\frac{\partial p'}{\partial x'} + \frac{1}{R} \frac{\partial^2 u'}{\partial x'^2} + \frac{\partial^2 u'}{\partial y'^2}$$

$$\frac{1}{R} \left[\frac{\partial v'}{\partial t'} + u' \frac{\partial v'}{\partial x'} + v' \frac{\partial v'}{\partial y'} \right] = -\frac{\partial p'}{\partial y'} + \frac{1}{R^2} \frac{\partial^2 v'}{\partial x'^2} + \frac{1}{R} \frac{\partial^2 v'}{\partial y'^2}$$

$$\frac{\partial u'}{\partial x'} + \frac{\partial v'}{\partial y'} = 0$$

Assuming that the derivatives appearing here remain finite as R the limiting form of the equations is as $R \rightarrow \infty$,

$$\frac{\partial u'}{\partial t'} + u' \frac{\partial u'}{\partial x'} + v' \frac{\partial u'}{\partial y'} = - \frac{\partial p'}{\partial x'} + \frac{\partial^2 u'}{\partial y'^2}$$

$$0 = - \frac{\partial p'}{\partial y'} \quad (2.12)$$

$$\frac{\partial u'}{\partial x'} + \frac{\partial v'}{\partial y'} = 0$$

which are the non-dimensional forms of equations (2.10).

Strictly speaking the application of these boundary layer equations does not require the presence of a wall. The conditions for application are, expressed non-dimensionally, that u/U_0 change rapidly from one finite value to another over a length normal to the basic streamline, of order $R^{-1/2}d$, while changes in the direction of the streamline are not rapid, i.e., $\frac{d}{U_0} \frac{\partial u}{\partial x}$, etc. are of order $\frac{u}{U_0}$. Wherever the curvature of the basic streamline or the rate of change of that curvature becomes infinite the equations are no longer valid.

From the preceding discussion and review we can make several conclusions. We expect the boundary layer theory to give us information in our problem of flow around a cylinder when R is large. When R is small we expect the motion in this problem to be determined by the equations obtained through the use of the Oseen approximation (equation 2.9). At the present time there is no formal mathematical means by which the problem for intermediate values of R may be attacked. For that reason, a portion of this thesis is

devoted to observing experimentally what happens in this range as a function of the parameters s/a and R . It is important to determine the ranges over which the analytical solutions for the extreme limits of R might be useful. The transition between the two types of solution is also observed experimentally, and seems to be related to the relative stability of the two types of flow.

Chapter III

The Calculation for the Case of Large Reynolds Numbers

Starting with the Navier-Stokes equations for an incompressible viscous fluid in two dimensions and the equation of continuity, we have seen that it is possible to obtain the Prandtl boundary layer equations which give a valid description of the fluid motion near a rigid boundary for the case of flow at high Reynolds numbers. The boundary layer equations are

$$\frac{\partial u}{\partial t} + u \frac{\partial u}{\partial x} + v \frac{\partial u}{\partial y} = - \frac{1}{\rho} \frac{\partial p}{\partial x} + \nu \frac{\partial^2 u}{\partial y^2} \quad (3.1)$$

$$\frac{\partial u}{\partial x} + \frac{\partial v}{\partial y} = 0 \quad (3.2)$$

where u and v are the x and y components of velocity, respectively. The boundary conditions are $u = v = 0$ at $y = 0$; $u = U(x,t)$ at $y = \infty$. The kinematic viscosity coefficient is ν , and p and ρ are the pressure and density. The coordinate x is measured along the boundary and y in the direction normal to the boundary. The function $U(x,t)$ represents the "outside" stream velocity. We recall that the derivation of these equations assumes that the boundary layer or transition region near the wall in which the stream velocity goes from free stream value to zero, has a thickness small compared to a characteristic length of the boundary. In addition

equation (3.1) is valid as long as the rate of change of the radius of curvature along the boundary is small.

The term $-\frac{1}{\rho} \frac{\partial p}{\partial x}$ has been shown to be equivalent to

$$-\frac{1}{\rho} \frac{\partial p}{\partial x} = \frac{\partial U}{\partial t} + U \frac{\partial U}{\partial x} \quad (3.3)$$

since to the order of approximation in deriving (3.1), $-\frac{1}{\rho} \frac{\partial p}{\partial x}$ in the boundary layer is the same as in the outside stream. Equation (3.3) can be looked upon as the limiting form of (3.1) as one moves away from the boundary. The equations governing motion in the boundary layer are thus

$$\frac{\partial u}{\partial t} + u \frac{\partial u}{\partial x} + v \frac{\partial u}{\partial y} = \frac{\partial U}{\partial t} + U \frac{\partial U}{\partial x} + v \frac{\partial^2 u}{\partial y^2} \quad (3.4)$$

$$\frac{\partial u}{\partial x} + \frac{\partial v}{\partial y} = 0$$

with the boundary conditions $u = v = 0$ at $y = 0$; $u = U(x, t)$ at $y = \infty$.

It has been mentioned in the first chapter that Schlichting⁷ has used these boundary layer equations to calculate the steady flow near a cylinder for the case corresponding to large R , and has compared his results with experiment. ($R \sim 1000$.) Schlichting's calculation is based on a perturbation approach and considers terms to second order. In this thesis the calculation is extended to terms in fourth order and an expression for the steady flow stream function

is obtained which shows a change in the flow pattern with the parameter s/a .

Schlichting's Treatment

In treating the problem of oscillating flow along a boundary, Schlichting assumes that the outside flow can be represented by $U(x,t) = U_0(x)\cos\omega t$. The perturbation procedure is carried out by assuming that u and v can be expanded in a power series in the parameter ϵ . The first, second, etc., powers of ϵ correspond to the first, second, etc., orders of the perturbation calculation. Thus the expressions $u = \epsilon u_1 + \epsilon^2 u_2 \dots$; $v = \epsilon v_1 + \epsilon^2 v_2 \dots$ are put into equations (3.4) and the resulting expressions are separated according to powers of ϵ . The ϵ , having served the purpose of separating the various order terms, is finally set equal to unity. Following this procedure and assuming that $\frac{\partial U}{\partial t}$ is of first order while $U \frac{\partial U}{\partial x}$ is of second order, Schlichting obtained the following equations.

$$\frac{\partial u_1}{\partial t} - \nu \frac{\partial^2 u_1}{\partial y^2} = \frac{\partial U}{\partial t} = -\omega U_0(x)\sin\omega t; \quad \frac{\partial u_1}{\partial x} + \frac{\partial v_1}{\partial y} = 0 \quad (3.5)$$

$$\begin{aligned} \frac{\partial u_2}{\partial t} - \nu \frac{\partial^2 u_2}{\partial y^2} &= U \frac{\partial U}{\partial x} - (u_1 \frac{\partial u_1}{\partial x} + v_1 \frac{\partial u_1}{\partial y}) \\ &= \frac{1}{2} U_0(x) \frac{dU_0}{dx} (1 + \cos 2\omega t) - (u_1 \frac{\partial u_1}{\partial x} + v_1 \frac{\partial u_1}{\partial y}) \end{aligned} \quad (3.6)$$

$$\frac{\partial u_2}{\partial x} + \frac{\partial v_2}{\partial y} = 0$$

The solution to second order is then $u = u_1 + u_2$, $v = v_1 + v_2$. The boundary conditions for equations (3.5) and (3.6) are $u_1 = v_1 = 0$ at $y = 0$, and $u_1 = \overset{U(x,t)}{U_0(x)}$ at $y = \infty$; $u_2 = v_2 = 0$ at $y = 0$ and u_2 is finite at $y = \infty$. The imposition of boundary conditions at $y = \infty$ is a mathematical simplification of the physical picture in which the velocities approach "outside" stream values away from the boundary. Since the velocity expressions consist of constant terms plus terms in y which decrease very rapidly as y increases, this is a valid simplification.

In solving the equations it is convenient to introduce the variable $\eta = y \sqrt{\frac{\omega}{\nu}}$ where the quantity $\sqrt{\frac{\nu}{\omega}} = \delta$ is usually considered to be a rough measure of the boundary layer thickness. Since equations (3.5) and (3.6) are linear, the principle of superposition may be used, and it is convenient to write the time variation as the real part of an exponential, i.e., $e^{i\omega t}$ for example. However, only real expressions can be used in calculating the nonlinear inhomogeneous terms for the next step.

The solutions to (3.5) and (3.6) are in appendix 1. The solutions u_1 and v_1 to (3.5) are periodic with frequency ω . The solutions u_2 and v_2 to (3.6) have a D.C. part and a periodic part of frequency 2ω . The steady part of the solution u_2 approaches a constant value as $y \rightarrow \infty$. This limiting value $u_2(x, \infty, t)$ is $-\frac{3}{4\omega} U_0 \frac{dU_0}{dx}$ which Schlichting interprets as the steady velocity of the circulating fluid just outside

the boundary layer. At points where $u_{2st} = 0$, i.e., $U_o \frac{dU_o}{dx} = 0$, the flow becomes normal to the boundary. The physical extent of the circulations at least along the boundary is thus determined by his result.

The steady portions of u_2 and v_2 represented in terms of a steady stream function are

$$\begin{aligned} \psi_{2st} &= \sqrt{\frac{v}{\omega}} \cdot \frac{1}{\omega} U_o \frac{dU_o}{dx} \int_{2b}(\eta) \\ u_{2st} &= \frac{\partial \psi_{2st}}{\partial y} = \frac{1}{\omega} U_o \frac{dU_o}{dx} \int_{2b}'(\eta) \\ v_{2st} &= -\frac{\partial \psi_{2st}}{\partial x} = -\sqrt{\frac{v}{\omega}} \cdot \frac{1}{\omega} \left[U_o \frac{d^2 U_o}{dx^2} + \left(\frac{dU_o}{dx} \right)^2 \right] \int_{2b}(\eta) \end{aligned} \quad (3.7)$$

The functions \int_{2b}' and \int_{2b} are plotted as functions of η in figure 1.

The Higher Order Terms

In proceeding to a calculation of higher order terms we shall write $U(x,t) = A_2(x) + A_4(x) + U_o \cos \omega t$, that is, include a time-independent part in the "outside" velocity. We shall assume that $A_2(x)$ is of second order and $A_4(x)$ of fourth order, while $U_o(x)$ is of first order. The expression for $\frac{\partial U}{\partial t}$ is the same as before. $\frac{\partial U}{\partial t} = -\omega U_o \sin \omega t$. The expression for $U \frac{\partial U}{\partial x}$ is modified by the inclusion of the terms $A_2(x)$ and $A_4(x)$.

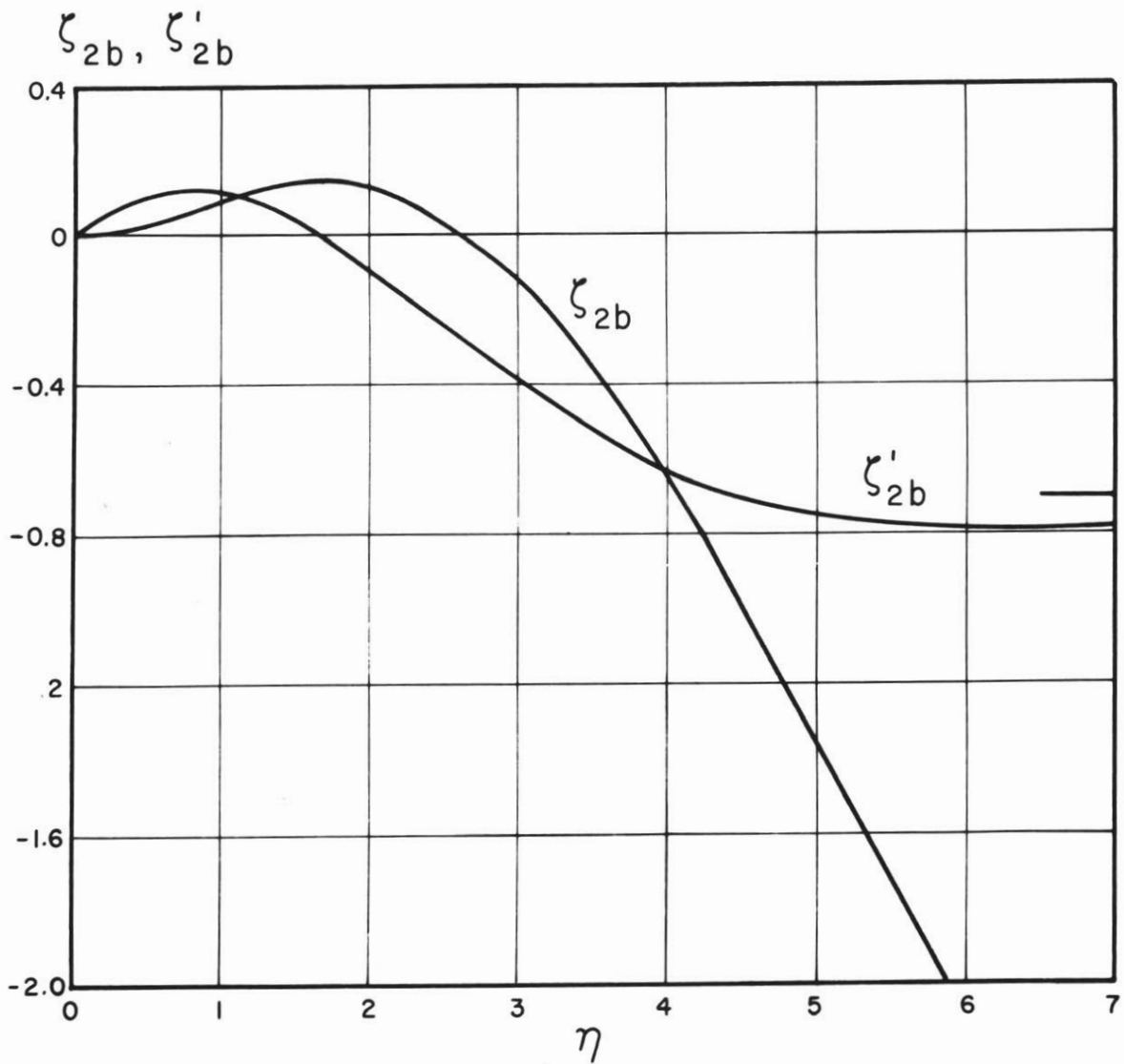


Figure 1 : The functions ζ_{2b}, ζ'_{2b} which appear in the time independent second order solution to the boundary layer equations, plotted as a function of $\eta = y/\delta$. (See equations 3.7)

$$U \frac{\partial U}{\partial x} = \frac{1}{2} U_0 \frac{dU_0}{dx} (1 + \cos 2\omega t) + \left(\frac{dA_2}{dx} U_0 + A_2 \frac{dU_0}{dx} \right) \cos \omega t + A_2 \frac{dA_2}{dx}$$

+ (cross products of fifth, sixth, and eighth order)

Since $A_2(x) \sim \epsilon^2$ and $A_2 \frac{dA_2}{dx} \sim \epsilon^4$, a separation according to powers of ϵ gives for the equations governing the first four orders of magnitude:

$$\frac{\partial u_1}{\partial t} - v \frac{\partial^2 u_1}{\partial y^2} = \frac{\partial U}{\partial t} = -\omega U_0 \sin \omega t \quad \frac{\partial u_1}{\partial x} + \frac{\partial v_1}{\partial y} = 0 \quad (3.8)$$

$$\frac{\partial u_2}{\partial t} - v \frac{\partial^2 u_2}{\partial y^2} = \frac{1}{2} U_0 \frac{dU_0}{dx} (1 + \cos 2\omega t) - \left(u_1 \frac{\partial u_1}{\partial x} + v_1 \frac{\partial v_1}{\partial y} \right) \quad (3.9)$$

$$\frac{\partial u_2}{\partial x} + \frac{\partial v_2}{\partial y} = 0$$

$$\begin{aligned} \frac{\partial u_3}{\partial t} - v \frac{\partial^2 u_3}{\partial y^2} &= \left(U_0 \frac{dA_2}{dx} + A_2 \frac{dU_0}{dx} \right) \cos \omega t \\ &\quad - \left(u_1 \frac{\partial u_2}{\partial x} + v_1 \frac{\partial u_2}{\partial y} + u_2 \frac{\partial u_1}{\partial x} + v_2 \frac{\partial u_1}{\partial y} \right) \end{aligned} \quad (3.10)$$

$$\frac{\partial u_3}{\partial x} + \frac{\partial v_3}{\partial y} = 0$$

$$\begin{aligned} \frac{\partial u_4}{\partial t} - v \frac{\partial^2 u_4}{\partial y^2} &= A_2 \frac{dA_2}{dx} - \left[u_1 \frac{\partial u_3}{\partial x} + u_2 \frac{\partial u_2}{\partial x} + u_3 \frac{\partial u_1}{\partial x} \right. \\ &\quad \left. + v_1 \frac{\partial u_3}{\partial y} + v_2 \frac{\partial u_2}{\partial y} + v_3 \frac{\partial u_1}{\partial y} \right] \end{aligned} \quad (3.11)$$

$$\frac{\partial u_4}{\partial x} + \frac{\partial v_4}{\partial y} = 0$$

The complete solution to fourth order is

$$u = u_1 + u_2 + u_3 + u_4$$

$$v = v_1 + v_2 + v_3 + v_4$$

The boundary conditions can also be separated according to powers of ϵ . The condition $u = v = 0$ at $y = 0$ gives $u_1, u_2, u_3, u_4, v_1, v_2, v_3, v_4$ all equal to zero at $y = 0$ ($\eta = 0$). At $y = \infty$ the functions u_1, u_2, u_3, u_4 must remain finite, and in addition $u_1 = U_0 \cos \omega t$, $u_2 = A_2(x)$, $u_4 = A_4(x)$. The solutions to (3.8) and (3.9) are the same as in the Schlichting case. The condition that $u_2 = A_2(x)$ at $y = \infty$ determines $A_2(x) = -\frac{3}{4\omega} U_0 \frac{dU_0}{dx}$ and this is put into equations (3.10) and (3.11).

Logically it seems that Schlichting should have included the $A_2(x)$ in the "outside" stream velocity. We have seen from (3.8) and (3.9) that his equations (3.5) and (3.6) for u_1, u_2, v_1, v_2 would have been unchanged. The steady portion of u_2 remaining finite at $y = \infty$ would not have been left dangling, but would have been fitted into the scheme of boundary conditions in a self-consistent manner as with $A_2(x)$ and $A_4(x)$ here.

In calculating the higher order terms it is necessary to assume the $A(x)$ terms in the "outside" velocity in order to obtain a solution. Had we not included these terms, the term $A_2 \frac{dA_2}{dx}$ in (3.11) would be absent, and the term $u_2 \frac{\partial u_2}{\partial x}$ on

the right-hand side of (3.11) which has a constant part would cause difficulty. The $A_2 \frac{dA_2}{dx}$ just cancels this constant term which upon integration would have given a component for u_4 which approached infinity as y^2 .

Since we are only interested in the time-independent part of u_4 , the work can be simplified. One may note from the expressions for u_1, u_2, v_1, v_2 in appendix 1 that the solution for u_3, v_3 in (3.10) will have no D.C. component. The solution to (3.11) will have a D.C. component obtainable from the time-independent portion of (3.11). The functions u_3, v_3 will have terms in ω and 3ω . However, the ω terms are the only ones contributing to the steady part of u_4 , and it is thus only necessary to obtain the ω components of u_3, v_3 .

The results of the calculation for the "fundamental" terms for u_3 and v_3 are given by:

$$\begin{aligned} \psi_{3(\omega)} = & -\sqrt{\frac{v}{\omega}} \frac{1}{2\omega^2} \text{R.P.} \left[U_0^2 \frac{d^2 U_0}{dx^2} \int_{3a}(\eta) e^{i\omega t} \right. \\ & \left. + U_0 \left(\frac{dU_0}{dx} \right)^2 \int_{3b}(\eta) e^{i\omega t} \right] \\ u_{3(\omega)} = & \text{R.P.} \left[-\frac{1}{2\omega^2} U_0^2 \frac{d^2 U_0}{dx^2} \int_{3a}'(\eta) e^{i\omega t} \right. \\ & \left. - \frac{1}{2\omega^2} U_0 \left(\frac{dU_0}{dx} \right)^2 \int_{3b}'(\eta) e^{i\omega t} \right] \end{aligned} \quad (3.12)$$

and

$$\begin{aligned}
 v_3(\omega) = \text{R.P.} \left\{ \sqrt{\frac{v}{\omega}} \frac{1}{2\omega^2} \left[U_0^2 \frac{d^3 U_0}{dx^3} + 2U_0 \frac{dU_0}{dx} \frac{d^2 U_0}{dx^2} \right] \int_{3a}(\eta) e^{i\omega t} + \right. \\
 \left. + \sqrt{\frac{v}{\omega}} \frac{1}{2\omega^2} \left[2U_0 \frac{dU_0}{dx} \frac{d^2 U_0}{dx^2} + \left(\frac{dU_0}{dx} \right)^3 \right] \int_{3b}(\eta) e^{i\omega t} \right\} \quad (3.13)
 \end{aligned}$$

where \int_{3a} , \int_{3b} , \int_{3a} , \int_{3b} are given in appendix 1.

The equation for the time-independent part of u_4 can be written:

$$\begin{aligned}
 -v \frac{\partial^2 u_4}{\partial y^2} = A_2 \frac{dA_2}{dx} - \overline{(u_1 \frac{\partial u_3}{\partial x} + u_2 \frac{\partial u_2}{\partial x} + u_3 \frac{\partial u_1}{\partial x})}^t \\
 - \overline{(v_1 \frac{\partial u_3}{\partial y} + v_2 \frac{\partial u_2}{\partial y} + v_3 \frac{\partial u_1}{\partial y})}^t \quad (3.14)
 \end{aligned}$$

The solution is:

$$\begin{aligned}
 u_{4st} = -\frac{1}{4\omega^3} \left[U_0^3 \frac{d^3 U_0}{dx^3} \int_{4a}(\eta) + U_0 \left(\frac{dU_0}{dx} \right)^3 \int_{4b}(\eta) \right. \\
 \left. + U_0^2 \frac{dU_0}{dx} \frac{d^2 U_0}{dx^2} \int_{4c}(\eta) \right] \quad (3.15)
 \end{aligned}$$

From the equation of continuity, we can introduce the stream function

$$\begin{aligned}
 \psi_{4st} = -\sqrt{\frac{v}{\omega}} \frac{1}{4\omega^3} \left[U_0^3 \frac{d^3 U_0}{dx^3} \int_{4a}(\eta) + U_0 \left(\frac{dU_0}{dx} \right)^3 \int_{4b}(\eta) + \right. \\
 \left. U_0^2 \frac{dU_0}{dx} \frac{d^2 U_0}{dx^2} \int_{4c}(\eta) \right] \quad (3.16)
 \end{aligned}$$

where:

$$v_4 = -\frac{\partial \psi_{4st}}{\partial x} \quad u_4 = \frac{\partial \psi_{4st}}{\partial y}$$

The expressions ψ'_{4a} , ψ'_{4b} , ψ'_{4c} , ψ_{4a} , ψ_{4b} , ψ_{4c} are given in appendix 1. In the limit of large distances from the boundary the functions ψ'_{4a} , ψ'_{4b} , ψ'_{4c} approach constant values

$$\psi'_{4a}(\infty) = \frac{17,839}{12,000} + \frac{1}{8\sqrt{2}} = 1.58$$

$$\psi'_{4b}(\infty) = -\frac{69,367}{3,000} - \frac{74,161}{23,000\sqrt{2}} = -25.4$$

$$\psi'_{4c}(\infty) = -\frac{1,280,027}{36,000} - \frac{236,121}{27,000\sqrt{2}} = -41.5$$

The functions ψ'_{4a} , ψ'_{4b} , ψ'_{4c} , ψ_{4a} , ψ_{4b} , ψ_{4c} are plotted in figures 2, 3, and 4.

The complete time-independent solution including both the second order and fourth order terms is thus

$$\psi_{st} = \sqrt{\frac{v}{\omega}} \frac{1}{\omega} \left\{ U_0 \frac{dU_0}{dx} \psi_{2b}(\eta) - \frac{1}{4\omega^2} \left[U_0^3 \frac{d^3 U_0}{dx^3} \psi_{4a}(\eta) + U_0 \left(\frac{dU_0}{dx} \right)^3 \psi_{4b}(\eta) + U_0^2 \frac{dU_0}{dx} \frac{d^2 U_0}{dx^2} \psi_{4c}(\eta) \right] \right\} \quad (3.17)$$

$$u_{st} = \frac{\partial \psi_{st}}{\partial y} = \frac{1}{\omega} \left\{ U_0 \frac{dU_0}{dx} \psi'_{2b}(\eta) - \frac{1}{4\omega^2} \left[U_0^3 \frac{d^3 U_0}{dx^3} \psi'_{4a} + U_0 \left(\frac{dU_0}{dx} \right)^2 \psi'_{4b} + U_0 \frac{dU_0}{dx} \frac{d^2 U_0}{dx^2} \psi'_{4c}(\eta) \right] \right\} \quad (3.18)$$

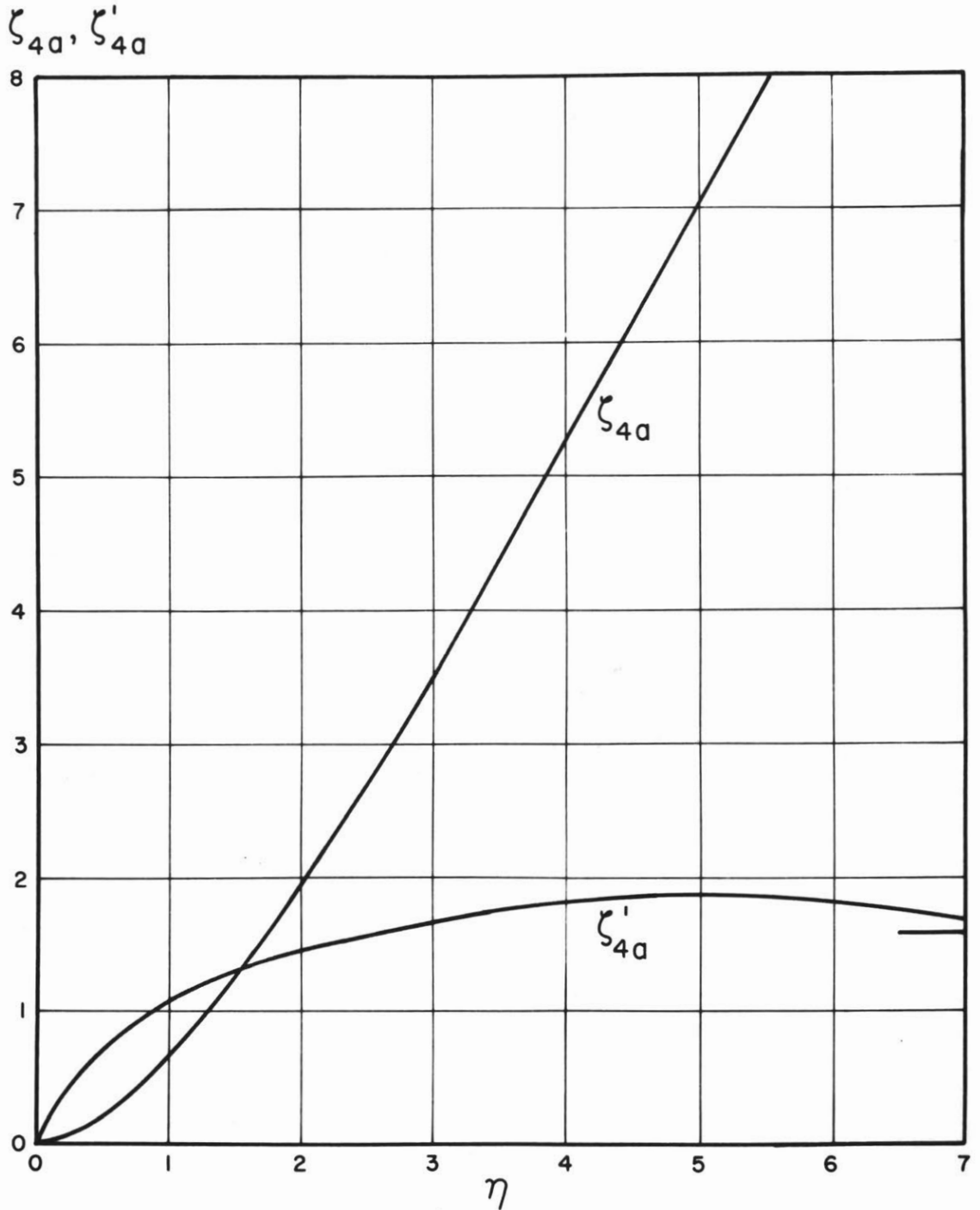


Figure 2: The functions ζ_{4a}, ζ'_{4a} which appear in the time independent fourth order solution to the boundary layer equations, plotted as a function of $\eta = y/\delta$.

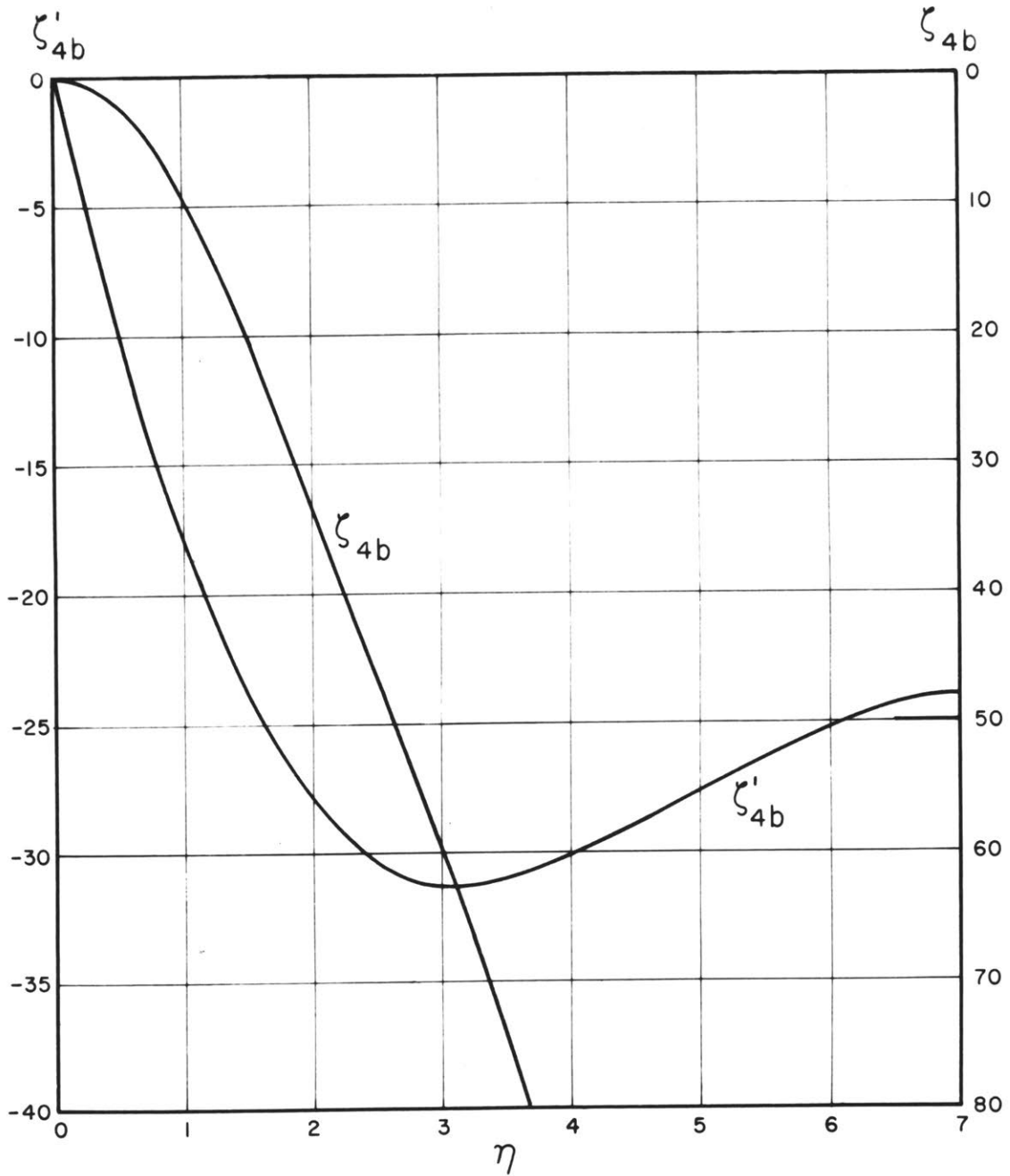


Figure 3: The functions ζ_{4b}, ζ'_{4b} which appear in the time independent fourth order solution to the boundary layer equations, plotted as a function of $\eta = y/\delta$.

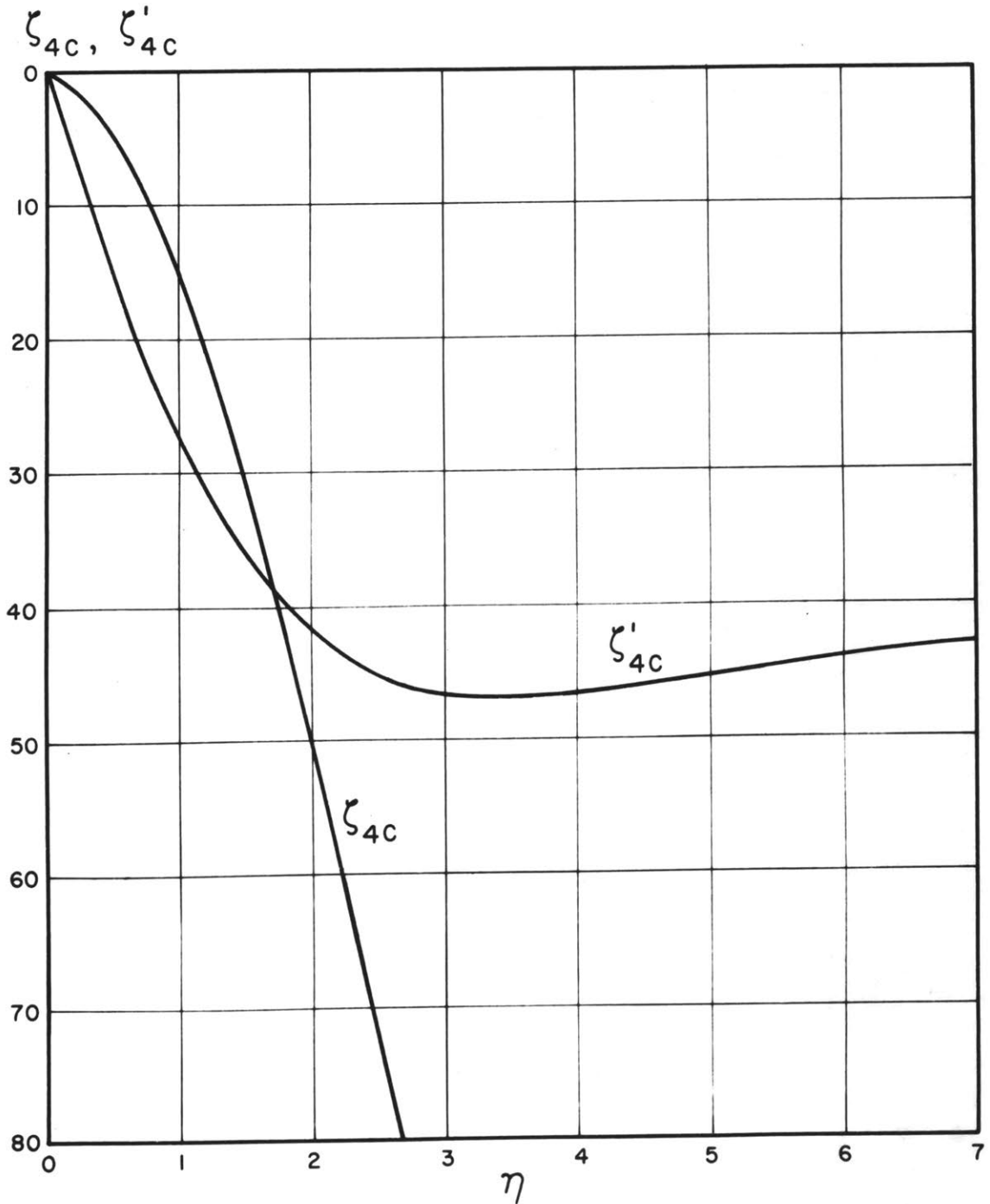


Figure 4: The functions ζ_{4c}, ζ'_{4c} which appear in the time independent fourth order solution to the boundary layer equations, plotted as a function of $\eta = y/\delta$.

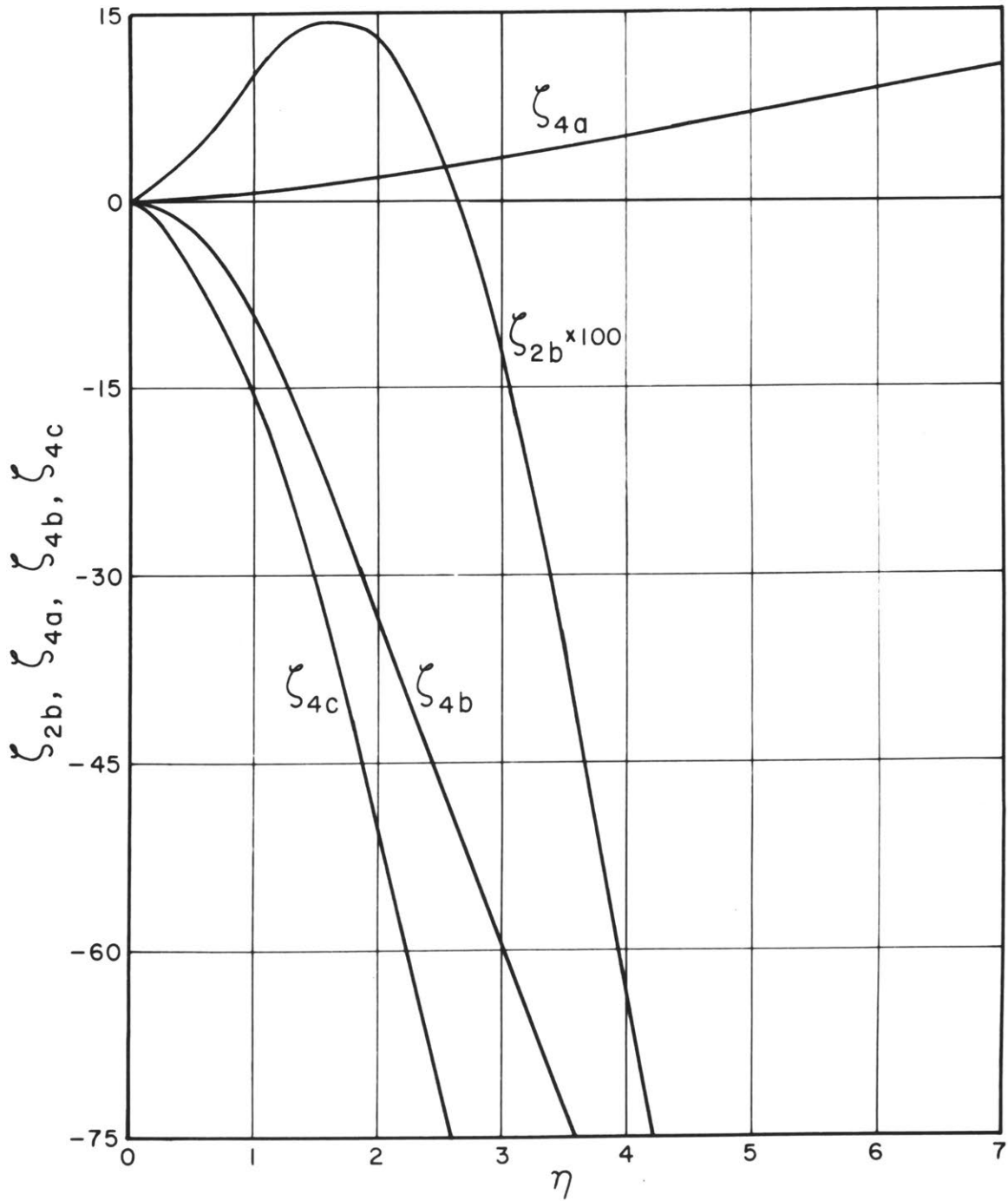


Figure 5: The functions $\zeta_{2b}, \zeta_{4a}, \zeta_{4b}, \zeta_{4c}$ which appear in the complete time independent stream function. (See equation 3.17)

$$\begin{aligned}
 V_{st} = -\frac{\partial \psi_{st}}{\partial x} = & -\sqrt{\frac{\nu}{\omega}} \cdot \frac{1}{\omega} \left\{ \left[U_0 \frac{d^2 U_0}{dx^2} + \left(\frac{dU_0}{dx} \right)^2 \right] \int_{2b}(\eta) \right. \\
 & - \frac{1}{4\omega^2} \left[\left(U_0 \frac{d^4 U_0}{dx^4} + 3U_0^2 \frac{dU_0}{dx} \frac{d^3 U_0}{dx^3} \right) \int_{4a}(\eta) \right. \\
 & + \left. \left. \left(3U_0 \left(\frac{dU_0}{dx} \right)^2 \frac{d^2 U_0}{dx^2} + \left(\frac{dU_0}{dx} \right)^4 \right) \int_{4b}(\eta) \right. \right. \\
 & \left. \left. + \left(U_0^2 \frac{dU_0}{dx} \frac{d^3 U_0}{dx^3} + U_0^2 \left(\frac{d^2 U_0}{dx^2} \right)^2 + 2U_0 \left(\frac{dU_0}{dx} \right)^2 \frac{d^2 U_0}{dx^2} \right) \int_{4c}(\eta) \right] \right\} \quad (3.19)
 \end{aligned}$$

The functions \int_{2b} , \int_{4a} , \int_{4b} , \int_{4c} appearing in (3.17) are plotted together in figure 5.

For the example in which we are primarily interested, i.e., the case of oscillating flow around a circular cylinder, the function $U(x,t) = 2U_0 \sin \frac{x}{a} \cos \omega t$. Thus $U_0(x) = 2U_0 \sin \frac{x}{a} = 2U_0 \sin \phi$ where x is measured along the boundary from a stagnation point. In this case

$$\frac{dU_0}{dx} = \frac{2U_0}{a} \cos \frac{x}{a} = \frac{2U_0}{a} \cos \phi \quad \frac{d^2 U_0}{dx^2} = -\frac{2U_0}{a^2} \sin \phi$$

$$\frac{d^3 U_0}{dx^3} = -\frac{2U_0}{a^3} \cos \phi \quad \frac{d^4 U_0}{dx^4} = +\frac{2U_0}{a^4} \sin \phi$$

The expressions for the stream function and the velocity components become:

$$\psi_{st} = \sqrt{\frac{\nu}{\omega}} \cdot \frac{2U_o^2}{\omega a} \cdot \sin 2\phi \left\{ \int_{2b}(\eta) + \left(\frac{s}{a}\right)^2 \cdot \left[(\int_{4a} + \int_{4c}) \sin^2 \phi - \int_{4b} \cos^2 \phi \right] \right\} \quad (3.20)$$

$$u_{st} = \frac{2U_o^2}{\omega a} \sin 2\phi \left\{ \int'_{2b}(\eta) + \left(\frac{s}{a}\right)^2 \cdot \left[(\int'_{4a} + \int'_{4c}) \sin^2 \phi - \int'_{4b} \cos^2 \phi \right] \right\}$$

$$v_{st} = -\sqrt{\frac{\nu}{\omega}} \frac{4U_o^2}{\omega a^2} \cos 2\phi \left\{ \int_{2b}(\eta) - \left(\frac{s}{a}\right)^2 \left[(\int_{4a} + \int_{4c}) \sin^4 \phi + \int_{4b} \cos^4 \phi - 3(\int_{4a} + \int_{4b} + \int_{4c}) \sin^2 \phi \cos^2 \phi \right] \right\}$$

The expression for the stream function can be written in terms of dimensionless quantities as:

$$\psi_{st} = \frac{2U_o^2}{\omega} \sin 2\phi \cdot \left(\frac{1}{a/\delta}\right) \left\{ \int_{2b}\left(\frac{y}{a} \cdot \frac{a}{\delta}\right) + \left(\frac{s}{a}\right)^2 \cdot \left[(\int_{4a} + \int_{4c}) \sin^2 \phi - \int_{4b} \cos^2 \phi \right] \right\} \quad (3.21)$$

$$\delta = \sqrt{\frac{\nu}{\omega}}$$

When the fourth order terms are neglected, equation (3.21) indicates that for a given value of a/δ the streamline patterns are geometrically similar. Thus photographs taken of the flow

lines should look identical if the value of a/δ is the same, even though the absolute size of the pattern might differ. When the fourth order terms are included it is necessary that s/a and a/δ both be the same for two flows to be geometrically similar. Thus, as long as s/a is small enough for these higher order terms to be neglected, a/δ alone is enough, and as s/a increases both s/a and a/δ are needed to specify the geometry of the flow. The parameter a/δ can be written $a/\delta = R' = \sqrt{\frac{a}{s} \cdot \frac{U_o a}{\nu}} = \sqrt{\frac{a}{s}} R$, and can be looked upon as a modified Reynolds number.

Another simple example to which the above calculation may be applied is that of circulating flow in a Kundt's tube. When standing waves are set up in such a tube the "outside" velocity function can be represented by

$$U(x,t) = U_o \sin \frac{2\pi x}{\lambda} \cos \omega t$$

Thus,

$$\begin{aligned} U_o(x) &= U_o \sin \frac{2\pi x}{\lambda} & \frac{dU_o}{dx} &= 2\pi \frac{U_o}{\lambda} \cos \frac{2\pi x}{\lambda} \\ \frac{d^2 U_o}{dx^2} &= -\frac{4\pi^2 U_o}{\lambda^2} \sin \frac{2\pi x}{\lambda} & \frac{d^3 U_o}{dx^3} &= -\frac{8\pi^3}{\lambda^3} U_o \cos \frac{2\pi x}{\lambda} \end{aligned}$$

The expression for the stream function determining the flow within the Kundt's tube is given by the expression

$$\psi_{st} = \sqrt{\frac{v}{\omega}} 2U_0^2 \left(\frac{\pi}{\omega\lambda}\right) \sin\frac{4\pi x}{\lambda} \left\{ \int_{2b}(\gamma) + \left(\frac{U_0\pi}{\omega\lambda}\right)^2 \cdot \left[\left(\int_{4a} + \int_{4c} \right) \sin^2 \frac{2\pi x}{\lambda} - \int_{4b} \cos^2 \frac{2\pi x}{\lambda} \right] \right\} \quad (3.22)$$

In this example the size of the fourth order term is seen to depend upon the ratio $\frac{U_0\pi}{\omega\lambda} = \frac{s\pi}{\lambda} = \frac{U_0}{c}$, where c is the velocity of sound. In most cases this ratio is extremely small, and as a result the fourth order terms can be neglected. The fact that these higher order terms may be significant in one case and not in another highlights the fact that the geometry of the obstacle plays an important role in determining the size of these terms.

Discussion

The streamlines given by the relation $\psi_{st} = \text{constant}$, are plotted in figures 6 and 7. In figure 6 the fourth order terms are completely neglected. The flow consists of a small circulating flow within the boundary layer itself and an outer flow which is also rotational. The directions of rotation of these flows are indicated and are seen to be in opposite directions, as of course they must be. In figure 7 the fourth order terms are taken into account. For this figure, $a\sqrt{\frac{\omega}{v}}$ has been taken to be 10 while the ratio of the oscillation amplitude to the radius of the cylinder, s/a , has the value 1/10. It is seen from figure 7 that the presence of the higher order terms distorts the flow somewhat in the direction of oscillation. Indeed as s/a is increased the distortion is

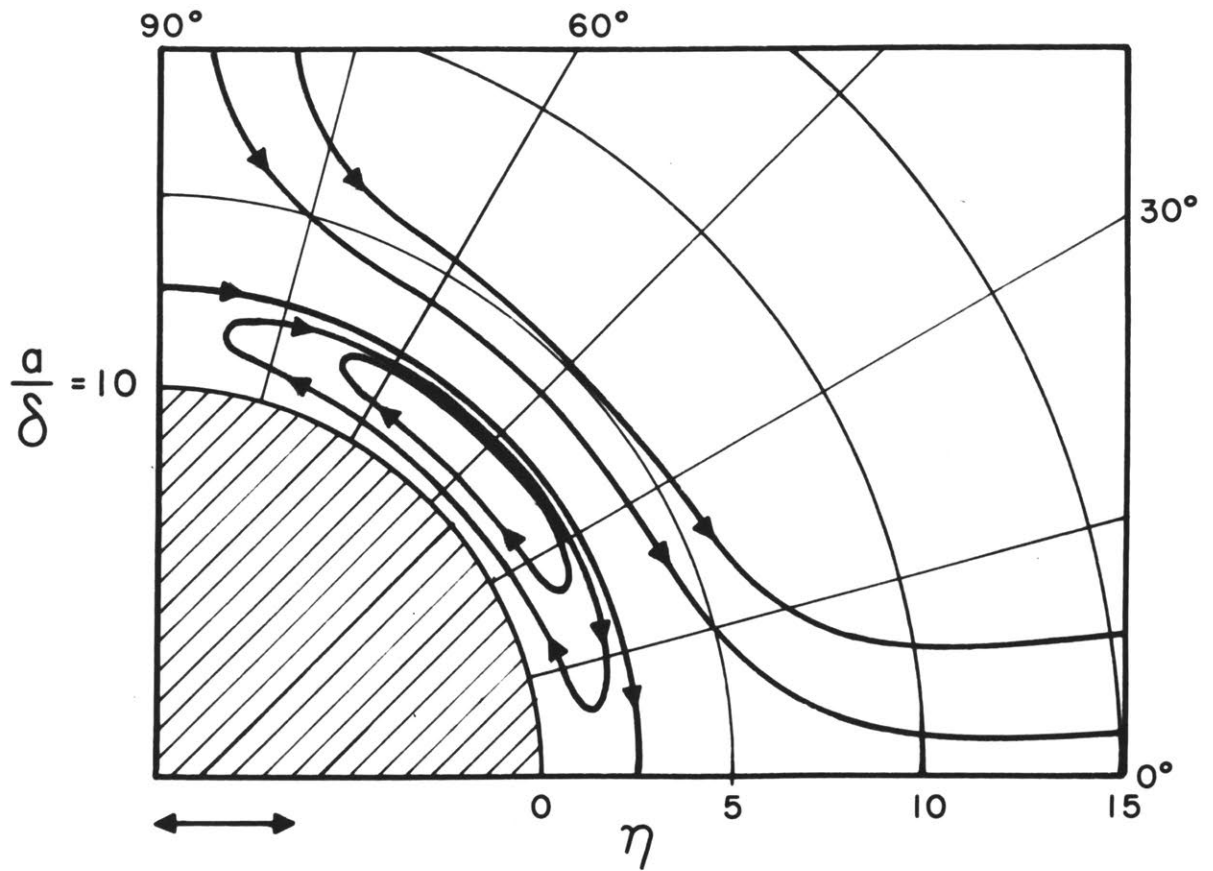


Figure 6: Steady flow streamlines produced by a sound wave passing by a cylinder in the direction indicated by the double arrow. Plotted from the stream function for large R neglecting higher order terms. (See equation 3.20). The flow pattern is symmetrical about the cylinder and only one quadrant is shown.

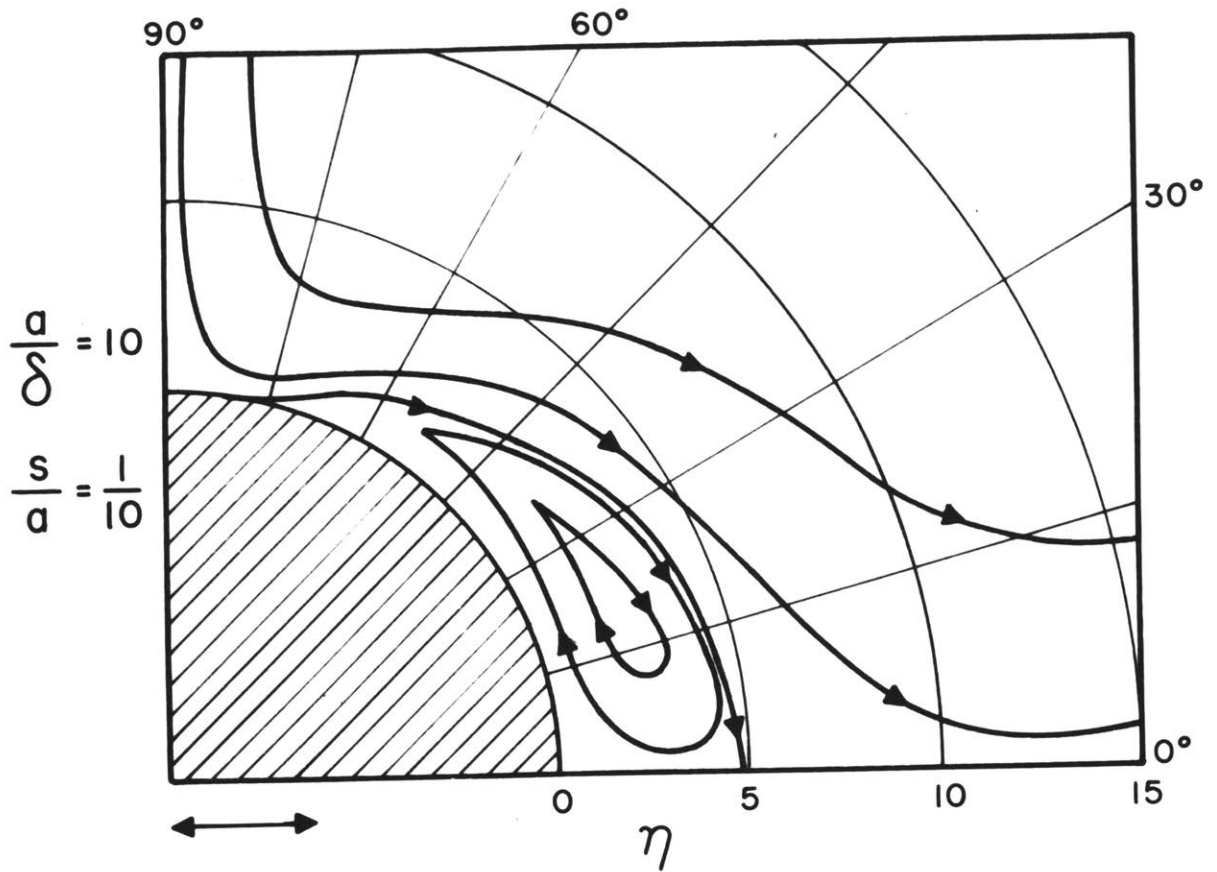


Figure 7: Steady flow streamlines produced by a sound wave passing by a cylinder in the direction indicated by the double arrow. Plotted from stream function for large R taking the fourth order terms into account. (See equation 3.20). In this figure $s/a = 1/10$, and $a/\delta = 10$.

increased further, and this may easily be seen to put a limit upon the range of application of the calculations to this particular example. As s/a increases, the distance from the cylinder at which the streamline $\psi_{st} = 0$ intersects the $\phi = 0$ line increases, and this intercept can be looked upon as a measure of the distortion of the boundary layer circulation. From equation (3.20) we see that for the streamline $\psi_{st} = 0$, the quantity

$$\int_{2b}(\eta) + \left(\frac{s}{a}\right)^2 \left[\left(\int_{4a} + \int_{4c} \right) \sin^2 \phi - \int_{4b} \cos^2 \phi \right]$$

must equal zero. For $\phi = 0$ this becomes

$$\int_{2b}(\eta) - \left(\frac{s}{a}\right)^2 \int_{4b} = 0$$

and for values of η larger than 5 or 6 the expressions \int_{2b} and \int_{4b} can be approximated by

$$\begin{aligned} \int_{2b} &\approx - .75 + 2.30 \\ \int_{4b} &\approx - 25 + 2.29 \end{aligned}$$

Thus

$$(25\eta + 2.29) \left(\frac{s}{a}\right)^2 - .75\eta + 2.30 = 0$$

determines the point of intersection, and the value of η representing this point is given by

$$\eta_c \approx \frac{2.30}{.75 - 25\left(\frac{s}{a}\right)^2}$$

For the example of the cylinder this is seen to become infinite when s/a reaches the value $s/a = \sqrt{\frac{3}{100}} = 0.17$.

Since this inner boundary circulation can be looked upon as representing the boundary layer thickness, it is to be expected that the results of our boundary layer calculation cannot be used to describe the steady motion in the neighborhood of small ϕ for values of greater than $s/a \approx .17$. It will be remembered that the derivation of the boundary layer equations is based upon the assumption that the boundary layer is very thin compared with the characteristic dimension of the obstacle.

Some experimental observations of the flow near a circular cylinder have been made for the large Reynolds number case which indicate that as s/a is increased to a value in the neighborhood of 0.2 the inner circulation is abruptly swept away. Thus this observation may possibly correspond to the theoretical indication that the inner circulation becomes elongated along the axis of oscillation. More will be said about this in the chapter on experiment.

A numerical example will give an estimate of the magnitude of the steady velocities indicated by equation (3.20). Let us consider just the first term of the expression for u_{st} . As the distance from the boundary increases the function $\int_{2b}^1(\eta)$ approaches the value $-3/4$. Thus

$$u_{st} = -\frac{3}{4\omega} \frac{2U_0^2}{a} \sin 2\phi = -\frac{3U_0}{2} \left(\frac{s}{a}\right) \sin 2\phi$$

Suppose that we have a plane sound wave of intensity 133 db and frequency 500 cps incident upon a cylinder of radius 1 cm.

Then $s/a = 0.01$ cm and $R = 209$. Thus the maximum value of u_{st} is 0.47 cm/sec. The magnitude of this velocity is directly proportional to the square of the particle velocity of the incident wave, and is inversely proportional to the frequency for a given U_0 .

In concluding this chapter it is worth while to sum up the assumptions made in the mathematical treatment presented here. In the first place the Reynolds number R must be large in order that the Prandtl boundary layer equations describe the region near the obstacle satisfactorily. In addition the curvature of the obstacle must not change too rapidly or become too large. Finally, for the case of the cylindrical obstacle, the parameter s/a must be small or the perturbation solution of the boundary layer equations will break down. We have seen that the maximum value it can take is of the order of 0.2.

Values of R of the order of 1000 should give good agreement with the calculations presented here as long as s/a is less than the value 0.2. This means that for the case of a circular cylinder in a sound field in air, the radius of the cylinder should be of the order of 0.5 cm with frequencies greater than several hundred cycles per second.

Chapter IV

The Calculation for the Case of Small Reynolds Numbers

In the last chapter a calculation was made for the case of a cylinder in a periodic flow field for large values of R . Earlier R has been defined as $\frac{U_0 a}{\nu}$, where U_0 is the particle velocity amplitude of the periodic flow, a is the radius of the cylinder, and ν is the kinematic viscosity coefficient.

In this chapter the corresponding problem will be treated for the case when R is small. In chapter II the equations governing this case were derived (equations 2.9) through the use of the Oseen approximation. These equations furnish our starting point here. If we introduce for $U(t)$, the expression:

$$U(t) = U_0 \cos \omega t \quad (4.1)$$

which represents a periodic flow, the equations governing the motion become

$$\begin{aligned} \frac{\partial}{\partial t}(U_0 \cos \omega t) + \frac{\partial u'}{\partial t} + U_0 \cos \omega t \frac{\partial u'}{\partial x} &= -\frac{1}{\rho} \frac{\partial p}{\partial x} + \nu \nabla^2 u' \\ \frac{\partial v'}{\partial t} + U_0 \cos \omega t \frac{\partial v'}{\partial x} &= -\frac{1}{\rho} \frac{\partial p}{\partial y} + \nu \nabla^2 v' \end{aligned} \quad (4.2)$$

$$\frac{\partial u'}{\partial x} + \frac{\partial v'}{\partial y} = 0$$

We now assume that u' and v' can be represented as series of decreasing terms, i.e., $u' = u_1 + u_2 \dots$,

$v' = v_1 + v_2 \dots$, where u_1 is of frequency ω , u_2 contains the frequency 2ω and a time-independent part, and u_3 has the frequencies 3ω and ω , etc. The problem is to find the time-independent part of u_2 and v_2 , which represents the steady streaming.

The equations for u_1, v_1 are, from (4.2)

$$\frac{\partial (U_0 \cos \omega t + u_1)}{\partial t} = - \frac{1}{\rho} \frac{\partial p_1}{\partial x} + \nu \nabla^2 u_1$$

$$\frac{\partial v_1}{\partial t} = - \frac{1}{\rho} \frac{\partial p_1}{\partial y} + \nu \nabla^2 v_1 \quad (4.3)$$

$$\frac{\partial u_1}{\partial x} + \frac{\partial v_1}{\partial y} = 0$$

In solving for u_1, v_1 it is convenient to introduce the complex quantity $e^{i\omega t}$ for the time dependence. In the expression for u_2 and v_2 it will be necessary to return to the real quantities since several product terms appear. Equations (4.3) can be written

$$i\omega U_0 \bar{i} + i\omega \bar{q}_1 = - \frac{1}{\rho} \nabla p_1 - \nu \text{curl curl } \bar{q}_1$$

where

$$\bar{q}_1 = u_1 \bar{i} + v_1 \bar{j}. \quad (\bar{i}, \bar{j}, \bar{k} \text{ are unit vectors})$$

This equation can be satisfied by:

$$\bar{q}_1 = - U_0 \bar{i} - \frac{1}{i\omega\rho} \nabla p_1 + \text{curl } \bar{A} \quad (4.4)$$

where

$$-\text{curl curl } \bar{A} = \nabla^2 \bar{A} = \frac{i\omega}{\nu} \bar{A}$$

and

$$\nabla^2 p_1 = 0.$$

In the case of cylindrical symmetry \bar{A} has only one component $A_z = \psi_1$, which is an ordinary stream function. The first order velocity \bar{q}_1 is then given by

$$\begin{aligned} u_1 &= -U_0 - \frac{1}{i\omega\rho} \frac{\partial p_1}{\partial x} + \frac{\partial \psi_1}{\partial y} \\ v_1 &= -\frac{1}{i\omega\rho} \frac{\partial p_1}{\partial y} - \frac{\partial \psi_1}{\partial x} \end{aligned} \quad (4.5)$$

where

$$\nabla^2 p_1 = 0$$

and

$$\nabla^2 \psi_1 = \frac{i\omega}{\nu} \psi_1$$

Correspondingly the vorticity is

$$\bar{\omega}_1 = \text{curl } \bar{q}_1 = \text{curl curl } \bar{A} = -\nabla^2 \bar{A} = -\frac{i\omega}{\nu} \bar{A} = -\frac{i\omega}{\nu} \psi_1 \quad (4.6)$$

Considering now the case of an oscillatory flow past a cylinder of radius a , the boundary conditions imposed upon the solution to equations (4.5) are

$$\left. \begin{aligned} u_1 + U &= 0 \\ v_1 &= 0 \end{aligned} \right\} \quad \text{for } r = a$$

$$u_1 = v_1 = 0 \quad \text{for } r = \infty \quad (4.7)$$

Once the solutions u_1 and v_1 have been found, the time-independent part of u_2 and v_2 are found by taking the time average of the equations (4.2) in which the real parts u_{1r} and v_{1r} of u_1 and v_1 have been inserted, i.e.,

$$\begin{aligned} \overline{U_0 \cos \omega t \frac{\partial u_{1r}}{\partial x}} &= -\frac{1}{\rho} \overline{\frac{\partial p_2}{\partial x}} + \nu \overline{\nabla^2 u_2} \\ \overline{U_0 \cos \omega t \frac{\partial v_{1r}}{\partial x}} &= -\frac{1}{\rho} \overline{\frac{\partial p_2}{\partial y}} + \nu \overline{\nabla^2 v_2} \end{aligned} \quad (4.8)$$

and

$$\overline{\frac{\partial u_2}{\partial x} + \frac{\partial v_2}{\partial y}} = 0$$

To simplify the notation let us in the following omit the bars and refer to the time average \bar{u}_2 and \bar{v}_2 by u_2 and v_2 themselves.

The equations (4.8) can then be written

$$\overline{U_0 \cos \omega t \frac{\partial \bar{q}_{1r}}{\partial x}} = -\frac{1}{\rho} \text{grad } p_2 - \nu \text{curl curl } \bar{q}_2$$

If we set

$$\bar{q}_2 = \text{curl } \bar{A}_2 = \text{curl } \psi_2 \bar{k}$$

and take the curl of this equation we find

$$\overline{U_0 \cos \omega t \frac{\partial \bar{q}_{1r}}{\partial x}} = -\nu \text{curl curl curl curl } \psi_2 \bar{k} = -\nu \nabla^4 \psi_2 \quad (4.9)$$

The last step in (4.9) is justified in the case of cylindrical and rectangular coordinates. The boundary condition is

$$\bar{q}_2 = 0 \quad \text{at} \quad r = a. \quad (4.10)$$

The Velocities u_1 and v_1

In cylindrical coordinates the appropriate solutions to (4.4) are

$$p_1 = i\omega\rho U_0 A_0 \log r - U_0 i\omega\rho \sum_{n=1}^{\infty} \frac{A_n}{n} \frac{\cos n\phi}{r^n} - i\omega\rho U_0 r \cos\phi$$

$$\psi_1 = U_0 \sum_{m=1}^{\infty} B_m K_m(kr) \sin m\phi \quad (4.11)$$

where

$$k^2 = \frac{i\omega}{\nu}$$

The $K_m(kr)$ is the solution to the modified Bessel equation which approaches zero as r becomes infinite.

For matching the boundary conditions we write (4.4) in cylindrical coordinates as

$$q_{1r} = -U_0 \cos\phi - \frac{1}{i\omega\rho} \frac{\partial p_1}{\partial r} + \frac{1}{r} \frac{\partial \psi_1}{\partial \phi}$$

$$q_{1\phi} = U_0 \sin\phi - \frac{1}{i\omega\rho} \frac{\partial p_1}{r \partial \phi} - \frac{\partial \psi_1}{\partial r}$$

Inserting (4.11) and recalling the boundary conditions

$q_{1r} = -U_0 \cos\phi$ and $q_{1\phi} = U_0 \sin\phi$ at $r = a$, we find

$$\begin{aligned}
 A_0 &= 0 \\
 A_1 &= a^2 K_2(ka) \\
 B_1 &= \frac{2}{kK_0(ka)} \\
 A_n &= B_n = 0 \quad \text{for } n > 1
 \end{aligned}
 \tag{4.12}$$

In obtaining A_1 the relations²⁸

$$K_1'(z) + \frac{1}{z} K_1(z) = -K_0(z)$$

and

$$zK_0(z) + 2K_1(z) = zK_2(z)$$

were used.

From (4.11) and (4.12) the stream function for the velocities u_1 and v_1 thus becomes

$$\psi_1 = 2U_0 a \frac{K_1(kr)}{kaK_0(ka)} \sin\phi e^{i\omega t} \tag{4.13}$$

where

$$k = 1/\delta ; \delta = \sqrt{\nu/\omega}$$

The Velocities u_2 and v_2

Having found ψ_1 we can now calculate the "driving" term in equation (4.9). From (4.6)

$$\omega_1 = -k^2 \psi_1 = -2U_0 k \frac{K_1(kr)}{K_0(ka)} \sin\phi e^{i\omega t}$$

and, with

$$\frac{\partial \omega_1}{\partial x} = \frac{\partial \omega_1}{\partial r} \cos \phi - \frac{\sin \phi}{r} \frac{\partial \omega_1}{\partial \phi}$$

we find, using the above recursion formula for K

$$\frac{\partial \omega_1}{\partial x} = U_0 e^{i\omega t} \left[\frac{k^2 K_2(kr)}{K_0(ka)} \right] \sin 2\phi \equiv U_0 e^{i\omega t} [X + iY] \sin 2\phi \quad (4.14)$$

Hence

$$\frac{\partial \omega_{1r}}{\partial x} = (X \cos \omega t - Y \sin \omega t) U_0 \sin 2\phi$$

in which

$$X = \operatorname{Re} \left[\frac{k^2 K_2(kr)}{K_0(ka)} \right] \quad Y = \operatorname{Im} \left[\text{---} \right]$$

From (4.9) and (4.14)

$$\nabla^4 \psi_2 = - U_0 \cos \omega t \frac{\partial \omega_{1r}}{\partial x} = - \frac{U_0^2}{2} X \sin 2\phi \quad (4.15)$$

Expressing X in terms of the functions $\ker_n x$ and $\operatorname{kei}_n x$ defined by²⁸

$$i^{-n} K_n(\sqrt{i} x) = \ker_n x + i \operatorname{kei}_n x$$

equation (4.15) can be written

$$\nabla^4 \psi_2 = \frac{U_0^2}{2v\delta^2 \Delta} \left[\ker_2 \frac{r}{\delta} \operatorname{kei}_0 \frac{a}{\delta} - \operatorname{kei}_2 \frac{r}{\delta} \ker_0 \frac{a}{\delta} \right] \sin 2\phi \quad (4.16)$$

where

$$\Delta = \ker_0^2 \frac{a}{\delta} + \text{kei}_0^2 \frac{a}{\delta}$$

and

$$\delta = \sqrt{\frac{\nu}{\omega}}$$

The functions \ker and kei do not satisfy the modified Bessel's equation. Instead, as shown in appendix 2, they satisfy the equations

$$\nabla^4 (\text{kei}_2 \frac{r}{\delta} \sin 2\phi) = k^4 \text{kei}_2 \frac{r}{\delta} \sin 2\phi$$

$$\nabla^4 (\ker_2 \frac{r}{\delta} \sin 2\phi) = k^4 \ker_2 \frac{r}{\delta} \sin 2\phi$$

Having proved this relationship a particular solution to (4.16) can be written down immediately.

$$\psi_{2p} = - \frac{U_0^2 \sin 2\phi}{2\omega \Delta} \left[\ker_2 \frac{r}{\delta} \text{kei}_0 \frac{a}{\delta} - \text{kei}_2 \frac{r}{\delta} \ker_0 \frac{a}{\delta} \right] \quad (4.17)$$

The homogeneous solution ψ_{2h} is a solution to the biharmonic equation

$$\nabla^4 \psi_{2h} = 0$$

From physical reasoning we expect the angular dependence to be expressed by $\sin 2\phi$ so that $\psi_{2h} = R(r)\sin 2\phi$. The equation for $R(r)$ then becomes

$$r^4 \frac{d^4 R}{dr^4} + 2r^3 \frac{d^3 R}{dr^3} - 9r^2 \frac{d^2 R}{dr^2} + 9r \frac{dR}{dr} = 0$$

The roots to the corresponding indicial equation are found to be $\rho = 0, \pm 2$, and 4. The corresponding solution for ψ_{2h} is found to be

$$\psi_{2h} = \left(\frac{C_1}{r^2} + C_2 + C_3 r^2 + C_4 r^4 \right) \sin 2\phi \quad (4.18)$$

Hence, the complete stream function is

$$\begin{aligned} \psi_2 = \psi_{2p} + \psi_{2h} = & \left[\frac{C_1}{r^2} + C_2 + C_3 r^2 + C_4 r^4 - \frac{U_0^2}{2\omega \Delta} \cdot \right. \\ & \left. \cdot \left(\ker_2 \frac{r}{b} \operatorname{kei}_0 \frac{a}{b} - \operatorname{kei}_2 \frac{r}{b} \ker_0 \frac{a}{b} \right) \right] \sin 2\phi \end{aligned} \quad (4.19)$$

With the condition

$$v_{2\phi} = - \frac{\partial \psi_2}{\partial r} = 0 \quad \text{at } r = \infty$$

we get

$$C_3 = C_4 = 0$$

The other two constants are determined from the condition

$$v_{2r} = v_{2\phi} = 0 \quad \text{at } r = a$$

Using the identities²⁸

$$\operatorname{kei}_2 x + \frac{x}{2} \operatorname{kei}_2' x = - \frac{x}{2} \operatorname{kei}_0' x$$

$$\ker_2 x + \frac{x}{2} \ker_2' x = - \frac{x}{2} \ker_0' x$$

we get

$$C_1 = - \frac{U_0^2 a^3}{4\omega \Delta \delta} \left(\text{ker}_2' \frac{a}{\delta} \text{kei}_0 \frac{a}{\delta} - \text{kei}_2' \frac{a}{\delta} \text{ker}_0 \frac{a}{\delta} \right)$$

$$C_2 = - \frac{U_0^2}{4\omega \Delta} \frac{a}{\delta} \left[\text{kei}_0 \frac{a}{\delta} \text{ker}_0' \frac{a}{\delta} - \text{ker}_0 \frac{a}{\delta} \text{kei}_0' \frac{a}{\delta} \right]$$

Hence, the final expression for ψ_2 is

$$\begin{aligned} \psi_2 = - \frac{U_0^2}{4\omega \Delta} & \left[\frac{a}{\delta} \frac{a^2}{r^2} \left(\text{ker}_2' \frac{a}{\delta} \text{kei}_0 \frac{a}{\delta} - \text{kei}_2' \frac{a}{\delta} \text{ker}_0 \frac{a}{\delta} \right) + \right. \\ & \frac{a}{\delta} \left(\text{kei}_0 \frac{a}{\delta} \text{ker}_0' \frac{a}{\delta} - \text{ker}_0 \frac{a}{\delta} \text{kei}_0' \frac{a}{\delta} \right) + \\ & \left. 2 \left(\text{ker}_2 \frac{r}{a} \frac{a}{\delta} \text{kei}_0 \frac{a}{\delta} - \text{kei}_1 \frac{r}{a} \frac{a}{\delta} \text{ker}_0 \frac{a}{\delta} \right) \right] \sin 2\phi \end{aligned} \quad (4.20)$$

$$\psi_2 = - \frac{U_0^2}{4\omega} f\left(\frac{r}{a}, \frac{a}{\delta}\right) \sin 2\phi$$

The streamlines of the steady streaming are given by

$$\psi_2 = \text{constant.}$$

In passing it might be mentioned that we now can estimate ψ_2/ψ_1 which should give an indication of the magnitude of the u_2 and v_2 terms compared with the u_1 and v_1 terms. From (4.20) and (4.13) it is seen that $\psi_2/\psi_1 \simeq s/a$. In order that the series for u and v be made up of decreasing terms as assumed earlier, s/a should be less than unity.

Discussion

The stream function appearing in (4.20) has been examined in some detail. The function $f\left(\frac{r}{a}, \frac{a}{\delta}\right)$ has been plotted as a

function of r/a for the values $a/\delta = 1, 2, 3,$ and 4 in figure 8. It is apparent that the quantity a/δ determines the general shape of the streamline pattern, as in the case for large R , and in any examples where a/δ is the same and the Reynolds number is small, one should expect to find a geometrically similar flow pattern. Figures 9, 10 and 11 are plots of the steady flow stream lines for the different values of $R' = 1, 2,$ and 3 . It is seen that for values of R' less than three, an "eddy" is formed outside the cylinder. When R' is increased the center of this "eddy" moves toward the cylinder and decreases in size. At the point of its disappearance ($R' = 3$), r/a is roughly 3 at the center of the "eddy." When R' is greater than 3, (figure 11), none of the flow lines close upon themselves for finite r/a .

Since

$$v_{2r} = \frac{1}{r} \frac{\partial \psi_2}{\partial \phi} \qquad v_{2\phi} = - \frac{\partial \psi_2}{\partial r}$$

we can write

$$v_{2r} = - \frac{U_0}{2} \cdot \frac{s}{a} \left[\frac{f(r/a, a/\delta)}{r/a} \right] \cos 2\phi \qquad (4.21)$$

and

$$v_{2\phi} = \frac{U_0}{4} \cdot \frac{s}{a} \left[f'(r/a, a/\delta) \right] \sin 2\phi \qquad (4.22)$$

where the prime indicates differentiation with respect to r/a . The functions $\frac{f(r/a, a/\delta)}{r/a}$ and $f'(r/a, a/\delta)$ representing the radial and tangential stream velocities, are plotted in figures 12 and 13 respectively for $R' = 1, 2,$ and 3 . It

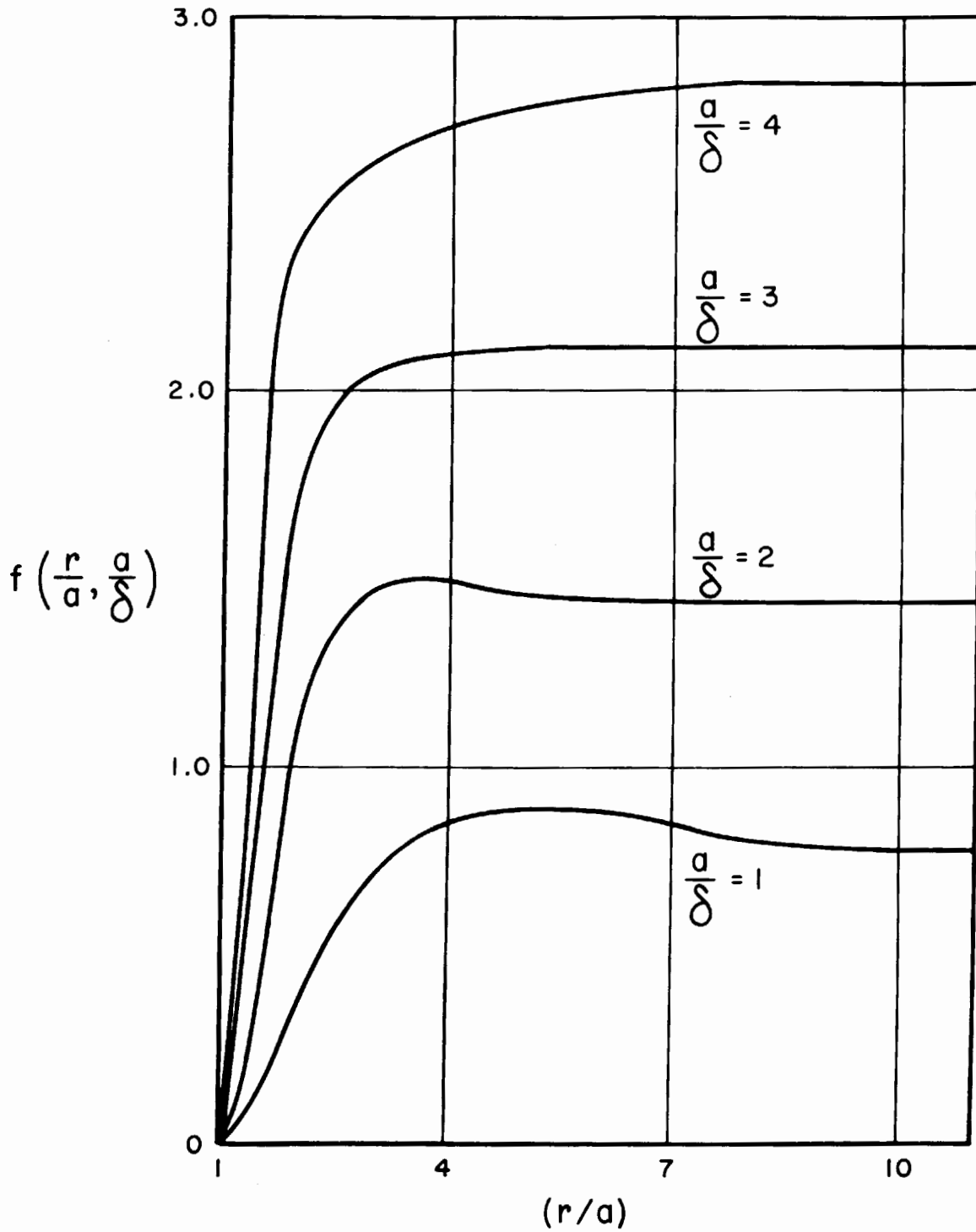


Figure 8: The radial part of the steady stream function, $f(r/a, a/\delta)$, which appears in the solution for small R , plotted as a function of r/a . (See equation 4.20).

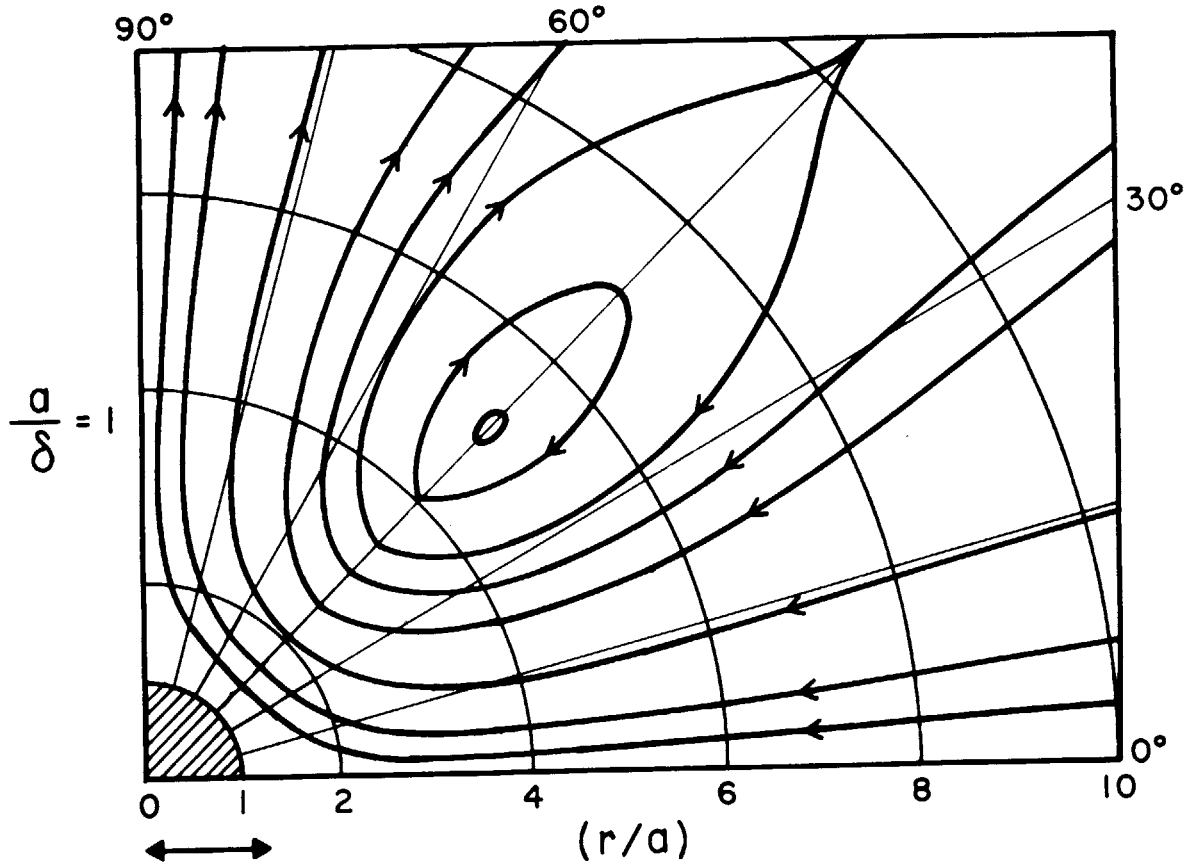


Figure 9: The steady flow pattern generated by a sound wave passing by a cylinder in the direction indicated by the double arrow for small R ($R < 10$). The parameter $R' = a/\delta$ has the value 1 in this figure.

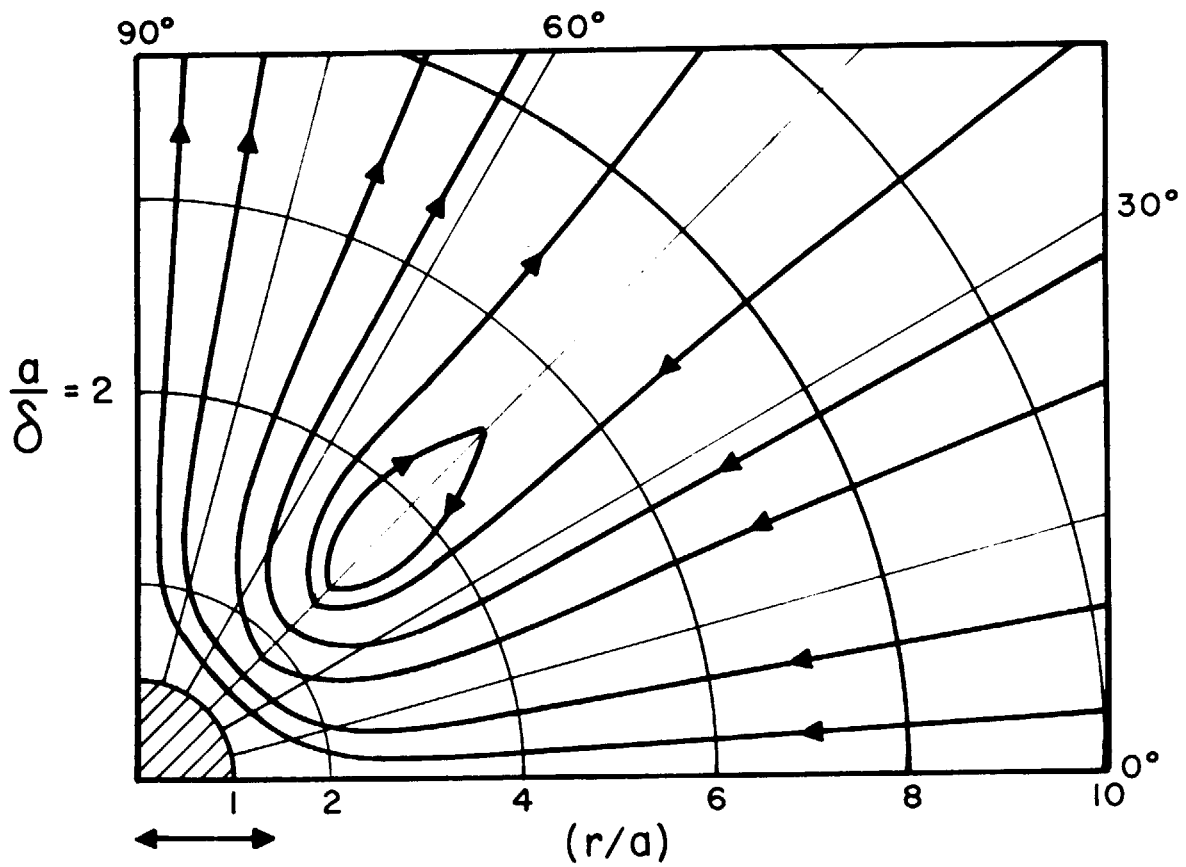


Figure 10: The steady flow pattern generated by a sound wave passing by a cylinder in the direction indicated by the double arrow for small R ($R < 10$). The parameter $R' = a/\delta$ has the value 2 in this figure.

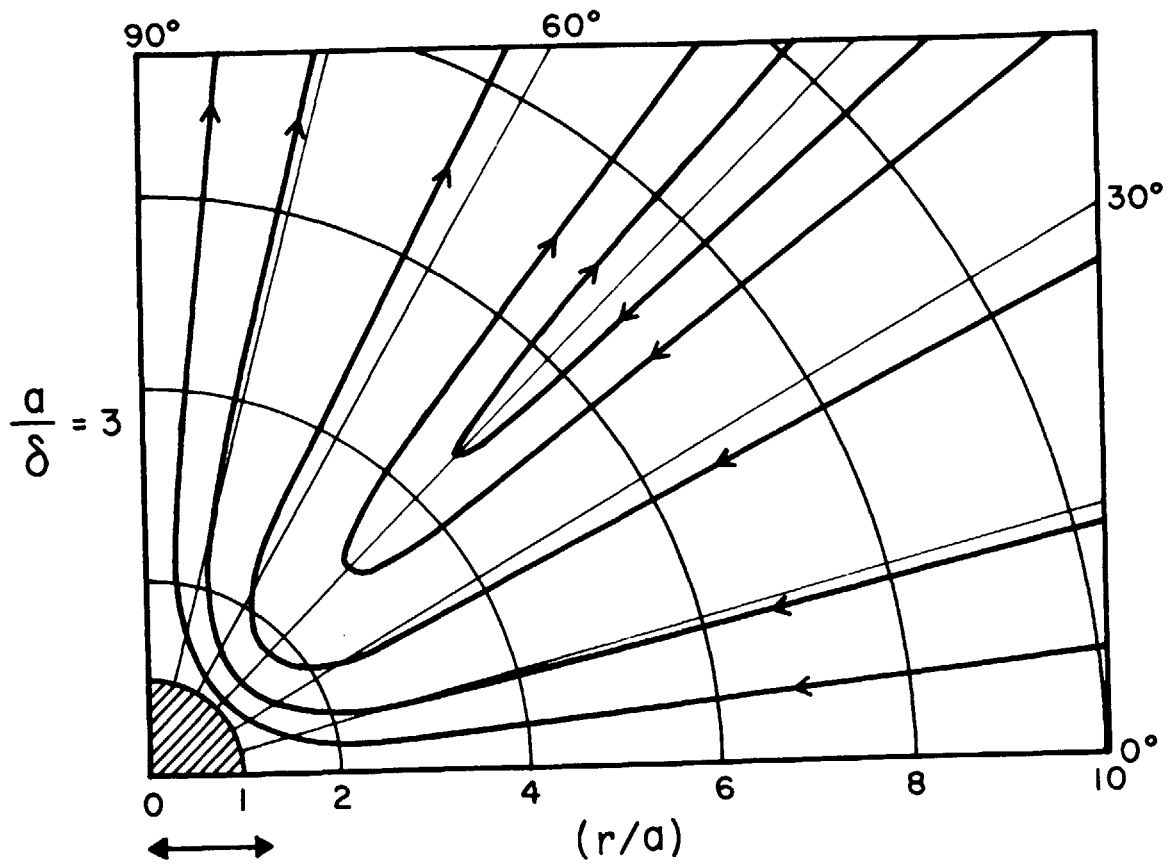


Figure 11: The steady flow pattern generated by a sound wave passing by a cylinder in the direction indicated by the double arrow for small R ($R < 10$). The parameter $R' = a/\delta$ has the value 3 in this figure.

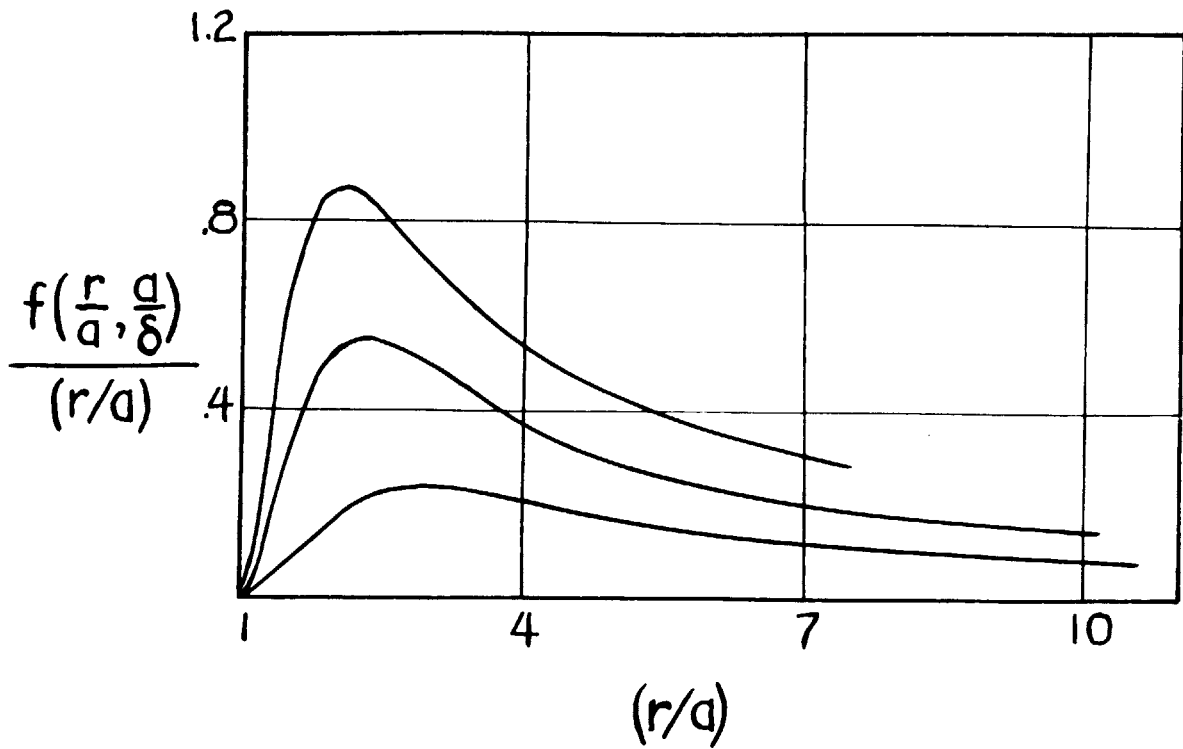


Figure 12: The radial velocity function $\frac{f(r/a, a/\delta)}{r/a}$ for the steady streaming shown in figures 9, 10, 11, plotted as a function of the distance from the cylinder for several values of $R' = a/\delta$.

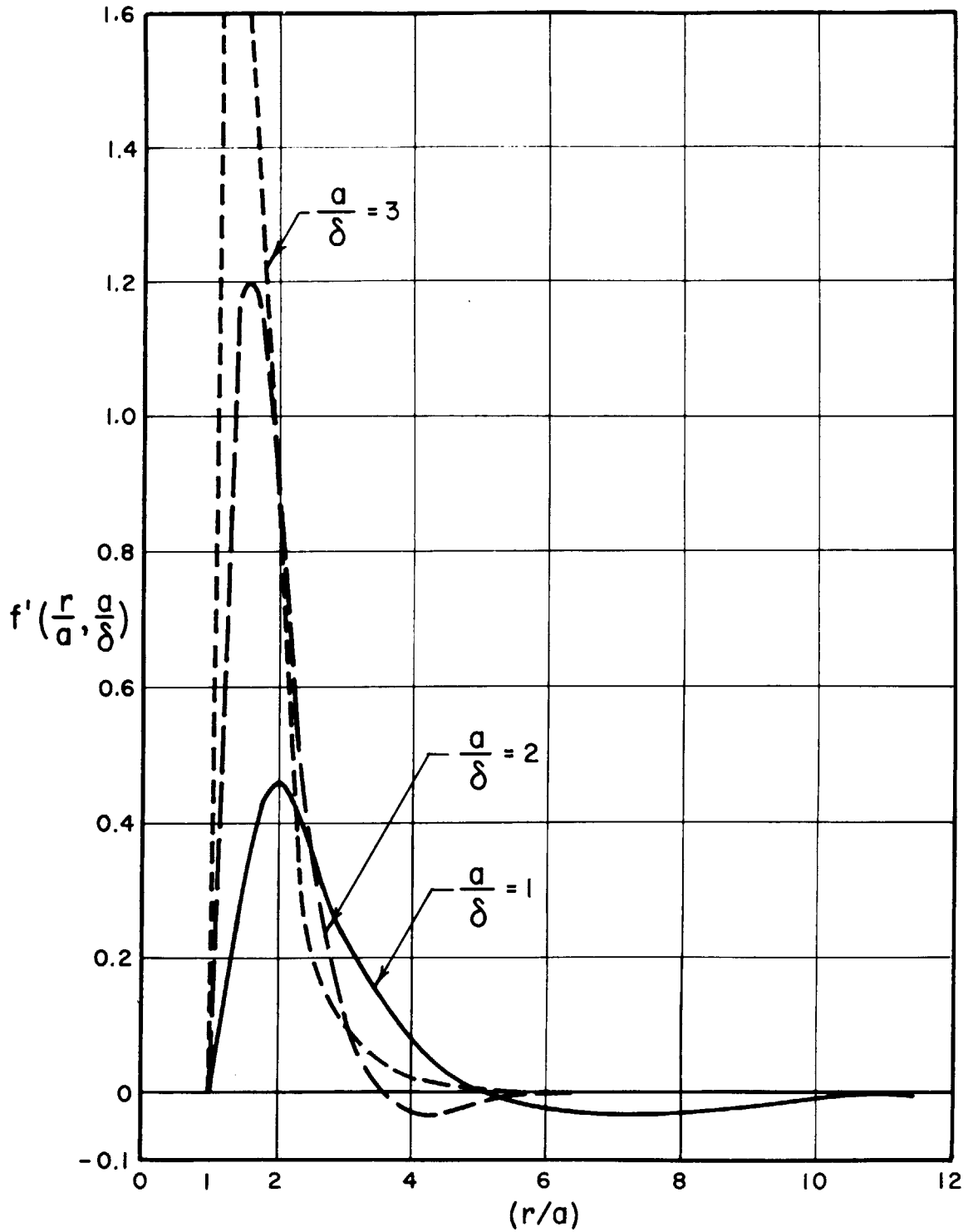


Figure 13: The tangential velocity function $f'(r/a, a/\delta)$ for the steady streaming shown in figures 9, 10, 11, plotted as a function of the distance from the cylinder for several values of R' .

is noted from (4.21) that v_{2r} is negative for ϕ between 0 and $\pi/4$. Thus the direction of the flow lines is toward the cylinder in the direction of the sound propagation.

A numerical example will give an estimate of the magnitude of the steady velocities. Suppose an incident sound wave of intensity 100 db and frequency 135 cps is travelling by a cylinder of radius 4×10^{-2} cm. Then $s = 0.79 \times 10^{-3}$ cm., and $R = 3$. The radial and tangential velocities have maximum values of

$$v_{2r} = 0.8 \times 10^{-2} U_0 = 5.7 \times 10^{-3} \text{ cm/sec}$$

$$v_{2\phi} = 1.1 \times 10^{-2} U_0 = 7.8 \times 10^{-3} \text{ cm/sec}$$

The magnitudes of these velocities are proportional to the square of the particle velocity of the incident wave, and decrease slowly with increasing frequency.

In concluding this chapter it is pointed out again that the preceding analysis is valid only for certain values of the parameters R and s/a , since the use of the Oseen approximation implies small values of R , and the analysis has pointed out that s/a must be small ($s/a < 1$). Preliminary experiments have shown that R should be less than 10 to get the flow described by this analysis. On the other hand, a typical value of R for which the reversed streaming exists is of the order of several hundred.

A comparison of the results of this analysis to the flows observed experimentally is given in chapter VI.

Chapter V

Calculation of the Viscous Dissipation due to an Obstacle

The calculation of the energy lost to viscous friction in a fluid is of practical interest. In acoustics such a calculation of the energy loss in periodic flow along a surface, or through an orifice is of importance in determining the resistive portion of the acoustic impedance of these configurations.

A distinction between the cases for large and small values of the Reynolds number, R , must be made again here. As has been previously pointed out, for the case of large R the flow velocity changes very rapidly from its midstream value to zero in a thin region near a boundary. Within the thin boundary layer the forces of viscosity are appreciable, and it might be expected that most of the energy lost due to viscous forces would be lost in this layer. Thus for large R the boundary layer is the region to be examined if a theoretical treatment of viscous losses near surfaces is to be made.

For the case of very small R there is no such sharp transition zone in which the shear forces are very large. As a consequence the total energy dissipated throughout the entire medium must be computed.

Fortunately the calculations made in Chapters III and IV have given all of the quantities needed for the calculation of the viscous dissipation due to the presence of a

circular cylinder in an incompressible oscillating flow. The following calculations can be regarded as by-products of the earlier work.

The Case for Large R

In a viscous, incompressible fluid the rate at which energy is dissipated is given by²⁹

$$W = \mu \int_V (\nabla \times \bar{v})^2 d\tau + 2\mu \int_S \left\{ \bar{n} \cdot (\bar{v} \times (\nabla \times \bar{v})) - \frac{1}{2} \frac{\partial v^2}{\partial n} \right\} dS \quad (5.1)$$

If the fluid is enclosed within fixed boundaries at which $\bar{v} = 0$ the surface integral of (5.1) is zero, for there is assumed to be no slipping of viscous fluid at a fixed boundary. In this case the rate of dissipation is:

$$W = \mu \int_V (\nabla \times \bar{v})^2 d\tau \quad (5.2)$$

In two dimensions

$$\text{curl } \bar{v} = \bar{k} \left(\frac{\partial v}{\partial x} - \frac{\partial u}{\partial y} \right)$$

and

$$(\text{curl } \bar{v})^2 = \left(\frac{\partial v}{\partial x} \right)^2 + \left(\frac{\partial u}{\partial y} \right)^2 - 2 \left(\frac{\partial u}{\partial y} \right) \left(\frac{\partial v}{\partial x} \right) \quad (5.3)$$

If the methods used in chapter II are applied and (5.3) is examined as to the relative magnitude of the terms appearing, it is seen that in the boundary layer one can write

$$(\text{curl } \bar{v})^2 \simeq \left(\frac{\partial u}{\partial y} \right)^2$$

Let us assume that this relation is a valid description of the situation in the boundary layer and calculate the rate of dissipation of energy there which is

$$W = \mu \int_V \left(\frac{\partial u}{\partial y}\right)^2 d\tau \quad (5.4)$$

where the volume of interest is the boundary layer.

In earlier calculations (chapter III) we determined the velocity u to terms of higher order in the amplitude of oscillation. Thus consider $u = u_1 + u_2 + u_3$ where u_1 , u_2 , u_3 are of first, second and third order respectively, as before. Then, to fourth order,

$$\left(\frac{\partial u}{\partial y}\right)^2 = \left(\frac{\partial u_1}{\partial y}\right)^2 + 2\left(\frac{\partial u_1}{\partial y}\right)\left(\frac{\partial u_2}{\partial y}\right) + 2\left(\frac{\partial u_1}{\partial y}\right)\left(\frac{\partial u_3}{\partial y}\right) + \left(\frac{\partial u_2}{\partial y}\right)^2 + \dots \quad (5.5)$$

all higher order terms having been omitted. In calculating the dissipation, the quantity of importance is the time average of the dissipation. It is to be recalled (see appendix 1) that u_1 is periodic with frequency ω ; u_2 has a periodic part of frequency 2ω and a DC part; u_3 has an ω and a 3ω component.

As a result, when the time average of (5.5) is taken it is seen that

$$\overline{\left(\frac{\partial u_1}{\partial y}\right)\left(\frac{\partial u_2}{\partial y}\right)} = 0$$

and that

$$\overline{\left(\frac{\partial u_1}{\partial y}\right)\left(\frac{\partial u_3}{\partial y}\right)}^t$$

contains a DC part only from the ω component of u_3 .

Since all of the quantities appearing in the expression

$$\overline{\left(\frac{\partial u}{\partial y}\right)^2}^t = \overline{\left(\frac{\partial u_1}{\partial y}\right)^2}^t + 2\overline{\left(\frac{\partial u_1}{\partial y}\right)\left(\frac{\partial u_3}{\partial y}\right)}^t + \overline{\left(\frac{\partial u_2}{\partial y}\right)^2}^t$$

are available from earlier calculation it is not difficult to evaluate the integral giving the rate of viscous dissipation in an oscillating boundary layer.

$$\overline{\left(\frac{\partial u_1}{\partial y}\right)^2}^t = \frac{\omega}{2\nu} U_0^2 \left(\int_{1r}''^2 + \int_{1i}''^2 \right) = \frac{\omega}{2\nu} U_0^2 \int_1'' \int_1'' \quad (5.6)$$

$$\overline{\left(\frac{\partial u_2}{\partial y}\right)^2}^t = \frac{\omega}{2\nu} \frac{1}{\omega^2} U_0^2 \left(\frac{dU_0}{dx}\right)^2 \left[\int_{2ar}''^2 + \int_{2ai}''^2 + \int_{2b}''^2 \right] \quad (5.7)$$

$$\begin{aligned} \overline{2\left(\frac{\partial u_1}{\partial y}\right)\left(\frac{\partial u_3}{\partial y}\right)}^t &= -\frac{\omega}{2\nu} \frac{U_0}{\omega^2} \left[U_0^2 \frac{d^2 U_0}{dx^2} \left(\int_{3ar}'' \int_{1r}'' + \int_{3ai}'' \int_{1i}'' \right) \right. \\ &\quad \left. + U_0 \left(\frac{dU_0}{dx}\right)^2 \left(\int_{3br}'' \int_{1r}'' + \int_{3bi}'' \int_{1i}'' \right) \right] \quad (5.8) \end{aligned}$$

It is convenient to consider separately the integrals of (5.6), (5.7) and (5.8). The integral of (5.6)

$$I_1 = \mu \int \overline{\left(\frac{\partial u_1}{\partial y}\right)^2}^t d\tau$$

is most easily treated. The function \int_1'' has the value

$$\int_0^{\infty} \eta'' = \frac{1+i}{\sqrt{2}} e^{-\frac{(1+i)\eta}{\sqrt{2}}}$$

and thus

$$\int_0^{\infty} \eta'' \bar{\eta}'' = e^{-\sqrt{2}\eta}$$

and

$$I_1 = \mu \frac{\omega}{2\nu} \int_{\nu} U_0^2 e^{-\sqrt{2}\eta} d\tau$$

Now $d\tau = dx dy = \delta dx d\eta$ where $\eta = y \sqrt{\frac{\omega}{\nu}} = \frac{y}{\delta}$

Thus

$$I_1 = \delta \mu \int_x \int_{\eta} e^{-\sqrt{2}\eta} \frac{\omega}{2\nu} U_0^2 dx d\eta \quad (5.9)$$

The integral over η can be taken from 0 to ∞ since there is virtually no contribution to it outside the boundary layer, and these limits simplify the integration. All η integrations are of the general form

$$\int_0^{\infty} \eta^n e^{-a\eta} d\eta = \frac{n!}{a^{n+1}}$$

Thus

$$I_1 = \frac{\delta \mu \omega}{2\nu} \frac{1}{\sqrt{2}} \int_x U_0^2(x) dx = \sqrt{\nu \omega} \cdot \frac{\rho}{2} \frac{1}{\sqrt{2}} \int_x U_0^2(x) dx \quad (5.10)$$

The integral

$$\begin{aligned}
 I_2 &= \delta\mu \int_x \int_0^{\infty} \overline{\left(\frac{\partial u_2}{\partial y}\right)^2} dx d\eta \\
 &= \delta\mu \frac{\omega}{2\nu} \frac{1}{\omega^2} \int_x U_0^2 \left(\frac{dU_0}{dx}\right)^2 dx \int_0^{\infty} \left[\int_{2a}'' \bar{\int}_{2a}'' + \int_{2b}''^2 \right] d\eta
 \end{aligned}$$

is treated in detail in appendix 3. The result is that

$$I_2 = \sqrt{\nu\omega} \cdot \frac{\rho}{2} \frac{1}{\omega^2} \left[-\frac{5}{36} + \frac{3829}{7200\sqrt{2}} \right] \int_x U_0^2 \left(\frac{dU_0}{dx}\right)^2 dx \quad (5.11)$$

Similarly

$$\begin{aligned}
 I_3 &= -\frac{\delta\mu\omega}{2\nu} \frac{1}{\omega^2} \left\{ \int \int U_0^3 \frac{d^2 U_0}{dx^2} \text{R.P.} \left[\int_{3a}'' \bar{\int}_1'' \right] dx d\eta \right. \\
 &\quad \left. + \int \int U_0^2 \left(\frac{dU_0}{dx}\right)^2 \text{R.P.} \left[\int_{3b}'' \bar{\int}_1'' \right] dx d\eta \right\}
 \end{aligned}$$

and

$$\begin{aligned}
 I_3 &= -\sqrt{\nu\omega} \cdot \frac{\rho}{2} \frac{1}{\omega^2} \left[\left(-\frac{1}{24} + \frac{33}{80\sqrt{2}} \right) \int_x U_0^3 \frac{d^2 U_0}{dx^2} dx \right. \\
 &\quad \left. + \left(-\frac{193}{450} + \frac{4373}{3600\sqrt{2}} \right) \int_x U_0^2 \left(\frac{dU_0}{dx}\right)^2 dx \right] \quad (5.12)
 \end{aligned}$$

Combining I_1 , I_2 , and I_3 , one gets the power dissipated in the boundary layer to be

$$\begin{aligned}
 W &= \sqrt{\nu\omega} \cdot \frac{\rho}{2} \left\{ \frac{1}{\sqrt{2}} \int_x U_0^2 dx - \frac{1}{\omega^2} \left[(.250) \int_x U_0^3 \left(\frac{d^2 U_0}{dx^2}\right) dx \right. \right. \\
 &\quad \left. \left. + (.212) \int_x U_0^2 \left(\frac{dU_0}{dx}\right)^2 dx \right] \right\} \quad (5.13)
 \end{aligned}$$

or with a partial integration

$$W = \sqrt{\nu\omega} \cdot \frac{\rho}{2} \left\{ \frac{1}{\sqrt{2}} \int_x^{x_2} U_o^2 dx - \frac{1}{\omega^2} \left[(.250) U_o^3 \left(\frac{dU_o}{dx} \right) \Big|_x^{x_2} - (0.538) \int_x^{x_2} U_o^2 \left(\frac{dU_o}{dx} \right)^2 dx \right] \right\} \quad (5.14)$$

The first term is the same as that often considered in obtaining viscous dissipation near boundaries. It is usually derived by considering the effect of viscosity upon the oscillatory "shearing" motion of an infinite plane. The other terms give an additional contribution to the dissipation which is a function of the amplitude of the oscillatory motion and the form of the velocity function along the boundary, $U_o(x)$.

For the example of the cylinder in an oscillating flow which has been treated in chapter III, we have

$$U_o(x) = 2U_o \sin \frac{x}{a} = 2U_o \sin \phi \quad \frac{dU_o}{dx} = \frac{2U_o}{a} \cos \phi$$

$$\frac{d^2U_o}{dx^2} = - \frac{2U_o}{a^2} \sin \phi$$

If these expressions are put into the integrals in (5.13) one obtains

$$\int_x^{x_2} U_o^2 dx = 4a \int_0^{\pi/2} U_o^2 \sin^2 \phi d\phi = 4a U_o^2 \cdot \frac{1}{2} \cdot \frac{\pi}{2}$$

$$\int_x^{x_2} U_o^3 \frac{d^2U_o}{dx^2} dx = - 16a \int_0^{\pi/2} \frac{U_o^4}{a^2} \sin^4 \phi d\phi = - \frac{a U_o^4}{a^2} \cdot 16 \cdot \frac{3}{8} \cdot \frac{\pi}{2}$$

$$\int_x U_o^2 \left(\frac{dU_o}{dx} \right)^2 dx = 16a \int_0^{\pi/2} \frac{U_o^4}{a^2} \sin^2 \phi \cos^2 \phi d\phi = 16a \frac{U_o^4}{a^2} \cdot \frac{1}{8} \cdot \frac{\pi}{2}$$

for integrations over one fourth of the cylinder. The expression for the power dissipated per unit length in the boundary layer for this example is

$$\begin{aligned} W &= \sqrt{v\omega} \cdot \frac{\rho}{2} \cdot a U_o^2 \cdot \frac{4\pi}{\sqrt{2}} \left[1 + \left(\frac{U_o}{\omega a} \right)^2 (.760) \right] \\ &= 4\pi v \cdot \frac{\rho}{2} \cdot U_o^2 \cdot \frac{1}{\sqrt{2}} \cdot \frac{a}{8} \left[1 + \left(\frac{U_o}{a} \right)^2 (.760) \right] \end{aligned} \quad (5.15)$$

This expression neglecting the higher order term is plotted in figure 14. For the case of standing waves in a Kundt's tube

$$U_o(x) = U_o \sin \frac{2\pi x}{\lambda} \quad \frac{dU_o}{dx} = \frac{2\pi U_o}{\lambda} \cos \frac{2\pi x}{\lambda}$$

$$\frac{d^2 U_o}{dx^2} = - \frac{4\pi^2 U_o}{\lambda^2} \sin \frac{2\pi x}{\lambda}$$

If we take the tube length to be $L = \frac{(2n+1)\lambda}{4}$ and the tube circumference as C, we get for the power dissipated

$$W = \sqrt{v\omega} \cdot \frac{\rho}{2} \cdot \frac{\lambda}{2\pi} \cdot U_o^2 \cdot \frac{(2n+1)\pi}{4\sqrt{2}} \cdot C \left[1 + \left(\frac{2\pi U_o}{\omega \lambda} \right)^2 (0.190) \right] \quad (5.16)$$

Numerical values for these cases will be given later.

The Case for Small R

For the case of small R we again must evaluate the integral

$$W = \mu \int_V (\text{curl } v)^2 d\tau$$

where this time the volume considered is the entire volume outside a cylinder of radius a . Only terms of first order shall be considered, and we thus shall represent $\text{curl } \bar{v}$ by $\text{curl } \bar{v}_1$.

From chapter IV equations (4.6) and (4.13) we have that

$$|\text{curl } \bar{v}_1| = |\bar{\omega}_1| = -k^2 \psi_1 = -2U_0 k \frac{K_1(kr)}{K_0(ka)} \sin \phi e^{i\omega t}$$

Since we want the time average dissipation, we take for $(\text{curl } v_1)^2$ the real part of ω_1 , squared, and averaged over time. If we write

$$\omega_1 = Z e^{i\omega t} = (X + iY)(\cos \omega t + i \sin \omega t)$$

Then

$$\text{R.P.}[\omega_1] = X \cos \omega t - Y \sin \omega t$$

and

$$\overline{[\text{R.P.}(\omega_1)]^2} = \frac{1}{2} (X^2 + Y^2) = \frac{1}{2} Z Z^* \quad (5.17)$$

Thus

$$\begin{aligned} W &= \frac{\mu}{2} \int_0^\infty \int_0^{2\pi} \frac{4U_0^2 k k^* K_1(kr) K_1^*(kr)}{K_0(ka) K_0^*(ka)} \sin^2 \phi r dr d\phi \\ &= 2\mu U_0^2 \frac{\omega}{v} \pi \int_0^\infty \frac{K_1(kr) K_1^*(kr)}{K_0(ka) K_0^*(ka)} r dr \end{aligned}$$

where

$$k = \sqrt{i}/\delta$$

$$K_1(kr) = K_1(\sqrt{i} \frac{r}{\delta})$$

$$K_1^*(kr) = K_1(\sqrt{-i} \frac{r}{\delta})$$

From Appendix 4 we have that:

$$\int_a^\infty K_1(\sqrt{i} \frac{r}{\delta}) K_1(\sqrt{-i} \frac{r}{\delta}) r dr = - a\delta \left[\ker_1 \frac{a}{\delta} \operatorname{kei}'_1 \frac{a}{\delta} - \operatorname{kei}_1 \frac{a}{\delta} \ker'_1 \frac{a}{\delta} \right]$$

where the ker and kei functions are defined in chapter IV by

$$\ker_n x + i \operatorname{kei}_n x = i^{-n} K_n(\sqrt{i} x)$$

Hence

$$W = - 4\pi v \frac{\rho}{2} U_0^2 \frac{a}{\delta} \frac{\left[\ker_1 \frac{a}{\delta} \operatorname{kei}'_1 \frac{a}{\delta} - \operatorname{kei}_1 \frac{a}{\delta} \ker'_1 \frac{a}{\delta} \right]}{\left[\ker_0^2 \frac{a}{\delta} + \operatorname{kei}_0^2 \frac{a}{\delta} \right]} \quad (5.18)$$

This expression is plotted in figure 14. Using several identities relating to the ker, kei functions²⁸ this may be written:

$$W = - 4\pi v \frac{\rho}{2} U_0^2 \frac{a}{\delta} \frac{Zk\left(\frac{a}{\delta}\right)}{Xk\left(\frac{a}{\delta}\right)}$$

where

$$Zk\left(\frac{a}{\delta}\right) = \ker_0 \frac{a}{\delta} \ker'_0 \frac{a}{\delta} + \operatorname{kei}_0 \frac{a}{\delta} \operatorname{kei}'_0 \frac{a}{\delta}$$

$$Xk\left(\frac{a}{\delta}\right) = \ker_0^2 \frac{a}{\delta} + \operatorname{kei}_0^2 \frac{a}{\delta}$$

The functions $Zk(x)$ and $Xk(x)$ are tabulated in a report of the British Association for Advancement of Science.³⁰

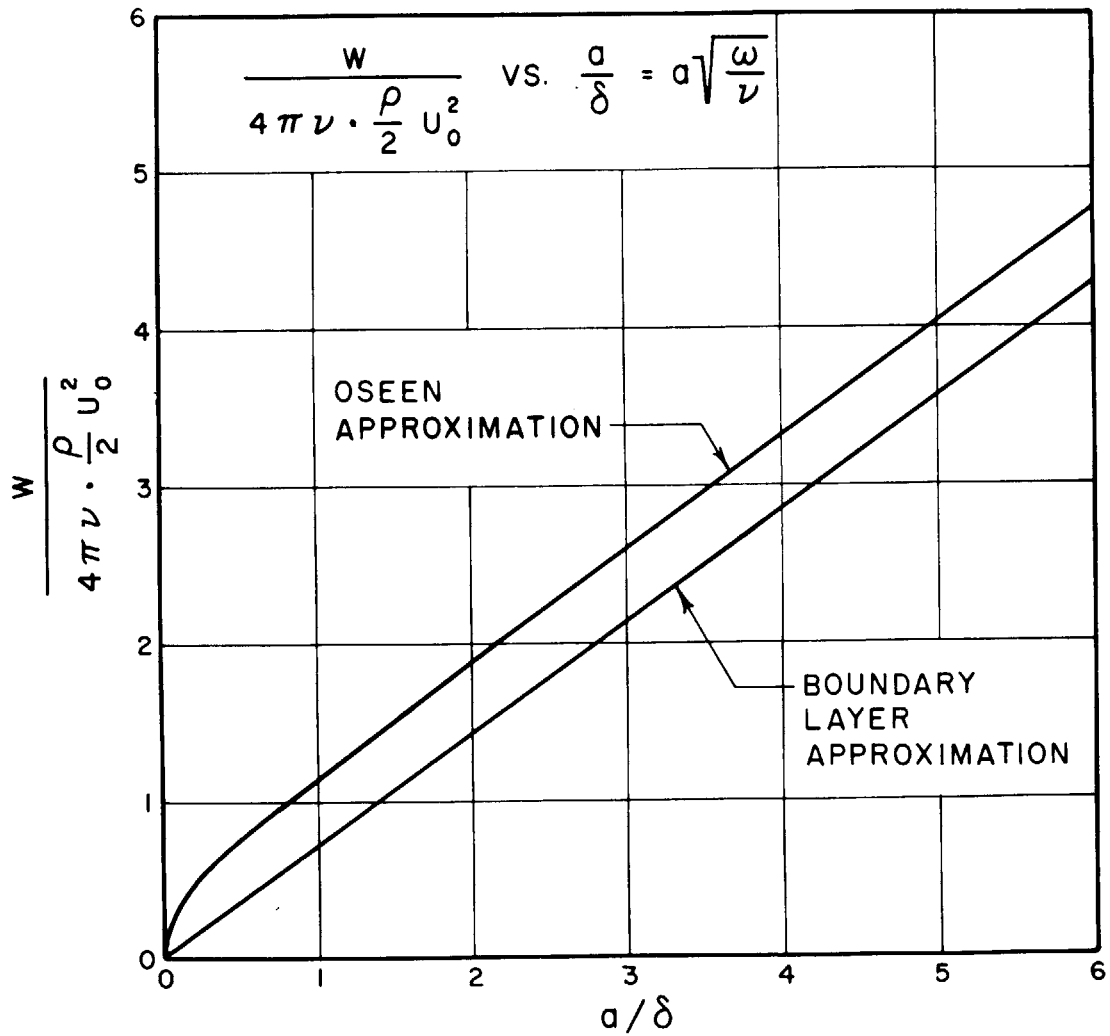


Figure 14: A plot of the viscous dissipation function $W/4\pi\nu\frac{\rho}{2} U_0^2$ as a function of a/δ for both the large R and small R cases. The small R case is plotted from equation (5.18), while the large R case is a plot of the first term of equation (5.15).

Discussion

It is useful to illustrate the above results through the use of some numerical examples. For the large Reynolds number case of a cylinder in an oscillating field, we can use the same numerical example given at the end of chapter III. In that case we had an incident plane sound wave of intensity 133 db and frequency 500 cps and a cylinder of radius 1 cm. Thus $s/a = 0.01$ and $R = 209$. The second term appearing in the bracket in expression (5.15) has the value 0.76×10^{-4} . This is really quite small compared with the unity term. An increase of 10 db increases this term by a factor of 10, and thus it still remains small except for very high intensities.

From the expression for the dissipation in a standing wave tube, equation (5.16), we can write an expression for the Q of such a system. Q is defined as

$$2\pi \frac{E_{\text{total}}}{\Delta E \text{ per cycle}}$$

The total energy is given by

$$\begin{aligned} E_T &= 2 (K.E.)_{\text{av}} = (K.E.)_{\text{max}} = \frac{\rho}{2} U_0^2 \int_0^L \sin^2 \frac{2\pi x}{\lambda} dx = \\ &= \frac{\rho}{2} \frac{\lambda}{2\pi} \cdot U_0^2 \cdot S \cdot \frac{1}{2} (2n + 1) \frac{\pi}{2} \end{aligned}$$

where S is the cross-sectional area of the tube. Also, from (5.16):

$$\Delta E/\text{cycle} = \sqrt{v\omega} \cdot \frac{\rho}{2} \cdot \frac{\lambda}{2\pi} \cdot U_0^2 \cdot \frac{(2n + 1)\pi}{4\sqrt{2}} \cdot c \cdot \frac{2\pi}{\omega} \left[1 + \left(\frac{U_0}{c}\right)^2 (.190) \right]$$

Hence,

$$Q = \frac{\omega R}{\sqrt{2\nu\omega}} \frac{1}{\left[1 + \left(\frac{U_0}{c}\right)^2 (.190)\right]} = \frac{1}{\sqrt{2}} \frac{R}{\delta} \cdot \frac{1}{\left[1 + \left(\frac{U_0}{c}\right)^2 (0.190)\right]} \quad (5.19)$$

where $\delta = \sqrt{\frac{\nu}{\omega}}$ is a measure of the boundary layer thickness and R is the tube radius. The contribution of the nonlinear viscous term to the total dissipation and to Q is negligible. Even at 160 db the second term in the bracket is 1.5×10^{-4} compared to the unity term.

The expressions giving the dissipation in the presence of a cylinder in an oscillating field are plotted for the case of large and small R in figure 14 as a function of the variable a/δ . For air the constant $4\pi\nu\frac{\rho}{2}$ has the value $1.13 \times 10^{-3} \text{ gm cm}^{-1} \text{ sec}^{-2}$. Thus for the example cited above where $R = 209$, we have $a/\delta = 144.5$, $U_0 = 31.4 \text{ cm/sec}$ and the power dissipated per unit length is $W = 113.6 \text{ ergs sec}^{-1} \text{ cm}^{-1}$. For the numerical example cited in chapter IV in which we had an incident sound wave of intensity 100 db and frequency 135 cps and a cylinder of radius 4×10^{-2} we had $s = 0.79 \times 10^{-3} \text{ cm}$, $U_0 = 0.67 \text{ cm/sec}$ and $R = 3$. Thus in that case $a/\delta = 3$ and the power dissipated per length is $1.33 \times 10^{-3} \text{ ergs sec}^{-1} \text{ cm}^{-1}$.

From the figure it is seen that the consideration of the curvature adds a bit to the dissipation. When a/δ is small as is usually the case for small R , this may be an appreciable

fraction of the whole, but when a/δ is large as would be the case for large R this contribution is negligible.

In closing this chapter perhaps a word should be mentioned about the viscous dissipation in orifices, since this is a problem of some import in acoustics. The geometry of orifices is not as simple as that of the cylinder problem treated in this thesis, and theoretical treatment may be seen to be quite complicated. For portions of the orifice having small radii of curvature, such as at sharp edges, the flow would be associated with small values of R . In other portions, which have less curvature, the flow would be characterized by a large value of R . In addition, as the intensity of an acoustic wave which is interacting with the orifice is changed, the nature of the flow in the different portions of the orifice may change from one type to another. Furthermore, since the range of intermediate values of R does not present itself to analytical attack, one must conclude that a complete treatment of the nonlinear orifice problem would be an impossible task.

Chapter VI

A Discussion of Certain Experimental Observations

This chapter contains a discussion of certain experimental observations made of the streaming motion near obstacles. Observations have been made of the streaming near circular cylinders for intermediate values of R as well as for the two limiting cases treated analytically in earlier chapters. A rough quantitative criterion for the transition point between the two types of flow will be given, in addition to descriptions and photographs of the flows for various combinations of R and s/a .

Experimental Setup

The experimental observations of the streaming around cylinders were carried out within a duct. The duct is made of three sections of aluminum tubing having a 3" inner diameter and a 3 1/2" outside diameter. These sections are (1) a driver section 18" in length, (2) a test section 10" in length, and (3) a terminating section 36" in length. The first two sections can be used together as a standing wave apparatus by putting a rigid metal plug at the end of the test section. (See figure 21.) The terminating section contains a Fiberglas wedge, and is used when travelling wave measurements are desired. (See figure 23.)

A fitting was machined with which a small horn driver unit can be fastened to the driver section. (See figure 25.)

This horn driver is designed to drive horn speakers on Navy vessels and is capable of handling up to 35 watts of power, with very little distortion. Its region of maximum efficiency is in the neighborhood of 1000 cps, but it is quite adequate as a sound source from 200 - 2000 cps. The driver section also has a small wall opening into which an Altec 621B condenser microphone can be push-fitted. When in place the microphone surface is flush with the inner wall of the tube. Actually during the observations, this hole was used for introducing smoke into the tube.

The driver section and the test section each contain two windows, 1" x 4", located for viewing the interior from points separated by 90° . A small threaded hole is opposite one of the windows in the test section, and it is through this hole that the cylindrical obstacles are introduced. (See figure 24.) Observations were made looking down upon the axis of the cylindrical obstacle, and illumination was provided through the window at the side. The source of illumination was a spotlight consisting of a 6 volt, 18 ampere projection bulb and a single lens for focusing. The beam was focused down to a $1/4$ inch diameter at the cylindrical obstacle. Even with this arrangement more light would have been desirable, since considerable difficulty was encountered in attempting to photograph the circulations. A small water bath was inserted in the path of the light beam to help minimize the radiant heating of the air within the

tube. It was hoped that this might cut down the convection currents which could interfere with the streaming currents. The spotlight was left unlit except during actual observations.

The driver unit was supplied from a Hewlett-Packard audio oscillator and a McIntosh 20 watt audio amplifier. Since most of the observations were made using the system as a standing wave tube, this arrangement furnished plenty of power. A few observations made using travelling waves indicated that some distortion occurred when the power input to the speaker was increased to levels needed to produce good streaming flows. This fact coupled with the fact that more general drift of the air seemed to occur with the longer termination made the resonance measurements more desirable.

The observations of the cylinder were made through a microscope which has a focal length of 40 mm and which gives a magnification of roughly 10. (See figure 22.) An eyepiece containing a scale furnished a means of determining the amplitude of oscillation of the smoke particles. When subjected to a sound field the illuminated smoke particles appear as shiny rods. It is actually rather difficult to measure the amplitude accurately since the smoke particles tend to obscure one another when large amplitudes are used. In addition the "shiny rods" are usually moving so that it is difficult to line them up with the scale in the ocular.

For photographing the particles through the microscope an Exakta 35 mm camera was used. (Figure 21.) An attachment

whereby the image is focused by the microscope directly upon a ground glass viewer made focusing quite easy. When the exposure is made the ground glass of course flips up out of the way.

A considerable amount of discussion is present in the literature concerning the use of smokes and dusts as a means of observing air flows. The article by Andrade⁶ dwells at some length on this subject, and other references are given in Beranek's book on "Acoustic Measurements."³¹ When smoke and dust particles are used to determine the amplitude of a periodic motion, it is important to know whether the particle is giving a true indication of the air motion. An expression giving the ratio of the particle velocity to the air velocity is given in Andrade's article. Thus:

$$\frac{w_o}{v_o} = \left(\frac{1 + 3b + \frac{9}{2} b^2 + \frac{9}{2} b^3 + \frac{9}{4} b^4}{a^2 + 3ab + \frac{9}{2} b^2 + \frac{9}{2} b^3 + \frac{9}{4} b^4} \right)^{\frac{1}{2}}$$

where w_o/v_o is the ratio of the maximum velocity or amplitude of the particle to that of the air, $a = \frac{2\sigma + 1}{3}$, $b = \frac{1}{R} \sqrt{\frac{\nu}{\pi f}}$, σ is the ratio of the particle density to that of air, R is the particle radius, ν the kinematic viscosity and f the frequency. For smoke particles, which are mainly water vapor, $R \simeq 5 \times 10^{-5}$ cm and even when the frequency is as high as 2000 cps, $w_o/v_o = 0.9988$. The measuring technique is a much

greater limitation of the accuracy in determining s/a , the ratio of particle amplitude to cylinder radius, than is the inability of the particle to follow the air motion.

Several types of smokes and dusts were tried during the course of the experiments. Ordinary cigarette smoke is the easiest to obtain and was used for most of the visual observations. Such smoke is quite dense, i.e., there are a great many particles in a given area of observation. As a result, when the particle amplitudes become of the order of several times the distance between the particles it is difficult to keep a given particle located. Since the particles of cigarette smoke are very small, each particle does not scatter much light. As a result such smoke particles are difficult to photograph, especially when in motion. Magnesium oxide formed by burning a strip of magnesium within the tube, while scattering somewhat more light than cigarette smoke, is too inconvenient to produce. It has a tendency to coat the inner surface of the tube and windows making observation difficult.

Titanium tetrachloride was examined briefly and found to produce smoke of the same density and light scattering power as cigarette smoke. It possesses the advantage of not smelling like cigarette smoke, but it is slightly corrosive, and fouls the interior of the tube more than does either magnesium oxide or cigarette smoke. Baby powder, a mixture of talc and boric acid, was blown into the tube and was

found to be much less dense than the smokes used. The particles are also about three times larger in radius than cigarette smoke particles, and consequently scatter more light. This combination of low density, i.e., low number of particles in a given area, plus the greater light scattering from each particle, makes it possible to photograph an individual particle track as it moves across the field simply by leaving the shutter open.

It is felt that the photographs of the streaming should give a picture of what is seen visually through the microscope. Thus when the streaming motion is rapid and the eye is unable to resolve individual particles, it is not necessary to resolve them in the photograph either. This makes photographing the large Reynolds number flow easy because the shutter can be left open for several seconds. Cigarette smoke can be photographed with these exposures, and was used for the pictures of this type of flow.

For streaming at small R , the eye can follow the individual particles, and it is desirable to resolve the individual particles in the photographs also. Thus the exposure time must be relatively short, i.e., short enough so that the tracks do not interfere with one another, but long enough so that some motion is indicated. Some experiments were made using a high speed flash arrangement of the type developed by Professor Edgerton at M.I.T. The flash time for the bulb is too short to indicate any motion at all,

and thus this type of illumination is not desirable for streaming photographs. It was thought that the baby powder would be suitable for the low R case. The shutter was left open for 5 to 10 seconds and the relatively few particles allowed to trace their paths upon the film. While very nice pictures of the paths were obtained, they did not give a true representation of the flow motion and could not be used. The photographs for the low R case were finally made using cigarette smoke with a 1/2 second exposure. This exposure seemed to be short enough to prevent the many particles from obscuring one another. In order to get enough light it was necessary to overload the projection bulb, and during the time of the exposure it was operated at 8 volts instead of 6 volts (190 watts instead of 108 watts).

Pictures were taken using both Plus X and Super XX film. These films were developed in fine grain developer (Kodak Microdol). In focusing the image upon the film, it was found necessary to compromise in the amount of magnification introduced through the use of the microscope. If the magnification is too great, the amount of light reaching the film from the particles is too small to produce a record. If the magnification is too small, the light intensity is quite adequate, but the image of the smoke particles is of the order of the film grain size. Some experimenting is necessary to determine the optimum magnification in any case.

The cylinders used as obstacles were of a variety of radii. The radii used were 0.0134 cm, 0.040 cm, 0.0828 cm,

0.160 cm, 0.240 cm, and 0.330 cm. The smaller cylinders were strands of wire, the intermediate were pieces of brazing rod, and the larger were machined from brass stock. (See figure 26.)

The resonant frequencies of the tube at which measurements were made were 230, 460, 1150, and 2100 cycles per second. The cylinders were located as near an antinode as possible. Any asymmetries observed were attributed to the cylinder not being precisely at such a point, and also to steady drifting of the smoke particles apparently resulting from temperature gradients within the tube.

Observations

The observations of the streaming motion near a cylindrical obstacle indicate that two main types of flow exist. For one range of s/a and R the flow qualitatively resembles that calculated using the Oseen approximation. (See figures 9, 10, 11, chapter IV.) Thus, a single circulating "loop" is present in each quadrant, and the flow is directed toward the cylinder along the line of oscillation (the axis of the tube). As the ratio s/a and/or R is increased the single circulation loops apparently become unstable, with part of the flow splitting away from the loop and flowing away from the cylinder along the axis of the tube. Thus an "outer" circulation is present in addition to the initial one, which now becomes the "inner" circulation. The flow

now resembles that calculated using the large Reynolds number approximation. (See figures 6, 7, chapter III.) As R is further increased the inner circulation shrinks down until it is confined to a thin region near the boundary (boundary layer). The transition between the two types of flow occurs rather sharply, and it is possible to determine a value of s/a and R associated with a particular transition. Photographs of the flow patterns for four combinations of s/a and R have been included in the thesis, and give an idea of the shapes and relative sizes of the circulations under these different conditions. (See figures 16--19.)

When observations were made using the larger cylinders ($a > 0.1$ cm) it was noted that another phenomenon occurred for high intensities of the incident wave. At a particular level, the inner circulation present in the boundary layer seems to be "squeezed out" and swept downstream along the axis of the tube (i.e., in the direction of oscillation). It seems likely that this occurrence corresponds to the point indicated in the higher order calculations of chapter IV, at which the inner circulation is deformed outward in such a manner. It is difficult to be conclusive on this point, however, since the air flow is nearly turbulent for the intensities at which this "squeeze-out" takes place, and a determination of s/a is difficult. The phenomenon is quite definite, however, for as the intensity is raised and lowered past the critical point, the inner circulation alternately disappears

and reappears. On some occasions a "flutter" between the two situations is seen. The value of s/a at the critical point seems to be of the order of 0.2 as the calculation would indicate, being more nearly 0.2 as R is increased. Several of the points at which this "squeeze-out" occurs are indicated in figure 15, and before-after photographs are included (Figures 20a, b).

Figure 15 can be looked upon as a map of the type of flow occurring for various combinations of s/a and R . The observed points of transition between the high and low Reynolds number types of flow for the various combinations of cylinder size and frequency are plotted in this figure. A line passing through these points divides the map into two parts. The points to the large R side of the line correspond to flows qualitatively resembling the flows calculated using the boundary layer approximation. The points on the small R side of the line correspond to the flows resembling the flows calculated using the Oseen approximation. In addition to the points observed by the author, there are points included which are calculated from data in Andrade's article.⁶ All of these latter points, except one, correspond to flow transitions for spheres instead of cylinders. (The value of R is calculated using for \underline{a} the radius of the sphere.) They are included on the map for the sake of completeness, and because the dividing line for the sphere case seems to be nearly the same as for the cylinder case.

Andrade does not explicitly identify his points with the transition between the two general types of flow, but he presents his points as representing what he calls the onset of "vortex motion," characterized by the appearance of a jet of air shooting outward from the obstacle. This "jet" apparently corresponds to the point at which the "outer" circulation of the large R flow begins. From figure 15 it is seen that for a wide range of values of s/a , the transition between the two types of flow takes place for $R \sim 10$. For the sake of clarity, the regions throughout which the theoretical treatments for large and small R are believed valid are also indicated in figure 15. A brief table containing the experimental data from which the points of transition and "squeeze-out" were calculated, appears below.

It is felt that the presentation of the data in the form of a map of the regions of flow is a good way to sum up the results of this thesis. Thus in figure 15 the manner in which the streaming motion changes from one general type to another is apparent at a glance. The regions throughout which the theoretical calculations might be expected to be valid are also indicated. Together with the photographs of the flows at various points, the map gives an indication of the flow behavior for large, medium and small values of R , and large and small values of s/a .

Possible future studies of the streaming near obstacles should include attempts to determine the line of transition

with more accuracy, and a closer examination of the "squeeze-out" phenomenon. Such measurements will require a more refined experimental arrangement than the one used here. Special attention should be given to a better means of measuring s/a with the microscope and the elimination of steady drifting of the smoke.

Tables

Experimental Data for Points of Transition

<u>a cm</u>	<u>f~</u>	<u>$\delta \times 10^2$ cm</u>	<u>a/δ</u>	<u>s/a</u>	<u>R</u>
.0134	230	1.02	1.31	3.4	5.85
	460	.722	1.86	2.2	7.6
	1150	.457	2.94	1.2	10.4
	2100	.338	3.96	~.6	~9
.040	230	1.02	3.92	.8	12.1
	460	.722	5.55	.37	11.3
	1150	.457	8.76	~.1	~8.8
	2100	.338	11.83	---	---
.0828	230	1.02	8.13	~.1	~9
	460	.722	11.5	~.05	~6
	1150	.457	---	---	---
	2100	.338	---	---	---

Experimental Data for Points of "Squeeze-out"

<u>a cm</u>	<u>f~</u>	<u>$\delta \times 10^2$ cm</u>	<u>a/δ</u>	<u>s/a</u>	<u>R</u>
.16	460	.722	22	.5	240
.24	460	.722	33	.4	440
.33	460	.722	46	.34	700

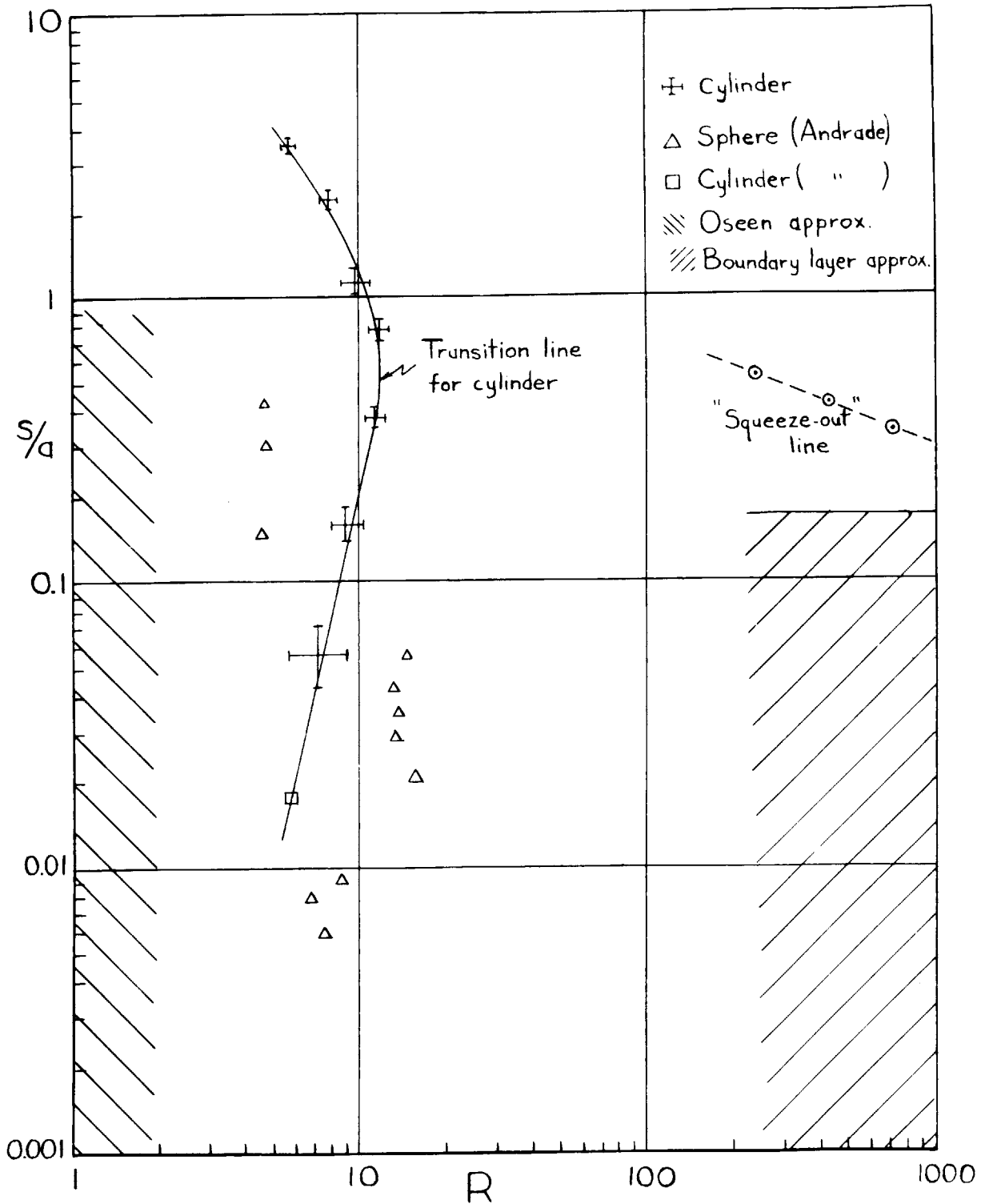


Figure 15: A "phase diagram" plot in s/a , R space. The experimental line of transition between the two types of flow, the regions of the validity of the calculations made for large and small R , and the experimental line of squeeze out of the inner circulation are shown.

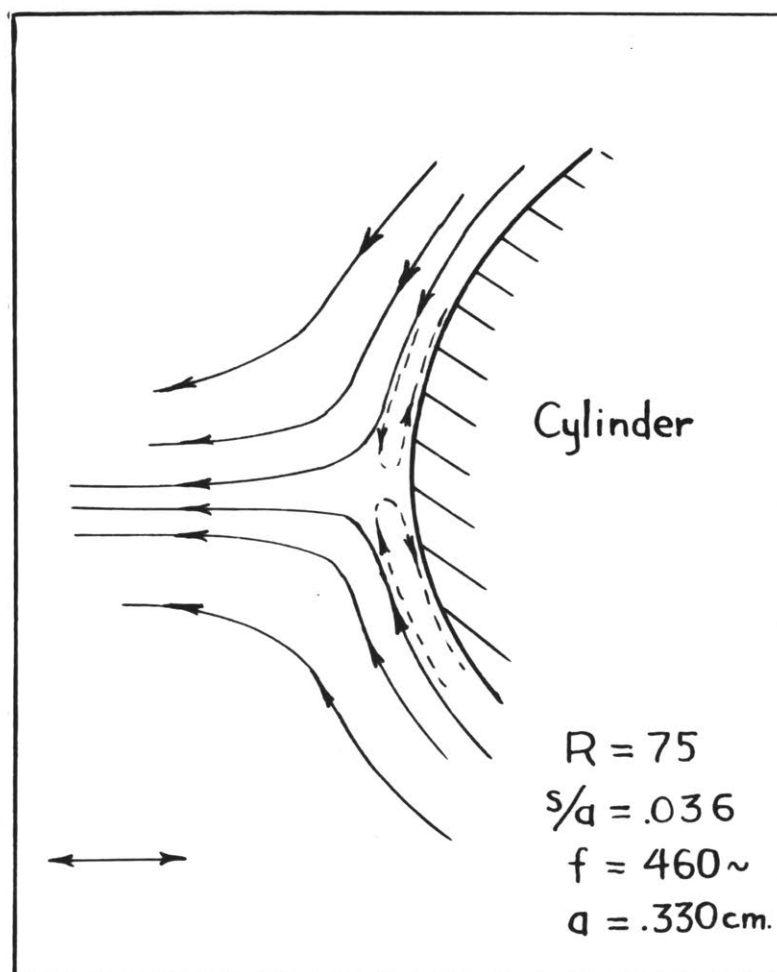


Figure 16 a,b : A photograph and schematic sketch of the streaming flow for $R = 75$, $s/a = .036$. The bright line indicates the edge of the cylinder. The double arrow in the schematic indicates the direction of oscillation. The exposure was 2 seconds on Kodak Super XX film.

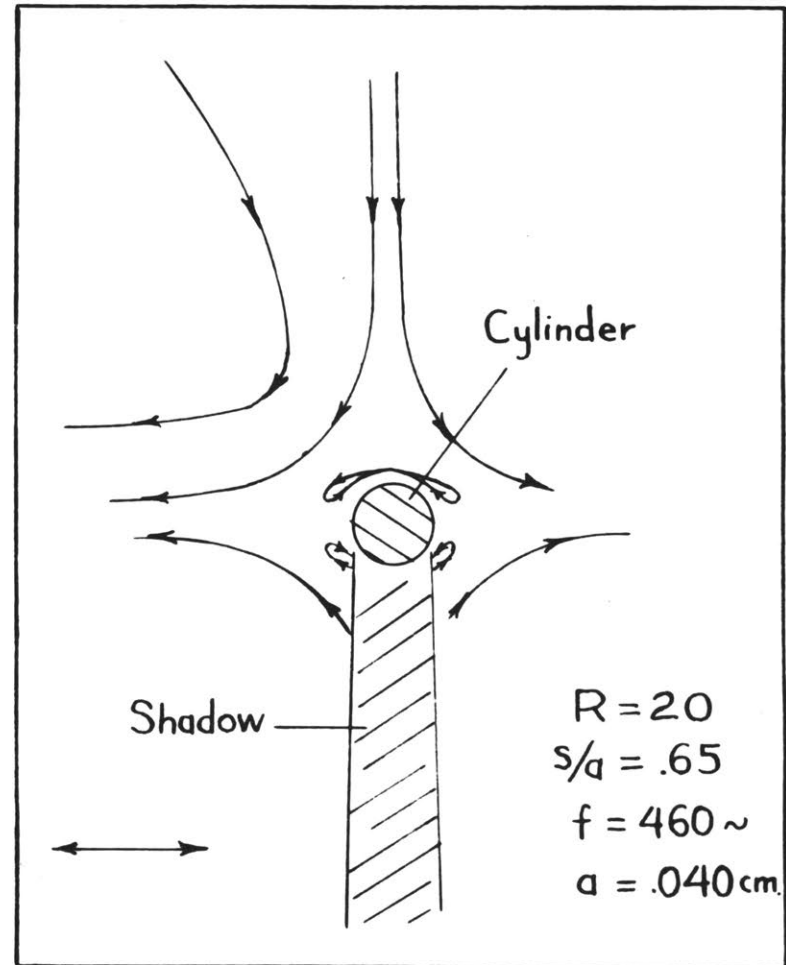


Figure 17 a,b : A photograph and schematic sketch of the flow for $R = 20$, $s/a = .65$. The edge of the cylinder is indicated by the dotted line on the photograph. The double arrow in the schematic indicates the direction of oscillation. The exposure was 2 seconds on Kodak Super XX film.

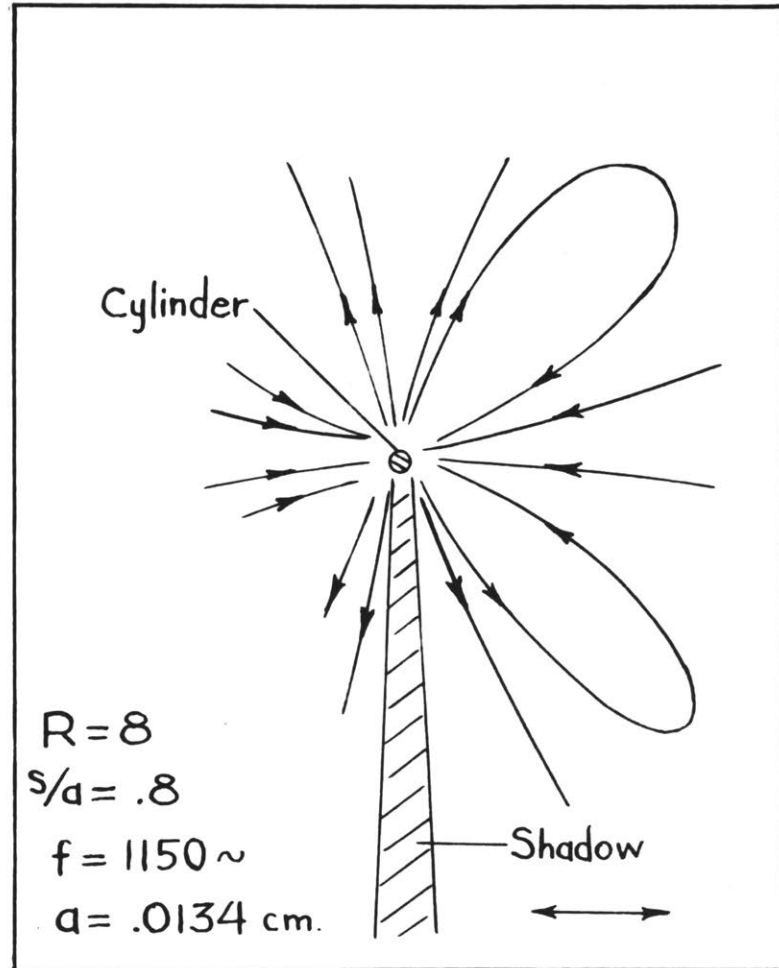
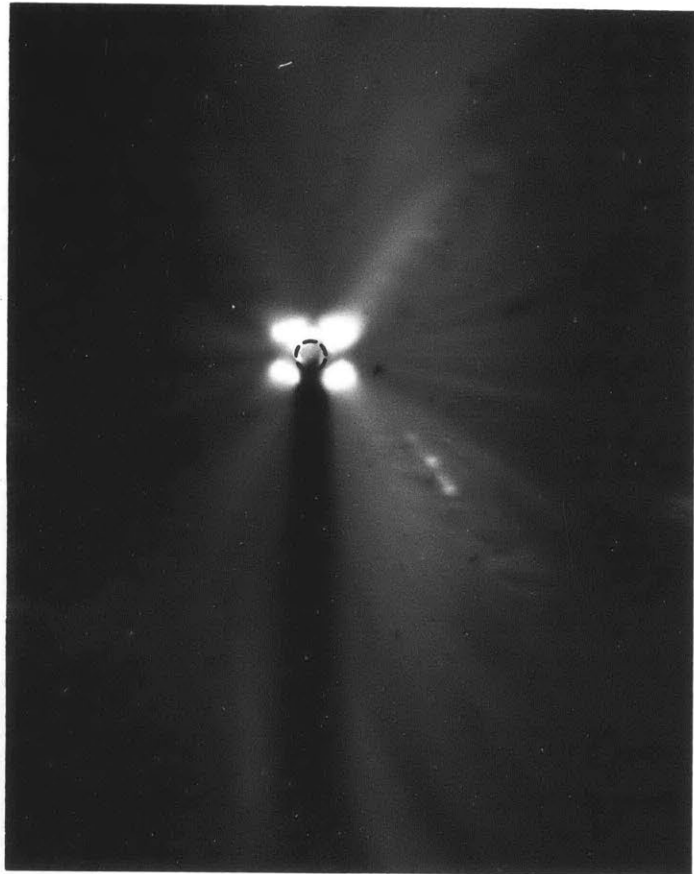


Figure 18 a,b : A photograph and schematic sketch of the flow for $R = 8$, $s/a = .8$. The edge of the cylinder is indicated by the dotted line on the photograph. The double arrow in the schematic indicates the direction of oscillation. The smoke particles tend to cluster at the points indicated by the four bright spots next to the cylinder. The exposure was $1/2$ second on Plus X film.

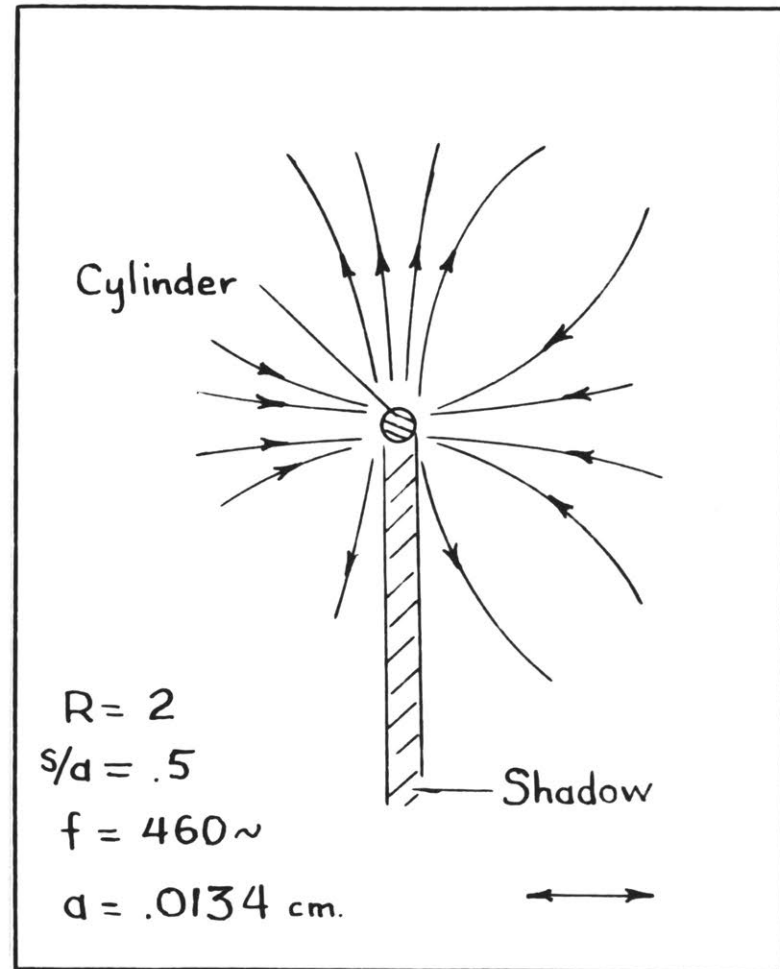
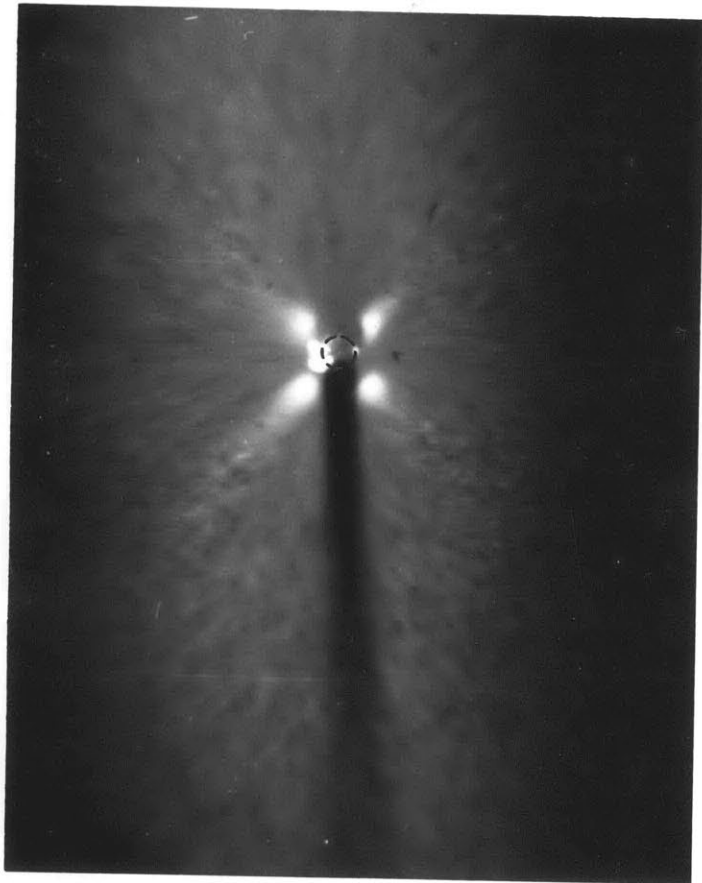


Figure 19 a,b : A photograph and schematic sketch of the flow for $R = 2$, $s/a = .5$. The edge of the cylinder is indicated by the dotted line on the photograph. The double arrow in the schematic indicates the direction of oscillation. The smoke particles tend to cluster at the points indicated by the four bright spots next to the cylinder. The exposure was $1/2$ second on Super XX film.



Figure 20 a,b : Photographs indicating the flow pattern before and after the inner boundary layer circulation is squeezed out and carried away. (The flow is similar to that in figure 16 a,b in direction and nature.) The squeeze out occurs for $R = 270$, $s/a = .55$. The exposure was 2 seconds on Super XX film.



Figure 21: Photograph showing the standing wave tube in which the streaming motions were observed. The camera and microscope arrangement is set up ready for taking photographs of the flow. The light source, amplifier, and audio oscillator are also shown.



Figure 22: Photograph showing the apparatus set up for making visual observations.



Figure 23 : Photograph showing the driver section, test section and termination section set up for making travelling wave observations.

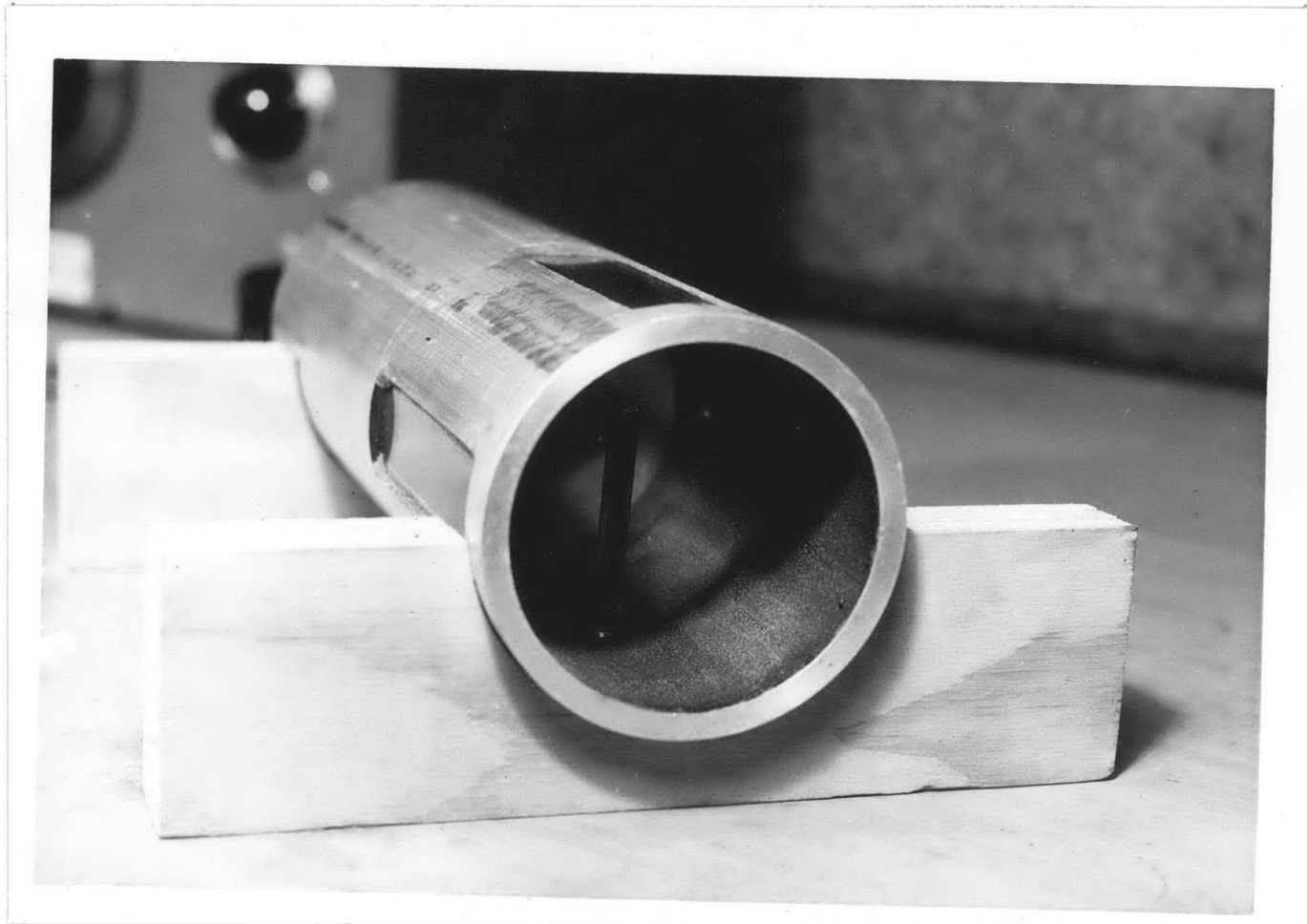


Figure 24 : A close-up photograph of the test section showing the windows for observation and illumination as well as one of the cylindrical obstacles in position.



Figure 25 : Photograph showing the speaker unit and the fitting with which it is coupled to the driver section.

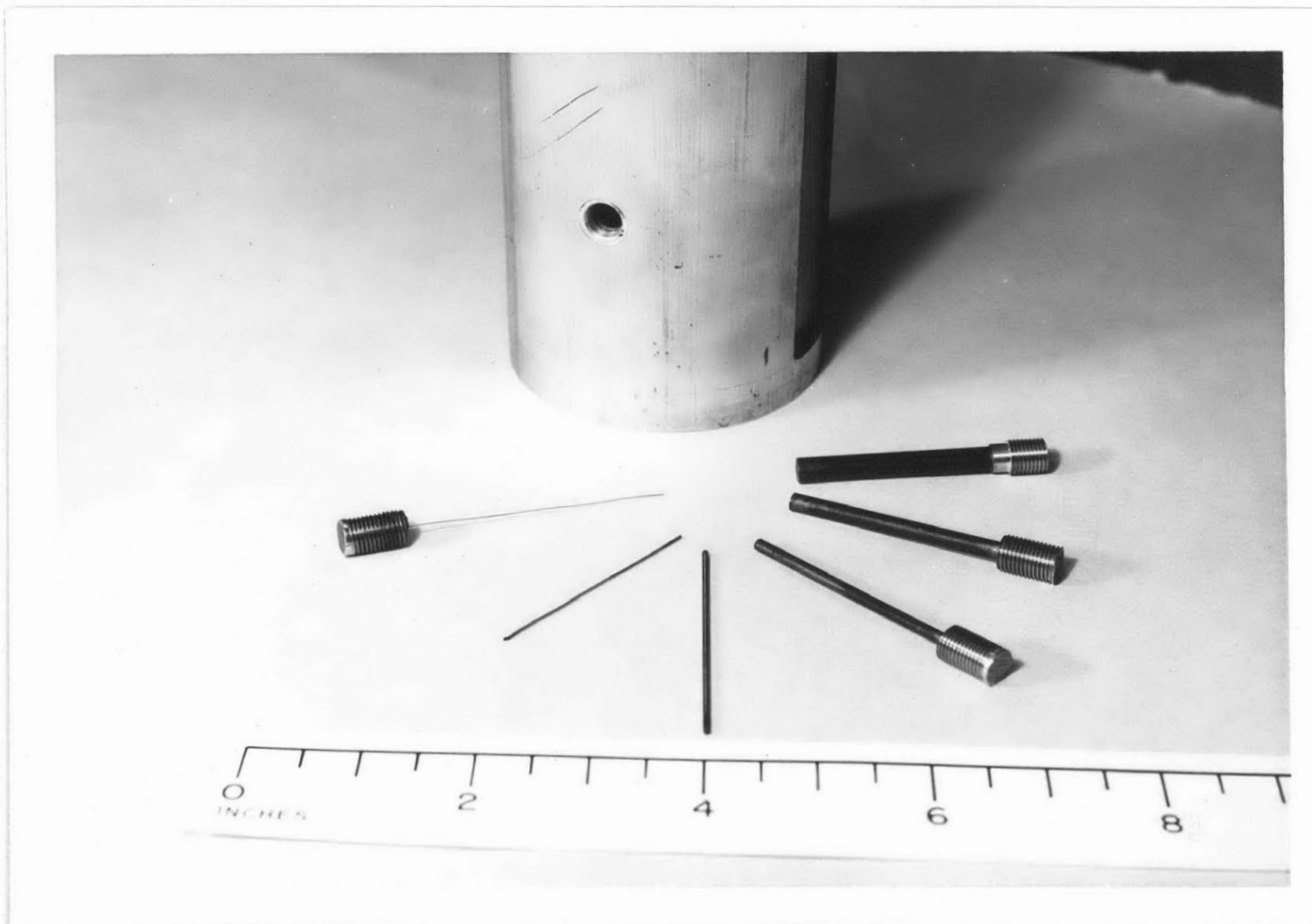


Figure 26: Photograph showing the cylindrical obstacles used for the streaming observations. The test section is oriented to show the hole through which the cylinders were introduced.

Appendix 1

The solution to equation (3.5) in terms of a stream function is:

$$\psi_1 = \text{R.P.} \left[\sqrt{\frac{\nu}{\omega}} U_0 \zeta_1 e^{i\omega t} \right] \quad (1)$$

$$u_1 = \frac{\partial \psi_1}{\partial y} = \text{R.P.} \left[U_0 \zeta_1' e^{i\omega t} \right]$$

$$v_1 = -\frac{\partial \psi_1}{\partial x} = -\sqrt{\frac{\nu}{\omega}} \frac{dU_0}{dx} \text{R.P.} \left[\zeta_1 e^{i\omega t} \right]$$

$$\zeta_1 = -\frac{(1-i)}{\sqrt{2}} + \eta + \frac{(1-i)}{\sqrt{2}} e^{-\frac{(1+i)\eta}{\sqrt{2}}}$$

$$\zeta_1' = 1 - e^{-\frac{(1+i)\eta}{\sqrt{2}}}$$

The solution to equation (3.6) is

$$\psi_2 = \sqrt{\frac{\nu}{\omega}} \cdot \frac{1}{\omega} \cdot U_0 \frac{dU_0}{dx} \text{R.P.} \left[\zeta_{2a} e^{i2\omega t} + \zeta_{2b} \right] \quad (2)$$

$$u_2 = \frac{\partial \psi_2}{\partial y} = \frac{1}{\omega} U_0 \frac{dU_0}{dx} \text{R.P.} \left[\zeta_{2a}' e^{i2\omega t} + \zeta_{2b}' \right]$$

$$v_2 = -\frac{\partial \psi_2}{\partial x} = -\sqrt{\frac{\nu}{\omega}} \cdot \frac{1}{\omega} \left[U_0 \frac{d^2 U_0}{dx^2} + \left(\frac{dU_0}{dx} \right)^2 \right] \cdot \left[\zeta_{2a} e^{i2\omega t} + \zeta_{2b} \right]$$

$$f_{2a} = \frac{1+i}{4} e^{-(1+i)\eta} + \frac{i}{2} \eta e^{-\frac{(1+i)\eta}{\sqrt{2}}} - \frac{1+i}{4}$$

$$f'_{2a} = -\frac{i}{2} e^{-(1+i)\eta} + \left[\frac{i}{2} + \frac{1-i}{2\sqrt{2}} \eta \right] e^{-\frac{(1+i)\eta}{\sqrt{2}}}$$

$$f_{2b} = -\frac{1}{4\sqrt{2}} e^{-\sqrt{2}\eta} - \left[\frac{3}{\sqrt{2}} \cos \frac{\eta}{\sqrt{2}} + \sqrt{2} \sin \frac{\eta}{\sqrt{2}} \right] e^{-\frac{\eta}{\sqrt{2}}} - \frac{\eta}{2} e^{-\frac{\eta}{\sqrt{2}}} \sin \frac{\eta}{\sqrt{2}} \\ - \frac{3}{4} \eta + \frac{13}{4\sqrt{2}}$$

$$f'_{2b} = \frac{1}{4} e^{-\sqrt{2}\eta} + 2e^{-\frac{\eta}{\sqrt{2}}} \sin \frac{\eta}{\sqrt{2}} + \frac{1}{2} e^{-\frac{\eta}{\sqrt{2}}} \cos \frac{\eta}{\sqrt{2}} \\ + \frac{\eta}{2\sqrt{2}} e^{-\frac{\eta}{\sqrt{2}}} \left(\sin \frac{\eta}{\sqrt{2}} - \cos \frac{\eta}{\sqrt{2}} \right) - \frac{3}{4}$$

The ω component of the solution to the third order equations (3.9) is given by

$$\psi_{3(\omega)} = -\frac{\sqrt{2}}{\omega} \cdot \frac{1}{2\omega^2} \text{R.P.} \left[U_0^2 \frac{d^2 U_0}{dx^2} f_{3a} e^{i\omega t} + U_0 \left(\frac{dU_0}{dx} \right)^2 f_{3b} e^{i\omega t} \right] \quad (3)$$

$$u_{3(\omega)} = \frac{\partial \psi_{3(\omega)}}{\partial y} = -\frac{1}{2\omega^2} \text{R.P.} \left[U_0^2 \frac{d^2 U_0}{dx^2} f'_{3a} e^{i\omega t} + U_0 \left(\frac{dU_0}{dx} \right)^2 f'_{3b} e^{i\omega t} \right]$$

$$v_{3(\omega)} = -\frac{\partial \psi_{3(\omega)}}{\partial x} = \frac{\sqrt{2}}{\omega} \cdot \frac{1}{2\omega^2} \text{R.P.} \left\{ \left[U_0^2 \frac{d^3 U_0}{dx^3} + 2U_0 \frac{dU_0}{dx} \frac{d^2 U_0}{dx^2} \right] f_{3a} e^{i\omega t} + \right. \\ \left. + \left[2U_0 \frac{dU_0}{dx} \frac{d^2 U_0}{dx^2} + \left(\frac{dU_0}{dx} \right)^3 \right] f_{3b} e^{i\omega t} \right\}$$

$$\begin{aligned}
 \rho_{3a} = & -\frac{(1-i)}{4} e^{-(1+i)\eta} - \left[\frac{1}{4} + \frac{151}{60\sqrt{2}} + i\left(\frac{1}{4} + \frac{4}{3\sqrt{2}}\right) - \frac{(3+4i)}{8} \eta + \right. \\
 & \left. + \frac{3\sqrt{2}}{16} (1-i)\eta^2 \right] e^{-\frac{(1+i)\eta}{\sqrt{2}}} - \frac{1}{3} \left[\left(\frac{1}{4} - \frac{1}{8\sqrt{2}}\right) - i\left(\frac{1}{4} + \frac{1}{8\sqrt{2}}\right) \right] e^{-\left[\left(1+\frac{1}{\sqrt{2}}\right) + \left(1-\frac{1}{\sqrt{2}}\right)i\right]\eta} \\
 & + \frac{(2+21i)}{10\sqrt{2}} e^{-\sqrt{2}\eta} + \left[\left(\frac{5}{4\sqrt{2}} - \frac{1}{8}\right) + i\left(\frac{7}{4\sqrt{2}} + \frac{1}{8}\right) + \frac{1}{4}\eta \right] e^{-\frac{(1-i)\eta}{\sqrt{2}}} \\
 & + \frac{\sqrt{2}}{40} i e^{-\left(\frac{3+i}{\sqrt{2}}\right)\eta} + \frac{(1-i)}{12\sqrt{2}} e^{-\sqrt{2}(1+i)\eta} + \left(\frac{17}{24} + \frac{113}{120\sqrt{2}}\right) - i\left(\frac{5}{24} + \frac{101}{40\sqrt{2}}\right)
 \end{aligned}$$

$$\begin{aligned}
 \rho'_{3a} = & \frac{1}{2} e^{-(1+i)\eta} + \left[\frac{29}{30} + i\left(\frac{97}{40} + \frac{1}{2\sqrt{2}}\right) - \frac{(5+i)}{8\sqrt{2}} \eta + \frac{3}{8} \eta^2 \right] e^{-\frac{(1+i)\eta}{\sqrt{2}}} \\
 & + \left(\frac{1}{8} - \frac{i}{4\sqrt{2}}\right) e^{-\left[\left(1+\frac{1}{\sqrt{2}}\right) + \left(1-\frac{1}{\sqrt{2}}\right)i\right]\eta} - \frac{(2+21i)}{10} e^{-\sqrt{2}\eta} \\
 & - \left[\frac{5}{4} + i\left(\frac{1}{4} + \frac{1}{4\sqrt{2}}\right) + \frac{(1-i)}{4\sqrt{2}} \eta \right] e^{-\frac{(1-i)\eta}{\sqrt{2}}} + \frac{(1-3i)}{40} e^{-\frac{(3+i)\eta}{\sqrt{2}}} - \frac{1}{6} e^{-\sqrt{2}(1+i)\eta}
 \end{aligned}$$

$$\begin{aligned}
 \rho_{3b} = & \left[-\frac{7}{4} + \frac{1}{2\sqrt{2}} + i\left(\frac{7}{4} + \frac{1}{2\sqrt{2}}\right) - \frac{1}{2}\eta \right] e^{-(1+i)\eta} - \left[\frac{299}{90\sqrt{2}} + \frac{47}{72} + i\left(\frac{53}{20\sqrt{2}} + \frac{7}{8}\right) + \right. \\
 & \left. + \frac{(13-14i)}{8} \eta + \frac{\sqrt{2}(7+i)}{16} \eta^2 \right] e^{-\frac{(1+i)\eta}{\sqrt{2}}} + \frac{1}{24} \left[-1 + \frac{5}{\sqrt{2}} + i\left(1 + \frac{5}{\sqrt{2}}\right) \right] e^{-\left[1+\frac{1}{\sqrt{2}}\right]\eta} \\
 & \cdot e^{-\left(1-\frac{1}{\sqrt{2}}\right)i\eta} - \left[\frac{17(1-2i)}{10\sqrt{2}} - \frac{i}{2}\eta \right] e^{-\sqrt{2}\eta} - \left(1-\frac{1}{\sqrt{2}}\right) \left[\frac{11}{72} + \frac{(1+i)}{12\sqrt{2}} \eta \right] e^{-\sqrt{2}(1+i)\eta} \\
 & + \left(\frac{49}{18} + \frac{173}{180\sqrt{2}}\right) - i\left(\frac{25}{24} + \frac{221}{24\sqrt{2}}\right)
 \end{aligned}$$

$$\begin{aligned}
 S'_{3b} = & \left[3 - \frac{j}{\sqrt{2}} + \frac{(1+j)\eta}{2} \right] e^{-(1+j)\eta} + \left[-\left(\frac{58}{45} + \frac{\sqrt{2}}{9}\right) + \left(\frac{341}{72} + \frac{55}{36\sqrt{2}}\right) i + \right. \\
 & \left. + \frac{(13-3i)\eta}{8\sqrt{2}} + \frac{(3+4i)\eta^2}{8} \right] e^{-\frac{(1+j)\eta}{\sqrt{2}}} - \left(\frac{1}{8} + \frac{j}{2\sqrt{2}}\right) e^{-\left[\left(1+\frac{1}{\sqrt{2}}\right) + \left(1-\frac{1}{\sqrt{2}}\right)j\right]\eta} \\
 & + \left[\frac{(17-29i)}{10} - i\frac{\eta}{\sqrt{2}} \right] e^{-\sqrt{2}\eta} - \left[\frac{13}{4} + i\left(\frac{7}{4} + \frac{1}{4\sqrt{2}}\right) + \frac{(9-5i)}{4\sqrt{2}}\eta - \frac{j}{4}\eta^2 \right] e^{-\frac{(1-j)\eta}{\sqrt{2}}} \\
 & + \frac{(3+i)}{40} e^{-\left(\frac{3+j}{\sqrt{2}}\right)\eta} + \left(1-\frac{1}{\sqrt{2}}\right) \left[\frac{2(1+j)}{9\sqrt{2}} + \frac{j}{6}\eta \right] e^{-\sqrt{2}(1+j)\eta}
 \end{aligned}$$

The time independent fourth order solution to equation (3.14) is

$$\psi_{4st} = -\sqrt{\omega} \cdot \frac{1}{4\omega^3} \left[U_0^3 \frac{d^3 U_0}{dx^3} \rho_{4a} + U_0 \left(\frac{dU_0}{dx}\right)^3 \rho_{4b} + U_0^2 \frac{dU_0}{dx} \frac{d^2 U_0}{dx^2} \rho_{4c} \right] \quad (4)$$

$$u_{4st} = \frac{\partial \psi_{4st}}{\partial y} = -\frac{1}{4\omega^3} \left[U_0^3 \frac{d^3 U_0}{dx^3} \rho'_{4a} + U_0 \left(\frac{dU_0}{dx}\right)^3 \rho'_{4b} + U_0^2 \frac{dU_0}{dx} \frac{d^2 U_0}{dx^2} \rho'_{4c} \right]$$

$$\begin{aligned}
 v_{4st} = -\frac{\partial \psi_{4st}}{\partial x} = & \sqrt{\omega} \cdot \frac{1}{4\omega^3} \left\{ \left[U_0^3 \frac{d^4 U_0}{dx^4} + 3U_0^2 \frac{dU_0}{dx} \frac{d^3 U_0}{dx^3} \right] \rho_{4a} + \right. \\
 & + \left[3U_0 \left(\frac{dU_0}{dx}\right)^2 \frac{d^2 U_0}{dx^2} + \left(\frac{dU_0}{dx}\right)^4 \right] \rho_{4b} + \left[U_0^2 \frac{dU_0}{dx} \frac{d^3 U_0}{dx^3} + U_0^2 \left(\frac{d^2 U_0}{dx^2}\right)^2 + \right. \\
 & \left. \left. + 2U_0 \left(\frac{dU_0}{dx}\right)^2 \frac{d^2 U_0}{dx^2} \right] \rho_{4c} \right\}
 \end{aligned}$$

$$\begin{aligned}
 S_{4a} &= \frac{1}{8} e^{-\eta} (\cos \eta + \sin \eta) - \left[\frac{1}{6} + \frac{59}{120\sqrt{2}} - 2\eta - \frac{3}{8\sqrt{2}} \eta^2 \right] e^{-\frac{\eta}{\sqrt{2}}} \cos \frac{\eta}{\sqrt{2}} \\
 &- \left[\frac{1}{3} + \frac{733}{120\sqrt{2}} + \frac{5}{8}\eta - \frac{3}{8\sqrt{2}} \eta^2 \right] e^{-\frac{\eta}{\sqrt{2}}} \sin \frac{\eta}{\sqrt{2}} + \left(\frac{1}{12} + \frac{7}{72\sqrt{2}} \right) e^{-(1+\frac{1}{\sqrt{2}})\eta} \cos(1-\frac{1}{\sqrt{2}})\eta \\
 &- \left(\frac{1}{18} + \frac{1}{24\sqrt{2}} \right) e^{-(1+\frac{1}{\sqrt{2}})\eta} \sin(1-\frac{1}{\sqrt{2}})\eta + \left[-\frac{1}{8} + \frac{14}{15\sqrt{2}} + \frac{5}{8}\eta + \frac{3}{16\sqrt{2}} \eta^2 \right] e^{-\sqrt{2}\eta} \\
 &+ \frac{1093}{7500\sqrt{2}} e^{-\frac{3\eta}{\sqrt{2}}} \cos \frac{\eta}{\sqrt{2}} + \frac{27}{625\sqrt{2}} e^{-\frac{3\eta}{\sqrt{2}}} \sin \frac{\eta}{\sqrt{2}} - \frac{5}{96\sqrt{2}} e^{-\sqrt{2}\eta} (\cos \sqrt{2}\eta + \sin \sqrt{2}\eta) \\
 &+ \frac{1}{144} (1+\frac{1}{\sqrt{2}}) e^{-(1+\sqrt{2})\eta} \cos(1-\sqrt{2})\eta - \frac{1}{144} (\frac{1}{\sqrt{2}} - 1) e^{-(1+\sqrt{2})\eta} \sin(1-\sqrt{2})\eta + \frac{1}{320\sqrt{2}} e^{-2\sqrt{2}\eta} \\
 &+ \left(\frac{17,839}{12,000} + \frac{1}{8\sqrt{2}} \right) \eta + \frac{11}{144} - \frac{77,113}{120,000\sqrt{2}} \\
 S'_{4a} &= -\frac{1}{4} e^{-\eta} \sin \eta - \left[\frac{97}{120} + \frac{1}{6\sqrt{2}} + \frac{15}{8\sqrt{2}} \eta \right] e^{-\frac{\eta}{\sqrt{2}}} \cos \frac{\eta}{\sqrt{2}} + \left[\frac{107}{40} + \frac{1}{2\sqrt{2}} \right. \\
 &\quad \left. - \frac{5}{8\sqrt{2}} \eta - \frac{3}{8} \eta^2 \right] e^{-\frac{\eta}{\sqrt{2}}} \sin \frac{\eta}{\sqrt{2}} - \left(\frac{1}{6} + \frac{1}{6\sqrt{2}} \right) e^{-(1+\frac{1}{\sqrt{2}})\eta} \cos(1-\frac{1}{\sqrt{2}})\eta \\
 &+ \left(\frac{1}{24} + \frac{1}{12\sqrt{2}} \right) e^{-(1+\frac{1}{\sqrt{2}})\eta} \sin(1-\frac{1}{\sqrt{2}})\eta - \left[\frac{37}{120} - \frac{1}{4\sqrt{2}} + \frac{7}{8\sqrt{2}} \eta + \frac{3}{16} \eta^2 \right] e^{-\sqrt{2}\eta} \\
 &- \frac{197}{1000} e^{-\frac{3\eta}{\sqrt{2}}} \cos \frac{\eta}{\sqrt{2}} - \frac{413}{3000} e^{-\frac{3\eta}{\sqrt{2}}} \sin \frac{\eta}{\sqrt{2}} + \frac{5}{48} e^{-\sqrt{2}\eta} \sin \sqrt{2}\eta \\
 &- \frac{1}{24\sqrt{2}} e^{-(1+\sqrt{2})\eta} \cos(1-\sqrt{2})\eta - \frac{1}{160} e^{-2\sqrt{2}\eta} + \frac{17,839}{12,000} + \frac{1}{8\sqrt{2}}
 \end{aligned}$$

$$\begin{aligned}
 \mathcal{Y}_{4b} = & \left[\frac{11}{2} + \frac{13}{4\sqrt{2}} + \frac{1}{\sqrt{2}}\eta - \frac{1}{4}\eta^2 \right] e^{-\eta} \cos \eta + \left[\frac{21}{4} - \frac{13}{4\sqrt{2}} + \frac{13}{4}\eta + \frac{1}{4}\eta^2 \right] e^{-\eta} \sin \eta \\
 & - \left[\frac{1445}{72\sqrt{2}} + \frac{241}{36} + \left(\frac{23}{18\sqrt{2}} - \frac{7}{18} \right) \eta - \frac{15}{8\sqrt{2}} \eta^2 - \frac{1}{4}\eta^3 \right] e^{-\frac{\eta}{\sqrt{2}}} \cos \frac{\eta}{\sqrt{2}} \\
 & + \left[\frac{391}{72} + \frac{913}{20\sqrt{2}} + \left(-\frac{2}{9\sqrt{2}} + \frac{571}{360} \right) \eta + \frac{31}{8\sqrt{2}} \eta^2 \right] e^{-\frac{\eta}{\sqrt{2}}} \sin \frac{\eta}{\sqrt{2}} + \frac{1}{81} \left[-\frac{39}{8} + \frac{591}{4\sqrt{2}} \right. \\
 & \left. + \frac{48}{\sqrt{2}} \eta \right] e^{-(1+\frac{1}{\sqrt{2}})\eta} \cos \left(1 - \frac{1}{\sqrt{2}} \right) \eta - \frac{1}{81} \left[\frac{39}{8} + \frac{591}{4\sqrt{2}} + \frac{69}{8} \eta \right] e^{-(1+\frac{1}{\sqrt{2}})\eta} \sin \left(1 - \frac{1}{\sqrt{2}} \right) \eta \\
 & + \left[-\frac{1}{9} + \frac{9143}{720\sqrt{2}} + \frac{267}{80} \eta + \frac{7}{8\sqrt{2}} \eta^2 \right] e^{-\sqrt{2}\eta} + \frac{1}{125} \left[-\frac{6217}{180\sqrt{2}} + \frac{472}{45} + \left(\frac{79}{12\sqrt{2}} - \frac{151}{24} \eta \right) \right] \cdot \\
 & \cdot e^{-\frac{3\eta}{\sqrt{2}}} \cos \frac{\eta}{\sqrt{2}} + \frac{1}{125} \left[\frac{11,363}{360\sqrt{2}} - \frac{1607}{360} + \left(-\frac{1}{4\sqrt{2}} + \frac{19}{8} \right) \eta \right] e^{-\frac{3\eta}{\sqrt{2}}} \sin \frac{\eta}{\sqrt{2}} \\
 & + \left[\frac{7}{72} + \frac{71}{288\sqrt{2}} - \frac{(\sqrt{2}-1)23}{288} \eta - \frac{(\sqrt{2}-1)}{24\sqrt{2}} \eta^2 \right] e^{-\sqrt{2}\eta} \cos \sqrt{2}\eta + \left[\frac{85}{288} + \frac{7}{144\sqrt{2}} + \right. \\
 & \left. + \frac{(\sqrt{2}-1)35}{288} \eta \right] e^{-\sqrt{2}\eta} \sin \sqrt{2}\eta - \frac{1}{6} \left(\frac{7}{72} + \frac{5}{36\sqrt{2}} \right) e^{-(1+\sqrt{2})\eta} \cos \left(1 - \sqrt{2} \right) \eta \\
 & - \frac{1}{6} \left(\frac{7}{72} - \frac{5}{36\sqrt{2}} \right) e^{-(1+\sqrt{2})\eta} \sin \left(1 - \sqrt{2} \right) \eta + \frac{1}{160\sqrt{2}} e^{-2\sqrt{2}\eta} + \frac{1}{16} e^{-2\eta} - \left[\frac{69,367}{3000} + \frac{74,161}{27,000\sqrt{2}} \right] \eta \\
 & + \frac{6403}{5625} + \frac{17,489}{7500\sqrt{2}}
 \end{aligned}$$

$$\begin{aligned}
 \mathcal{Y}_{4b}^1 = & \left[-\frac{1}{4} - \frac{11}{2\sqrt{2}} + \left(\frac{11}{4} - \frac{1}{\sqrt{2}} \right) \eta + \frac{1}{2}\eta^2 \right] e^{-\eta} \cos \eta - \left[\frac{15}{2} + \left(\frac{11}{4} + \frac{1}{\sqrt{2}} \right) \eta \right] e^{-\eta} \sin \eta + \left[\frac{23,399}{720} + \right. \\
 & \left. + \frac{781}{72\sqrt{2}} + \left(\frac{1781}{360\sqrt{2}} + \frac{19}{36} \right) \eta + \frac{1}{4}\eta^2 + \frac{5}{8\sqrt{2}} \eta^3 \right] e^{-\frac{\eta}{\sqrt{2}}} \cos \frac{\eta}{\sqrt{2}} - \left[\frac{2509}{240} - \frac{25}{24\sqrt{2}} - \left(\frac{3}{4} + \frac{231}{40\sqrt{2}} \right) \eta + \right. \\
 & \left. + \frac{7}{4}\eta^2 + \frac{1}{8\sqrt{2}} \eta^3 \right] e^{-\frac{\eta}{\sqrt{2}}} \sin \frac{\eta}{\sqrt{2}} - \left[\frac{317}{108\sqrt{2}} + \frac{1}{9} \left(\frac{35}{8\sqrt{2}} + \frac{29}{8} \right) \eta \right] e^{-(1+\frac{1}{\sqrt{2}})\eta} \cos \left(1 - \frac{1}{\sqrt{2}} \right) \eta + \\
 & + \left[\frac{397}{216} + \frac{1}{9} \left(\frac{29}{8} - \frac{35}{8\sqrt{2}} \right) \eta \right] e^{-(1+\frac{1}{\sqrt{2}})\eta} \sin \left(1 - \frac{1}{\sqrt{2}} \right) \eta - \left[\frac{337}{36} - \frac{2}{9\sqrt{2}} + \frac{197}{40\sqrt{2}} \eta + \frac{7}{8}\eta^2 \right] e^{-\sqrt{2}\eta} \\
 & + \frac{1}{25} \left[\frac{8827}{720} - \frac{2113}{360\sqrt{2}} - \left(2 - \frac{17}{4\sqrt{2}} \right) \eta \right] e^{-\frac{3\eta}{\sqrt{2}}} \cos \frac{\eta}{\sqrt{2}} - \frac{1}{25} \left[\frac{3989}{720} - \frac{191}{360\sqrt{2}} + \left(\frac{7}{12} + \frac{1}{6\sqrt{2}} \right) \eta \right] e^{-\frac{3\eta}{\sqrt{2}}} \sin \frac{\eta}{\sqrt{2}} \\
 & + (\sqrt{2}-1) \left[\frac{17}{144} + \frac{23}{72\sqrt{2}} \eta + \frac{1}{24}\eta^2 \right] e^{-\sqrt{2}\eta} \cos \sqrt{2}\eta - \left[\frac{13}{24\sqrt{2}} + \frac{5}{12} + \frac{(\sqrt{2}-1)}{12\sqrt{2}} \eta - \frac{(\sqrt{2}-1)}{24} \eta^2 \right] e^{-\sqrt{2}\eta} \sin \sqrt{2}\eta \\
 & + \frac{1}{9\sqrt{2}} e^{-(1+\sqrt{2})\eta} \cos \left(1 - \sqrt{2} \right) \eta - \frac{1}{72} e^{-(1+\sqrt{2})\eta} \sin \left(1 - \sqrt{2} \right) \eta - \frac{1}{80} e^{-2\sqrt{2}\eta} - \frac{1}{8} e^{-2\eta} \\
 & - \frac{69,367}{3000} - \frac{74,161}{27,000\sqrt{2}}
 \end{aligned}$$

$$\begin{aligned}
 \varphi_{4c} = & \left(\frac{25}{8} + \frac{3}{4\sqrt{2}}\right)e^{-\eta} \cos \eta + \left(\frac{23}{8} - \frac{3}{4\sqrt{2}} + \frac{3}{4}\eta\right)e^{-\eta} \sin \eta - \left[\frac{623}{72} + \frac{10,541}{360\sqrt{2}} + \left(\frac{662}{40} + \frac{1}{4\sqrt{2}}\right)\eta + \right. \\
 & \left. + \frac{15}{4\sqrt{2}}\eta^2\right]e^{-\frac{\eta}{\sqrt{2}}} \cos \frac{\eta}{\sqrt{2}} + \left[\frac{313}{72} + \frac{33,025}{360\sqrt{2}} + \frac{986}{120}\eta - \frac{7}{4\sqrt{2}}\eta^2 - \frac{3}{8}\eta^3\right]e^{-\frac{\eta}{\sqrt{2}}} \sin \frac{\eta}{\sqrt{2}} \\
 & + \frac{1}{81}\left[\frac{693}{8} + \frac{945}{8\sqrt{2}} + \frac{81}{4\sqrt{2}}\eta\right]e^{-(1+\frac{1}{\sqrt{2}})\eta} \cos\left(1-\frac{1}{\sqrt{2}}\right)\eta + \frac{1}{81}\left[\frac{513}{8} - \frac{873}{8\sqrt{2}} + \frac{81}{8}\eta\right]e^{-(1+\frac{1}{\sqrt{2}})\eta} \sin\left(1-\frac{1}{\sqrt{2}}\right)\eta \\
 & + \left[-1 + \frac{185}{16\sqrt{2}} + \frac{363}{80}\eta + \frac{15}{16\sqrt{2}}\eta^2\right]e^{-\sqrt{2}\eta} + \frac{1}{125\sqrt{2}}\left[\frac{4885}{60} + \frac{96}{5\sqrt{2}} + \left(\frac{17}{6} + \frac{191}{12\sqrt{2}}\right)\eta\right]e^{-\frac{3\eta}{5}} \cos \frac{\eta}{\sqrt{2}} \\
 & + \frac{1}{125\sqrt{2}}\left[\frac{1129}{90\sqrt{2}} + \frac{665}{180} + \left(\frac{31}{6} + \frac{13}{12\sqrt{2}}\right)\eta\right]e^{-\frac{3\eta}{5}} \sin \frac{\eta}{\sqrt{2}} - \left[\frac{31}{96\sqrt{2}} + \left(\frac{1}{24\sqrt{2}} - \frac{1}{48}\right)\eta\right]e^{-\sqrt{2}\eta} \cos \sqrt{2}\eta \\
 & + \left[\frac{17}{144} - \frac{13}{576\sqrt{2}} + \left(\frac{1}{24\sqrt{2}} - \frac{3}{16}\right)\eta\right]e^{-\sqrt{2}\eta} \sin \sqrt{2}\eta + \frac{1}{16\sqrt{2}}e^{-(1+\sqrt{2})\eta} \left[\cos\left(1-\sqrt{2}\right)\eta - \sin\left(1-\sqrt{2}\right)\eta\right] \\
 & + \frac{1}{320\sqrt{2}}e^{-2\sqrt{2}\eta} + \frac{1}{16}e^{-2\eta} - \left(\frac{1,280,027}{36,000} + \frac{236,121}{27,000\sqrt{2}}\right)\eta + \frac{159,571}{30,000} + \frac{1,088,329}{72,000\sqrt{2}}
 \end{aligned}$$

$$\begin{aligned}
 \varphi_{4c}^1 = & \left[-\left(\frac{1}{4} + \frac{3}{2\sqrt{2}}\right) + \frac{3}{4}\eta\right]e^{-\eta} \cos \eta - \left(\frac{21}{4} + \frac{3}{4}\eta\right)e^{-\eta} \sin \eta + \left[\frac{1055}{24} + \frac{51}{4\sqrt{2}} + \left(\frac{1}{8} + \frac{259}{15\sqrt{2}}\right)\eta + \right. \\
 & \left. + \eta^2 - \frac{3}{8\sqrt{2}}\eta^3\right]e^{-\frac{\eta}{\sqrt{2}}} \cos \frac{\eta}{\sqrt{2}} + \left[-\left(\frac{2071}{90} - \frac{155}{36\sqrt{2}}\right) + \left(\frac{1}{8} + \frac{29}{6\sqrt{2}}\right)\eta + \frac{13}{8}\eta^2 + \frac{3}{8\sqrt{2}}\eta^3\right]e^{-\frac{\eta}{\sqrt{2}}} \sin \frac{\eta}{\sqrt{2}} \\
 & - \left[\frac{1}{3} + \frac{53}{12\sqrt{2}} + \frac{3}{8\sqrt{2}}\eta\right]e^{-(1+\frac{1}{\sqrt{2}})\eta} \cos\left(1-\frac{1}{\sqrt{2}}\right)\eta - \left[\frac{1}{3} - \frac{1}{6\sqrt{2}} + \frac{3}{8\sqrt{2}}\eta\right]e^{-(1+\frac{1}{\sqrt{2}})\eta} \sin\left(1-\frac{1}{\sqrt{2}}\right)\eta \\
 & - \left[\frac{281}{40} - \frac{2}{\sqrt{2}} + \frac{36}{5\sqrt{2}}\eta + \frac{15}{16}\eta^2\right]e^{-\sqrt{2}\eta} - \frac{1}{25}\left[\frac{8087}{360} + \frac{709}{180\sqrt{2}} + \left(\frac{1}{3} + \frac{14}{3\sqrt{2}}\right)\eta\right]e^{-\frac{3\eta}{5}} \cos \frac{\eta}{\sqrt{2}} \\
 & - \frac{1}{25}\left[\frac{1097}{120} + \frac{93}{20\sqrt{2}} + \left(\frac{11}{6} + \frac{23}{12\sqrt{2}}\right)\eta\right]e^{-\frac{3\eta}{5}} \sin \frac{\eta}{\sqrt{2}} + \left[\frac{17}{72} + \frac{7}{36\sqrt{2}} + \left(\frac{1}{12} - \frac{5}{12\sqrt{2}}\right)\eta\right] \cdot \\
 & \cdot e^{-\sqrt{2}\eta} \cos \sqrt{2}\eta - \left[\frac{7}{36\sqrt{2}} - \frac{35}{144} - \frac{7}{3\sqrt{2}}\right]e^{-\sqrt{2}\eta} \sin \sqrt{2}\eta - \frac{1}{8\sqrt{2}}e^{-(1+\sqrt{2})\eta} \cos\left(1-\sqrt{2}\right)\eta \\
 & + \frac{1}{8}e^{-(1+\sqrt{2})\eta} \sin\left(1-\sqrt{2}\right)\eta - \frac{1}{160}e^{-2\sqrt{2}\eta} - \frac{1}{8}e^{-2\eta} - \frac{1,280,027}{36,000} - \frac{236,121}{27,000\sqrt{2}}
 \end{aligned}$$

Appendix 2

Differential equation for ker and kei functions

$K_p(kr) \sin p\phi$ is a solution to the equation
 $(\nabla^2 - k^2)\psi = 0$ in cylindrical coordinates.

Thus

$$\left[\frac{\partial^2}{\partial r^2} + \frac{1}{r} \frac{\partial}{\partial r} + \frac{1}{r^2} \frac{\partial^2}{\partial \phi^2} - k^2 \right] K_p(kr) \sin p\phi = 0 \quad (1)$$

$K_p(kr)$ satisfies the equation

$$\left[r^2 \frac{d^2}{dr^2} + r \frac{d}{dr} - (p^2 + k^2 r^2) \right] K_p(kr) = 0 \quad (2)$$

In our case k^2 is pure imaginary $= i\alpha^2$

Thus

$$\left[r^2 \frac{d^2}{dr^2} + r \frac{d}{dr} - (p^2 + i\alpha^2 r^2) \right] K_p(iar) = 0 \quad (3)$$

If we write $K_p(iar) = X_p(ar) + iY_p(ar)$ where X_p and Y_p are the real and imaginary parts of the function, then we can separate the real and imaginary parts of (3) and get

$$\begin{aligned} r^2 \frac{d^2 X_p}{dr^2} + r \frac{dX_p}{dr} - p^2 X_p + \alpha^2 r^2 Y_p &= 0 \\ r^2 \frac{d^2 Y_p}{dr^2} + r \frac{dY_p}{dr} - p^2 Y_p - \alpha^2 r^2 X_p &= 0 \end{aligned} \quad (4)$$

Or

$$\begin{aligned}\nabla^2 X_p \sin p \phi &= -\alpha^2 Y_p \sin p \phi \\ \nabla^2 Y_p \sin p \phi &= \alpha^2 X_p \sin p \phi\end{aligned}\tag{5}$$

Hence

$$\nabla^4 X_p \sin p \phi = -\alpha^2 \nabla^2 Y_p \sin p \phi = -\alpha^4 X_p \sin p \phi = k^4 X_p \sin p \phi\tag{6}$$

$$\nabla^4 Y_p \sin p \phi = k^4 Y_p \sin p \phi$$

In our case

$$K_2(\sqrt{i} \frac{r}{\delta}) = -\ker_2 \frac{r}{\delta} - kei_2 \frac{r}{\delta} = X_2 + i Y_2\tag{7}$$

Thus

$$\nabla^4 \left[\ker_2 \frac{r}{\delta} \sin 2 \phi \right] = k^4 \ker_2 \frac{r}{\delta} \sin 2 \phi$$

and

$$\nabla^4 \left[kei_2 \frac{r}{\delta} \sin 2 \phi \right] = k^4 kei_2 \frac{r}{\delta} \sin 2 \phi\tag{8}$$

Appendix 3

An Evaluation of the Three Integrals I_1 , I_2 , and I_3
Discussed in Chapter V

$$I_1 = \delta\mu \cdot \frac{\omega}{2v} \int_x U_0^2 dx \int_0^{\infty} (\zeta_{1r}''^2 + \zeta_{1i}''^2) d\eta$$

$$\text{Since, } \zeta_{1r}''^2 + \zeta_{1i}''^2 = \zeta_1'' \bar{\zeta}_1'' = e^{-\sqrt{2}\eta}$$

$$I_1 = \sqrt{2}\omega \cdot \frac{\rho}{2} \cdot \frac{1}{\sqrt{2}} \int_x U_0^2(x) dx \quad (1)$$

$$I_2 = \delta\mu \cdot \frac{\omega}{2v} \cdot \frac{1}{\omega^2} \int_x U_0^2 \left(\frac{dU_0}{dx}\right)^2 dx \int_0^{\infty} (\zeta_{2a}'' \bar{\zeta}_{2a}'' + \zeta_{2b}''^2) d\eta$$

$$\zeta_{2a}'' \bar{\zeta}_{2a}'' = \frac{1}{2} e^{-2\eta} - \left[\frac{1}{\sqrt{2}} - \frac{(1+i)\eta}{4} \right] e^{-\left[\left(1+\frac{1}{\sqrt{2}}\right) - \left(1-\frac{1}{\sqrt{2}}\right)i\right]\eta}$$

$$- \left[\frac{1}{\sqrt{2}} - \frac{(1-i)\eta}{4} \right] e^{-\left[\left(1+\frac{1}{\sqrt{2}}\right) + \left(1-\frac{1}{\sqrt{2}}\right)i\right]\eta} + \left[1 - \frac{1}{\sqrt{2}}\eta + \frac{1}{4}\eta^2 \right] e^{-\sqrt{2}\eta}$$

$$\zeta_{2b}''^2 = \frac{1}{8} e^{-2\sqrt{2}\eta} + \left[\frac{(-3+4i)}{8} + \frac{(1+2i)\eta}{4\sqrt{2}} + \frac{\eta^2}{16} \right] e^{-\sqrt{2}(1-i)\eta}$$

$$+ \left[-\frac{(3+4i)}{8} + \frac{(1-2i)\eta}{4\sqrt{2}} + \frac{\eta^2}{16} \right] e^{-\sqrt{2}(1+i)\eta} - \left[\frac{(1+2i)}{4} + \frac{\eta}{4\sqrt{2}} \right] e^{-\left(\frac{3-i}{\sqrt{2}}\right)\eta}$$

$$- \left[\frac{(1-2i)}{4} + \frac{\eta}{4\sqrt{2}} \right] e^{-\left(\frac{3+i}{\sqrt{2}}\right)\eta} + \left[\frac{5}{4} + \frac{\eta}{2\sqrt{2}} + \frac{\eta^2}{8} \right] e^{-\sqrt{2}\eta}$$

Thus,

$$I_2 = \sqrt{2}\omega \cdot \frac{\rho}{2} \cdot \frac{1}{\omega^2} \left[-\frac{5}{36} + \frac{3829}{7200\sqrt{2}} \right] \int_x U_0^2 \left(\frac{dU_0}{dx}\right)^2 dx \quad (2)$$

$$I_3 = -\delta\mu \cdot \frac{\omega}{2v} \cdot \frac{1}{\omega^2} \left\{ \int_x U_0^3 \frac{d^2 U_0}{dx^2} dx \int_0^\infty \text{R.P.} (\bar{p}_{3a}'' \bar{p}_1'') d\eta + \right. \\ \left. + \int_x U_0^2 \left(\frac{dU_0}{dx} \right)^2 dx \int_0^\infty \text{R.P.} (\bar{p}_{3b}'' \bar{p}_1'') d\eta \right\}$$

$$\bar{p}_{3a}'' \bar{p}_1'' = -\frac{1}{\sqrt{2}} e^{-[(1+\frac{1}{\sqrt{2}})+(1-\frac{1}{\sqrt{2}})i]\eta} + \left\{ -\frac{161}{120} - i\left(\frac{1}{2\sqrt{2}} + \frac{261}{120}\right) + \frac{(11-5i)}{8\sqrt{2}} \eta \right. \\ \left. - \frac{3}{8} \eta^2 \right\} e^{-\sqrt{2}\eta} + \frac{3}{8} i e^{-[(1+\sqrt{2})+(1-\sqrt{2})i]\eta} + \frac{(23+19i)}{10} e^{-\left(\frac{3-i}{\sqrt{2}}\right)\eta} \\ + \left\{ \left(\frac{1}{4} + \frac{1}{4\sqrt{2}}\right) - i - \frac{(1+i)}{4\sqrt{2}} \eta \right\} e^{-\sqrt{2}(1-i)\eta} + \frac{(1+7i)}{40} e^{-2\sqrt{2}\eta} + \frac{1}{3} e^{-\left(\frac{3+i}{\sqrt{2}}\right)\eta}$$

$$\bar{p}_{3b}'' \bar{p}_1'' = \left[-\frac{5}{\sqrt{2}} + i - \frac{(1+i)}{\sqrt{2}} \eta \right] e^{-[(1+\frac{1}{\sqrt{2}})+(1-\frac{1}{\sqrt{2}})i]\eta} - \left\{ -\left(\frac{689}{360} + \frac{2}{9\sqrt{2}}\right) + \right. \\ \left. + i\left(\frac{413}{72} + \frac{55}{36\sqrt{2}}\right) + \frac{(-1-5i)}{8\sqrt{2}} \eta + \frac{(3+4i)}{8} \eta^2 \right\} e^{-\sqrt{2}\eta} \\ + \left[\frac{5}{4\sqrt{2}} + i\frac{3}{8} \right] e^{-[(1+\sqrt{2})+(1-\sqrt{2})i]\eta} + \left[\frac{(7+41i)}{10} + \frac{(1+i)}{\sqrt{2}} \eta \right] e^{-\left(\frac{3-i}{\sqrt{2}}\right)\eta} \\ - \frac{(7-i)}{40} e^{-2\sqrt{2}\eta} + \left\{ \left(\frac{5}{4} + \frac{1}{4\sqrt{2}}\right) - i\frac{3}{2} - \frac{(3+7i)}{4\sqrt{2}} \eta - \frac{1}{4} \eta^2 \right\} e^{-\sqrt{2}(1-i)\eta} \\ + \left[\frac{-5(\sqrt{2}-1)(1+i)}{36} - \frac{(\sqrt{2}-1)i}{3\sqrt{2}} \eta \right] e^{-\left(\frac{3+i}{\sqrt{2}}\right)\eta}$$

Thus,

$$\begin{aligned} I_3 = & -\sqrt{2}\omega \cdot \frac{\rho}{2} \cdot \frac{1}{\omega^2} \left\{ \left(-\frac{1}{24} + \frac{33}{80\sqrt{2}} \right) \int_x U_0^3 \frac{d^2 U_0}{dx^2} dx + \right. \\ & \left. + \left(-\frac{193}{450} + \frac{4373}{3600\sqrt{2}} \right) \int_x U_0^2 \left(\frac{dU_0}{dx} \right)^2 dx \right\} \end{aligned} \quad (3)$$

Combining I_1, I_2, I_3 , we get

$$\begin{aligned} W/T = & \sqrt{2}\omega \cdot \frac{\rho}{2} \cdot \left\{ \frac{1}{\sqrt{2}} \int_x U_0^2(x) dx - \frac{1}{\omega^2} \left[(.250) \int_x U_0^3 \frac{d^2 U_0}{dx^2} dx \right. \right. \\ & \left. \left. + (.212) \int_x U_0^2 \left(\frac{dU_0}{dx} \right)^2 dx \right] \right\} \end{aligned} \quad (4)$$

Appendix 4

Evaluation of the Integral $\int_a^\infty K_1(kr)K_1^*(kr)rdr$

Let $u = R_n^0(k_p r)$ and $v = R_n^0(k_q r)$ be two solutions of the modified Bessel equation, i.e.

$$\frac{1}{r} \frac{d}{dr} \left(r \frac{du}{dr} \right) - \left(k_p^2 + \frac{n^2}{r^2} \right) u = 0 \quad (1)$$

$$\frac{1}{r} \frac{d}{dr} \left(r \frac{dv}{dr} \right) - \left(k_q^2 + \frac{n^2}{r^2} \right) v = 0 \quad (2)$$

Multiply (1) by rv , (2) by ru , subtract and integrate from a to ∞ .

Thus:

$$\begin{aligned} (k_p^2 - k_q^2) \int_a^\infty rvudr &= + \int_a^\infty \left[v \frac{d}{dr} \left(r \frac{du}{dr} \right) - u \frac{d}{dr} \left(r \frac{dv}{dr} \right) \right] dr \\ &= + \left[rv \frac{du}{dr} - ru \frac{dv}{dr} \right]_a^\infty \end{aligned}$$

This last step is obtained by an integration by parts. In our case $R_n^0(kr) = K_n(kr)$ which approaches zero as r becomes infinite. Thus the upper limit terms vanish.

$$\text{For } n = 1, k_p = \sqrt{i} \frac{1}{\delta}, k_q = \sqrt{-1} \frac{1}{\delta}, (k_p^2 - k_q^2) = \frac{2i}{\delta^2}$$

Thus:

$$\begin{aligned} I &= \int_a^\infty r K_1 \left(\sqrt{i} \frac{r}{\delta} \right) K_1 \left(\sqrt{-1} \frac{r}{\delta} \right) dr = \\ &= - \frac{a\delta}{2i} \left[\underbrace{\sqrt{i} K_1 \left(\sqrt{-1} \frac{a}{\delta} \right) K_1' \left(\sqrt{i} \frac{a}{\delta} \right)}_{X + iY} - \sqrt{-1} K_1 \left(\sqrt{i} \frac{a}{\delta} \right) K_1' \left(\sqrt{-1} \frac{a}{\delta} \right) \right] \end{aligned} \quad (3)$$

$X + iY$

Considering the first term in the bracket to be split into real and imaginary parts $X + iY$, we see that the integral has the value, $I = -a\delta Y$. Thus we need Y .

We have:

$$K_1(\sqrt{i} x) = -kei_1 x + iker_1 x$$

$$K_1(\sqrt{-i} x) = -kei_1 x - iker_1 x$$

$$\sqrt{i} K_1'(\sqrt{i} x) = -kei_1' x + iker_1' x$$

Thus

$$\begin{aligned} \sqrt{i} K_1(\sqrt{-i} x) K_1'(\sqrt{i} x) &= [kei_1 x kei_1' x + ker_1 x ker_1' x + \\ &+ i(ker_1 kei_1' x - kei_1 x ker_1' x)] \end{aligned}$$

Hence

$$Y = ker_1 \frac{a}{\delta} kei_1' \frac{a}{\delta} - kei_1 \frac{a}{\delta} ker_1' \frac{a}{\delta} \quad (4)$$

Thus finally:

$$\int_a^\infty r K_1(\sqrt{i} \frac{r}{\delta}) K_1(\sqrt{-i} \frac{r}{\delta}) dr = -a\delta [ker_1 \frac{a}{\delta} kei_1' \frac{a}{\delta} - kei_1 \frac{a}{\delta} ker_1' \frac{a}{\delta}] \quad (5)$$

Bibliography

References to Acoustic Streaming

1. V. Dvorak, Ann. Physik 157, 42 (1896).
2. Rayleigh, Theory of Sound (MacMillan Co. Ltd., London, 1896) v. II, p. 333.
3. A. Meissner, Z. Tech. Physik 7, 585 (1926).
4. Z. Carrière, J. Phys. et Radium 10, part 1, 198 (1929).
5. Z. Carrière, J. Phys. et Radium 12, 165 (1931).
6. E. N. Andrade, Proc. Roy. Soc. (London) A 134, 445 (1931).
7. H. Schlichting, Phys. Z. 33, 327 (1932).
8. H. Bouasse, Tourbillons (Delagrave, Paris, 1932) v. 2.
9. Z. Carrière, J. Phys. et Radium 1, 68 (1940).
10. K. Schuster and W. Matz, Akust. Z. 5, 349 (1940).
11. C. Eckart, Phys. Rev. 73, 68 (1948).
12. L. N. Lieberman, Phys. Rev. 75, 1415 (1949).
13. U. Ingard and S. Labate, J.A.S.A. 22, 211 (1950).
14. J. P. Walker and C. H. Allen, J.A.S.A. 22, 680A (1950).
15. F. Fox and K. Herzfeld, Phys. Rev. 78, 156 (1950).
16. G. D. West, Proc. Phys. Soc. B (London) 64, 483 (1951).
17. P. N. Kubanskii, J. Tech. Phys. (U.S.S.R.) 22, 585 (1952).
P. N. Kubanskii, J. Tech. Phys. (U.S.S.R.) 22, 593 (1952).
18. J. J. Markham, Phys. Rev. 86, 497 (1952).
19. P. J. Westervelt, J.A.S.A. 25, 60 (1953).
20. W. L. Nyborg, J.A.S.A. 25, 68 (1953).
21. H. Medwin and I. Rudnick, private communication.
22. J. Guittard, Acustica, v. 3, No. 1, 22--32 (1953).

General References

23. H. Schlichting, Grenzschicht-Theorie, (G. Braun, Karlsruhe, 1951) p. 90.
24. P. Bridgman, Dimensional Analysis (Yale, New Haven, 1922).
25. S. Goldstein, Modern Developments in Fluid Dynamics (Oxford, 1950) v. I.
26. Prandtl, Verhandlungen des dritten internationalen Mathematiker-Kongresses, Heidelberg, 1904 (Leipzig, 1905) pp. 484--491.
27. H. Lamb, Hydrodynamics, 6th ed. (Dover, New York, 1945) Ch. 11.
28. H. B. Dwight, Tables of Integrals and Other Mathematical Data (The MacMillan Co., New York, 1947).
29. L. M. Milne-Thomson, Theoretical Hydrodynamics (MacMillan, London, 1938) ch. 19.
30. H. G. Savidge, British Assoc. Report (1916) pp. 108-122.
31. L. L. Beranek, Acoustic Measurements (Wiley, New York, 1949) p. 159.

Biographical Sketch

John Milton Andres was born to Paul Arthur Andres and Sylvetta Fricker Andres at Santa Ana, California, on February 4, 1927. He attended public schools in southern California and graduated from the Garden Grove Union High School in 1944. He entered the California Institute of Technology in June, 1944, and completed the freshman year in February, 1945. From March, 1945, to July, 1946, he served as an Electronic Technician with the U.S. Navy. He resumed his work at Caltech in September, 1946, with a tuition scholarship, and was graduated with honor in 1949. He remained at Caltech as a teaching assistant in Physics and received his M.S. in June, 1950.

Since September, 1950, he has been at the Massachusetts Institute of Technology pursuing work leading to the Ph.D. degree. In September, 1951, he was appointed a Research Assistant at M.I.T. He is a member of Tau Beta Pi and an associate member of Sigma Xi.